PREDICTIVE KINETICS IN HOMOGENEOUS CATALYSIS

Ewa Natalia Szlapa

Supervisors:
Prof. J. N. Harvey
Prof. J. M. Ugalde

Members of the Examination Committee:
Prof. X. Lopez
Prof. A. Ceulemans
Prof. E. Van der Eycken
Prof. V. Van Speybroeck
Prof. W. De Borggraeve

Dissertation presented in partial fulfilment of the requirements for the degree of Doctor of Science

November

Uitgegeven in eigen beheer, Ewa Natalia Szlapa, Leuven

Preface

The main goal of this thesis is to make theoretical predictions of the course of catalytic reactions employing the tools that belong to the domain of computational chemistry. Hopefully the reader will find in this manuscript some evidence that it is possible to foresee, accurately enough, the mechanism, kinetics and selectivity of macroscopic homogenous processes using quantum chemical calculations. And furthermore, that computational simulations may be utilized to propose novel models of reaction routes and presumptive catalysts.

I would like to say “thank you” to so many people. Let’s do it in chronological order.

Firstly to my family and friends: Halina, Kazik, Gosia, Bogusia, Monika and Liu, for their constant support and encouragement.

My adventure with science began at Wroclaw University of Technology. I am very grateful to the supervisor of my engineer project and master thesis, Andrzej Miniewicz, who introduced me to the world of academic research.

Many, many thanks to my supervisor at KU Leuven, Jeremy Harvey, who has taught me everything I know about computational catalysis. Moreover, thank you to Rita, Leen, Indra and An for the help with bureaucracy at KU Leuven and to Hans for taking care of the computational resources. I was lucky to belong to such a great group of other students and postdocs in Quantum Chemistry and Physical Chemistry Section, many thanks to my colleagues there.

Thanks a lot to everybody engaged in the Theoretical Chemistry and Computational Modelling (TCCM) consortium, especially to Manuel Yañez and Wilson Rodriguez, for this PhD opportunity, the organization of the whole programme and all thirteen workshops and meetings. This project was often fun because of the other fourteen early stage researchers of this TCCM-European Joint Doctorate. I was a pleasure to meet you: Neus, Martina, Vani, Max, Francesco, Andi, Jelle, Stefano, Carles, Tomasso, Dyma, Gabriele, Meilani, María.

During my PhD project I spent three months in Alyatech company in Sabadell, Spain. I am very thankful to my hosts there, Lourdes Vega and Patricia Ruíz for the opportunity to become acquainted with the company environment and learn about the molecular dynamics.

In the last stage of my doctorate I was working at the University of the Basque Country. I would like to thank my supervisors there, Jesus Ugalde and Xabier Lopez for the research guidance, Izaskun, Idoia and Ana Maria for taking care of the administrative issues, Txema and Edu for the help with calculations and the great group of researchers and workers at the Donostia International Physics Centre.

Last but not least I wish to thank the taxpayers in European Union for financing my scholarship: European Union's Horizon 2020 research and innovation programme under the Marie Skłodowska-Curie grant agreement No.642294.

Abstract

This thesis is devoted to the theoretical chemistry studies of catalytic reactions. It includes two sorts of computational approach towards the prediction of the reaction course. The first one is to understand better the process that already exists. The conducted calculations, which approach the quantitative agreement with the experiment, provide a valuable insight into the mechanisms of the investigated reaction. The second approach is to employ the tools of computational chemistry in order to discover new catalysts and reaction routes that one day could be verified in a chemical laboratory and maybe even used by the industry.

A brief introduction encompassing the history and main concepts of catalysis together with the description of some important catalytic processes, is presented at the beginning of Chapter 1. Later on the scientific methods of theoretical chemistry employed in the conducted investigation are summarized including a short description of Hartree-Fock, coupled cluster and density functional theory methods used for electronic structure calculations, as well as collision theory and transition state theory concepts for prediction of reaction rates. Chapter 1 concludes with a description of industrial and research achievements in the field of hydroformylation and methane activation, the two reactions that have been investigated throughout this doctorate project.

The obtained results are presented in two chapters. In Chapter 2 the investigation devoted to alkene hydroformylation is described. This research was conducted on a well-known system of unmodified cobalt catalyzed hydroformylation of propene. The methods of computational chemistry, density functional theory and coupled cluster calculations of reaction potential energy surface together with transition state theory and microkinetic modelling were employed so as to understand the kinetics and the selectivity of the process in more detail. The mechanism of the reaction was studied with great care in order to reproduce the experimentally observed

rates of aldehydes production as a function of many factors: temperature, pressure and concentrations of reactants. The reasons behind the observed regioselectivity are addressed too. They include the competing pathway of reductive elimination by catalyst and treatment of permutational symmetry numbers that altogether lead to the experimentally observed higher yield of a linear aldehyde. Thus the first approach of theoretical chemistry, to understand better the operating processes, is demonstrated.

In Chapter 3 the putative reaction of methane activation with alternant X_2Y_2 (X = N or P, Y = O or S) radical cations forming ring-like structures is predicted with quantum-mechanical calculations. The reaction is studied on a gas-phase system under single-collision conditions, revealing that a hydrogen atom transfer from methane towards the nitrogen atom of a cluster may occur. Such a model, although idealized and simplified, enables to extract some useful information on electronic structure of reactants and transition states. This project is an example of the second employment of computational chemistry, namely to predict the novel reaction routes that might be used to solve some of the challenges of modern catalysis.

The last Chapter 4 contains an extensive summary of the obtained results. Both approaches of the conducted computational chemistry studies in the field of applied catalysis represented here by the research on hydroformylation and methane activation are compared and evaluated.

Samenvatting

Deze thesis is gewijd aan theoretische chemie studies van katalytische reacties. Het bevat twee types computationele strategieën voor de voorspelling van de reactie route. De eerste wordt gebruikt om het bestaande proces beter te begrijpen. De uitgevoerde berekeningen, die in kwantitatieve overeenstemming zijn met experiment, leveren een belangrijk inzicht in de mechanismen van de onderzochte reactie. De tweede methode gebruikt de middelen van de computationele chemie om nieuwe katalysatoren en reactie routes te ontdekken die misschien ooit bevestigd kunnen worden in het laboratorium en misschien zelfs bruikbaar zijn in de industrie

Een korte inleiding met daarin een geschiedenis van en de belangrijkste concepten uit de katalyse samen met een beschrijving van een aantal belangrijke katalytische processen, wordt gegeven in het begin van hoofdstuk 1. Daarna worden de wetenschappelijke methodes van de theoretische chemie die gebruikt werden in het uitgevoerde onderzoek samengevat met daarin een korte beschrijving van de Hartree-Fock, coupled cluster and density functional theorie methodes die gebruikt werden voor de electronic structure berekeningen, en van de concepten van de botsingstheorie en van de transitietoestandtheorie voor de voorspelling van reactiesnelheden. Hoofdstuk 1 sluit af met een beschrijving van industriële en onderzoek successen in het veld van hydroformylatie en methaan activatie, de twee reacties die werden onderzocht in dit doctoraatsproject.

De bereikte resultaten worden beschreven in twee hoofdstukken. In hoofdstuk 2 wordt het onderzoek naar alkeen hydroformylatie beschreven. Dit onderzoek werd uitgevoerd op een goed gekend systeem: de ongemodificeerde, kobalt gekatalyseerde hydroformylatie van propeen. De methodes van de computationele chemie, density functional theorie en coupled cluster berekeningen van het potentiële energieoppervlak van de reactie, samen met transitietoestand theorie en microkinetische modellen werden

gebruikt om de kinetiek en de selectiviteit van het proces beter te begrijpen. Het reactiemechanisme werd nauwkeurig onderzocht om de experimenteel geobserveerde snelheden van aldehyde productie te reproduceren in functie van verschillende factoren: temperatuur, druk en concentratie van de reactanten. Ook de oorzaken van de vastgestelde regioselectiviteit worden toegelicht. Deze omvatten de concurrerende reactie route van de reductieve eliminatie door de katalysator en de rol van de permutational symmetry numbers die samen leiden tot de hogere experimentele opbrengst van een lineair aldehyde. De eerste strategie van de theoretische chemie, het beter begrijpen van reeds gebruike processen, is aldus behandeld.

In hoofdstuk 3 wordt de reactie van methaan activatie met de alternanten X_2Y_2 (X = N of P, Y = O of S), radicale kationen die ring structuren vormen, voorspeld met quantummechanische berekeningen. De reactie wordt onderzocht in een systeem in gasfase onder “single-collision” omstandigheden waarbij wordt aangetoond dat een waterstofatoom van methaan naar het stikstofatoom van een cluster getransfereerd kan worden. Een dergelijk model, hoewel geïdealiseerd en vereenvoudigd, maakt het mogelijk nuttige informatie te verkrijgen over de elektronische structuur van de reactanten en de transitie toestanden. Dit project is een voorbeeld van de tweede strategie van de computationele chemie, namelijk het voorspellen van nieuwe reactie routes die mogelijk gebruikt kunnen worden om sommige problemen van de moderne katalyse op te lossen.

Het laatste hoofdstuk 4 bevat een uitgebreide samenvatting van de verkregen resultaten. Beide strategieën van de computationele chemie toegepast in het veld van de toegepaste katalyse, hier vertegenwoordigd door het onderzoek naar hydroformilatie en methaan activatie, worden vergeleken en geëvalueerd.

Resumen

Esta tesis está dedicada al estudio de las reacciones catalíticas en el ámbito de la química teórica. Incluye dos tipos de enfoque computacional hacia la predicción del transcurso de la reacción. El primero es para entender mejor el proceso que existe actualmente. Los cálculos llevados a cabo, que se aproximan cuantitativamente al experimento, proporcionan una valiosa información sobre los mecanismos de la reacción investigada. El segundo enfoque es emplear herramientas de la química computacional para descubrir nuevos catalizadores y rutas de reacción que algún día podrían ser verificaos en laboratorios químicos y tal vez incluso ser utilizados por la industria.

Al comienzo del Capítulo 1 se presenta una breve introducción que abarca la historia y los conceptos principales de la catálisis, junto con la descripción de algunos de los procesos catalíticos más importantes. Más adelante, se resumen los métodos científicos de química teórica empleados en las investigaciones ya realizadas, que incluyen una breve descripción de Hartree-Fock, cluster acoplado y teoría del funcional de la densidad son métodos usados para los cálculos de estructuras electrónicas, así como conceptos de teoría de colisión y estado de transición para la predicción de las velocidades de reacción. El Capítulo 1 concluye con una descripción de los logros industriales y de investigación en el campo de la hidroformilación y la activación de metano, las dos reacciones que se han investigado a lo largo de este doctorado.

Los resultados obtenidos se presentan en dos capítulos. En el Capítulo 2 se describe la investigación dedicada a la hidroformilación de alquenos.

Esta investigación se realizó sobre un sistema bien conocido de hidroformilación de propeno catalizada con cobalto no modificado. Los métodos de la química computacional, la teoría del funcional de la densidad y cálculos de cluster acoplado de la superficie de energía potencial de reacción, junto con la teoría del estado de transición y el modelado microcinético, se emplearon para comprender la

cinética y la selectividad del proceso con más detalle. El mecanismo de la reacción se estudió con gran cuidado para reproducir las tasas observadas experimentalmente de producción de aldehídos en función de muchos factores: temperatura, presión y concentraciones de reactivos. Las razones detrás de la regioselectividad observada se abordan también. Incluyen la vía competitiva de eliminación reductora por catalizador y el tratamiento de los números de simetría permutacional que en conjunto conducen al mayor rendimiento observado experimentalmente de un aldehído lineal. Así el primer enfoque de la química teórica, para comprender mejor los procesos operativos, queda demostrado.

En el Capítulo 3, la supuesta reacción de la activación de metano con cationes radicales alternantes X_2Y_2 (X = N o P, Y = O o S) que forman estructuras en forma de anillo se predice con cálculos cuántico-mecánicos. La reacción se estudia en un sistema de fase gaseosa en condiciones de colisión única, lo que revela que puede ocurrir una transferencia de un átomo de hidrógeno desde el metano hacia el átomo de nitrógeno de un grupo. Este modelo, aunque idealizado y simplificado, permite extraer información útil sobre la estructura electrónica de los reactivos y los estados de transición. Este proyecto es un ejemplo del segundo uso de la química computacional, esto es predecir las nuevas rutas de reacción que podrían usarse para resolver algunos de los desafíos de la catálisis moderna.

El último Capítulo 4 contiene un extenso resumen de los resultados obtenidos. Ambos enfoques de los estudios de la química computacional realizados en el campo de la catálisis aplicada son comparados y evaluados en esta tesis. Dichos enfoques son representados aquí por la investigación sobre hidroformilación y activación de metano.

List of Abbreviations

ab initio	from the beginning
AO	atomic orbital
BO	Born-Oppenhimer
CC	coupled cluster
CCSD(T)	coupled cluster singles and doubles with perturbative triples
D3	D3 version of Grimme's dispersion
D3BJ	D3 version of Grimme's dispersion with Becke-Johnson damping
DFT	density functional theory
GTO	Gaussian-type orbital
HAT	hydrogen atom transfer
HF	Hartree-Fock
in silico	performed on computer or performed employing computer simulation
IRC	intrinsic reaction coordinate
LCAO	linear combination of atomic orbitals
MA	methane aromatization
MO	molecular orbital
NOCM	non- oxidative coupling of methane
OCM	oxidative coupling of methane
PCET	proton-coupled electron transfer
PES	potential energy surface
RHF	restricted Hartree-Fock
ROHF	restricted open-shell Hartree-Fock
STO	Slater-type orbital
TCD	thermocatalytic decomposition
TOF	turnover frequency
TON	turnover number
TS	transition state (activated complex)
TST	transition state theory
UHF	unrestricted Hartree-Fock

Contents

Chapter 1

Introduction

1.1 Catalysis – the Historical Perspective

The deliberate use of catalysis has been accompanying the development of civilizations throughout the history, since the first intentional employment of the fermentation process for alcohol production [1] or bread making. But the scientific understanding of how catalytic reactions proceed came much, much later. In particular, when it comes to fermentation, the deeper comprehension is owed to Louis Pasteur, who was one of the first scientists to start the investigation, and Eduard Buchner, who presented a study on cell-free fermentation in 1897 [2]. Buchner was awarded the Nobel Prize for this contribution to chemistry twenty years later.

The outstanding advancements in the field of catalysis are due to the extensive and impressive work of scientists, philosophers, engineers and laborers throughout centuries. It is unfortunately impossible to describe all significant theories, experiments and developments. However some of the achievements are summarized in following paragraphs.

One of the first documented records of discussion of catalytic reactions is the work of Elizabeth Fulhame on oxidation-reduction reactions published in 1794 [3]. She observed that many reactions required water to proceed although the water itself was not consumed during the process. She had even proposed one of the first reaction mechanisms, for the wet charcoal combustion she was investigating, suggesting that the water actively participates in the reaction and is regenerated at the end of it [4]. Forty-one years later the term catalysis was for the first time used by Jöns Jacob Berzelius [5]. He managed to gather the existing knowledge on specific chemical reactions reported by other scientists and

formulate a general definition of catalysis. In these specific reactions a presence of a certain substance which exerted a catalytic force was a condition for the chemical transformation to occur, although this specific substance, the catalyst, was not consumed throughout. One of the processes that inspired the concept of catalysis presented by Berzelius was the combustion of hydrogen and gas of olefins in the presence of the platinum wire reported by Humphry Davy [6] while he was working on the safety lamp for miners (the invention he has never patented so that it could be commonly used for saving lives of workers). Another catalytic reaction would be the transformation of ethanol into ether affected by the addition of sulphuric acid investigated by Eilhard Mitscherlich [7]. The first process, the oxidation of the gases on platinum, may serve as a good example of heterogenous catalysis in which two phases are present throughout the reaction occuring at the interface, typically on the surface of the catalyst. The second reaction, acid-catalyzed dehydration of alcohol, is an instance of homogenous catalysis which proceeds in a single phase.

Catalysis was redefined by Wilhelm Ostwald and Paul Sabatier [8], with the former arguing that the role of the catalyst is only to speed up the reaction. His view brought up some resistance as many reactions were never to be observed without a catalyst. Nevertheless the catalyst definition of Ostwald has been commonly accepted as the reactions that do not appear to happen can be treated as having an infinitesimally small rate. The Ostwald's point of view on the catalysis was purely physical, which means that the catalyst did not take part in the reaction itself rather brought the substrates to the conditions in which they could react faster. On the contrary the theory of Sabatier was concerned with the formation of unstable species and intermediates throughout the catalytic process thus indicating an active participance of catalyst in the chemical transformation. Both of the opinions provide an invaluable insight into the field of catalysis even though in the times when physics and chemistry were distinct scientific

disciplines they could seem to be contradictory. The magnificent work of both gentlemen was recognized and Wilhelm Ostwald was awarded the Nobel Prize in 1909 for his contribution to the field of catalysis [9], while Paul Sabatier just three years later got his Nobel Prize for the development of catalyzed direct hydrogenation of organic compounds [10].

Catalytic reactions were not only studied in academia. They became very important for industry even before they drew the attention of the academic community [11]. Around the middle of the eighteenth century the price of sulphuric acid (H_2SO_4) dropped significantly due to the implementation of the *lead chamber process* in which sulphur was burned together with saltpetre (KNO_3) producing the acid. Potassium nitrate acted there clearly as a catalyst, as sulphuric acid was known already by that time not to include any nitrogen or potassium in its chemical formulae. The technical aspects of the process were improved along the way, mostly based on the trial and error approach. For example it was shown by Charles Bernard Desormes and Nicolas Clément that a continuous flow of air may reduce the amount of catalyst needed. It proved that the prime reaction was the recombination of sulphur dioxide with oxygen while small amounts of saltpetre were there just to speed up the process. Catalyst recovery was a serious problem of the sulphuric acid production, hence later on the combination of propositions of Joseph Louis Gay-Lussac for catalyst recovery and of John Glover for the incorporation of recycling tower were slowly accepted and incorporated in the manufacture design. During the 19th century a new *contact process* for the sulphuric acid production was being developed, which is a main industrial process used in modern times. Nowadays however the expensive platinum catalyst has been replaced by vanadium pentoxide [12].

Soon it was realized that catalysis could be an answer to certain problems faced by developing societies. For example a pull for the research on synthesis of ammonia (NH_3) was provided by

the increasingly faster growth of population that needed to be fed. It was already known that ammonia fertilizers would be invaluable for plant growth. Primarily however nitrogenous substances were used for the production of explosives. The scientists, including Wilhelm Ostwald, William Crooks, Fritz Haber and last but not least Walther Nernst were trying to implement a process that would enable the production of ammonia [13]. Still it was not until 1913 that the production on industrial scale would be possible, when the first ammonia producing plant started to operate in Oppau, employing the Bosch-Haber process. The large-scale synthesis of ammonia from nitrogen and hydrogen ($N_2 + 3H_2 \rightarrow 2NH_3$) would not have been possible if certain technological breakthroughs had not been in place. Firstly Alwin Mittasch discovered a much cheaper catalyst based on iron that is still being used nowadays. Secondly technologically advanced equipment withstanding high pressures had to be designed. And last but not least the process needed a reliable source of molecular hydrogen, which was supplied from synthesis gas (a mixture of hydrogen, carbon monoxide and/or carbon dioxide). Indeed, the production of synthesis gas in BASF company created much more opportunities for synthetic chemistry.

Around the same time as industrial ammonia production got under way, the prospect of creating fuel from synthesis gas started to be investigated as well. In 1913 Mittasch and Schneider discovered that a mixture of hydrogen and carbon monoxide (in excess) may be converted to liquid hydrocarbons in the presence of metal catalyst. Soon after, inspired by this notice, Franz Fischer and Hans Tropsch started to work on this process at the Kaiser Wilhelm Institute at Mulheim-Ruhr. After years of investigation of catalysts and optimization of reaction condition the first plant was built in 1936 to produce synthetic petrol called *Synthol* in Fischer-Tropsch process [14].

After World War II catalysis has expanded even more. It is nowadays employed in the production of polymers, detergents,

pesticides, pharmaceuticals, dyes, flavours and fragrance chemicals. As a matter of fact it is accepted that the production of 90% of chemical commodities involves catalysis in their manufacture [15]. Although industrial production of bulk chemicals is very efficient and well-established still there is place for improvement in some areas. Firstly there is an urge of transition to new feedstock as the supplies of petroleum are shrinking. Secondly the market for fine chemicals (medical drugs, speciality advanced polymers etc.) is growing [16]. Many innovations tailored for specific purposes appear in the field of catalysis. At the same time more and more stress is put on the environmental impact of the chemical large-scale processes [17]. Accurate laboratory small-scale experiments together with the development of computational modelling techniques assist the design of novel catalysts.

1.2 Catalysis – Definitions and Concepts

A catalyst may be defined as a substance which alters the pathway of a chemical reaction in such a way that the rate of the reaction increases [18]. It has no effect on the standard Gibbs free energy change (ΔG^{θ}) of the transformation, however it acts on the effective energy of activation (E_a) of the process. In other words it brings down the energy barrier that has to be overcome for the chemical transformation to occur. The reaction mechanism of a catalyzed process may be quite complicated, consisting of many elementary steps and intermediate species. Schematic energy profiles for an uncatalyzed and a catalyzed reaction are presented in Figure 1.1. A catalyst is regenerated at the end of a process and it may continue to operate and catalyse another cycle of the reaction. That is why the catalyst may be used in smaller amounts compared to the substrates which makes it very advantageous, especially if it is an expensive material.

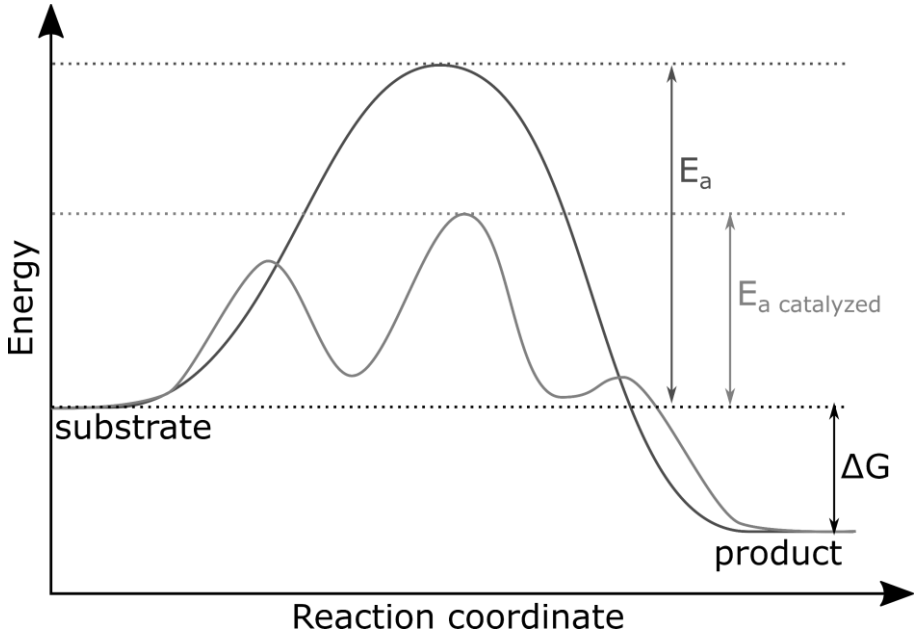

Figure 1.1 *Modus operandi* of a catalyst: schematic energy profiles of the uncatalyzed and the catalyzed reaction.

There are a number of properties of a catalyst that are used to evaluate its usefulness [19]. The catalytic *activity* informs of the speed of the reaction. It can be described in terms of the turnover number (TON) which measures the total number of product molecules produced by each catalyst molecule (or active site for heterogenous catalyst)

$$TON = \frac{moles\ of\ product\ formed}{moles\ of\ catalyst} \tag{1.1}$$

or in terms of the turnover frequency (TOF)

$$TOF = \frac{moles\ of\ product\ formed}{moles\ of\ catalyst\ \times time}\left[\frac{1}{s}\right] \tag{1.2}$$

which measures the number of product molecules per catalyst molecule (or site) and per unit time, which could be seconds or hours [20]. From the economic point of view the *conversion* of substrates to products is pivotal. It is defined as the ratio of the number of the substrate molecules converted into product S_C and

the initial number of the substrate molecules present at the beginning of the reaction S_0.

$$conversion = \frac{S_C}{S_0} \tag{1.3}$$

While high conversion is desirable, if the unconverted substrate can be recycled and fed to the reactor again the costs may be reduced even with low conversion. Another important factor is the *selectivity* towards the desired product represented by the number of moles of the substrate that produced the specific product S_P per number of moles of the converted substrate S_C.

$$selectivity = \frac{S_P}{S_C} \tag{1.4}$$

Not only does formation of side-products lead to a waste of part of the substrate, but also the mixture of main product and by-products may have to be separated which introduces another complication in the manufacture. The *yield* of the reaction is its *conversion* times *selectivity*. It measures the number of moles transformed into the certain product S_P compared to the initial number of moles of the substrate S_0.

$$yield = \frac{S_C}{S_0} \cdot \frac{S_P}{S_C} = \frac{S_P}{S_0} \tag{1.5}$$

Conversion, *selectivity* and *yield* can be conveniently measured in percent. The *stability* and the *strength* of the catalyst assess its resistance to the destructive factors throughout the operation period in the reactor. Thus the operating conditions of the process are in general monitored continuously to prevent unnecessary damage to the catalyst. Overheating, poisons, deposition of dust or coke on the catalyst are some of the factors leading to the drop of the initial *activity* and *yield* of the process [21].

Nowadays not only the economics of the process but also environmental safety aspects play a role in choosing a catalyst. The ones operating under milder pressure and temperature are

preferred due to smaller operational costs and energy demand. The emission of greenhouse gases and the side-production of hazardous substances may be a problem too. The necessity of development of sustainable, environmentally friendly chemical processes has been recognized [22]. The improvements can be done on many levels, from the search of new molecules employed in catalytic reaction through the development of heterogenous catalyst support to the optimization of the equipment and the operating conditions in manufacturing plants. Even the basic science providing fundamental understanding of the electronic structure of chemical species proved to be a useful tool in the field and the computational catalyst design may support the endeavours of creating sustainable chemical industry [23].

1.3 Computational Chemistry Methods

The prime concern of computational chemistry is to study molecular interactions *in silico* employing the developed methodologies. A most general classification would encompass static and dynamic methods for studying chemical phenomena. For studying chemical reactions the focus of the static treatment is on the 3N dimensional configuration space (N is the number of atoms), describing only the position of each atom. Time is left out of the picture. On the other hand dynamical methods are used for investigation of 6N-dimensional phase space, which accounts additionally for the three momentum coordinates. This means that the time evolution of a system is treated explicitly and followed during the simulation. *Ab initio*, density functional theory, semi-empirical, molecular mechanics belong to the first category of methods while molecular dynamics and Monte Carlo methods belong to the second category. Each of them has its own limitations, approximations, pros and cons therefore depending on the studied system one should choose wisely which methodology ought to be applied.

Computational chemistry provides information on many properties of the system, like the geometry of the molecule in its minimum-energy configuration, the vibrational frequencies, the charge distribution exhibited by the molecule, and energies of short-living species like transition states. When applied to the study of chemical reactions computational chemistry is used mainly to explore the potential energy surface of the reaction. This is a map in which the energy of the system is a function of reactants' geometries. It is used to guide chemists towards the most probable reaction mechanism. When the map is precise enough it may be used to predict the bottlenecks of a chemical transformation and ultimately the rates at which the products are formed.

1.3.1 *Ab initio* Methods

The purpose of *ab initio* methods is to solve as well as it is feasible the Schrödinger equation

$$\boldsymbol{H}\Psi = \varepsilon\Psi \tag{1.6}$$

where $\boldsymbol{H}$ is the Hamiltonian operator, Ψ is the wavefunction (a mathematical construct describing the quantum system) and ε is the total value of the energy. The total molecular Hamiltonian of a many-body system composed of electrons *e* and nuclei *n* contains the kinetic *T* and potential *V* energy terms.

$$\boldsymbol{H} = \boldsymbol{T}_e + \boldsymbol{V}_{ee} + \boldsymbol{V}_{ne} + \boldsymbol{T}_n + \boldsymbol{V}_{nn} \tag{1.7}$$

The operator for the kinetic energy of electrons is given by the expression below

$$\boldsymbol{T}_e = -\sum_{i=1}^{N} \frac{\nabla_i^2}{2} \tag{1.8}$$

The operator corresponding to the potential energy of the repulsive Coulomb forces acting between electrons is represented by the following term:

$$\boldsymbol{V}_{ee} = \sum_{i>j}^{N} \frac{1}{|\boldsymbol{r}_i - \boldsymbol{r}_j|} \tag{1.9}$$

The attractive Coulomb interactions between nuclei and electrons are written as the following operator:

$$\boldsymbol{V}_{ne} = -\sum_{i=1}^{N}\sum_{A=1}^{M} \frac{Z_A}{|\boldsymbol{r}_i - \boldsymbol{R}_A|} \tag{1.10}$$

The operator for the kinetic energy of nuclei is given as

$$\boldsymbol{T}_n = -\sum_{A=1}^{M} \frac{\nabla_A^2}{2m_A} \tag{1.11}$$

Finally, the contribution from the potential energy of nuclei is written as the operator:

$$\boldsymbol{V}_{nn} = \sum_{A>B}^{M} \frac{Z_A Z_B}{|\boldsymbol{R}_A - \boldsymbol{R}_B|} \tag{1.12}$$

In the above equations ∇^2 is the Laplacian operator, Z_A and Z_B are the atomic numbers of nuclei A and B respectively while $\boldsymbol{R}_A$ and $\boldsymbol{R}_B$ are their corresponding positions, m_A is the ratio of masses of the nucleus A and an electron, $\boldsymbol{r}_i$ and $\boldsymbol{r}_j$ are the positions of the i-th and j-th electrons respectively, atomic units are used throughout (q_e = m_e = $\bar{h}$ = c = 1) [24]. Unfortunately, even though the mathematical expression describing the chemical system is known it is too complicated to be solved analytically for any atom or molecule unless it is hydrogen or a hydrogen-like atom.

However incisive theories and algorithms together with the extending power of computational resources make it possible to estimate the solution of the Schrödinger equation, with various errors, depending on the level of theory, algorithm used and computing time applied to tackle a specific problem. There are basically three approximations that significantly simplify the calculations of molecular energies. These are the Born-

Oppenheimer (BO), Hartree-Fock (HF) and linear combination of atomic orbitals (LCAO) approximations.

The Born-Oppenheimer approximation is based on the fact that usually the big nuclei move much slower than the small electrons. Therefore the nuclei can be treated as fixed in space, so that the $\boldsymbol{T}_n$ term becomes zero. Moreover the movement of the nuclei may be decoupled from the movement of the electrons so that $\boldsymbol{V}_{nn}$ is a constant value added after the electronic energy is found. In this way the nuclei are treated classically because of fixing them in space-time domain. When the BO approximation is valid and the electronic and nuclear wavefunctions can be decoupled the calculations may be limited to solving only the electronic Schrödinger equation

$$\boldsymbol{H}_{\boldsymbol{el}}\Psi_{el} = \varepsilon_{el}\Psi_{el} \tag{1.13}$$

$$\boldsymbol{H}_{\boldsymbol{el}} = \boldsymbol{T}_e + \boldsymbol{V}_{ee} + \boldsymbol{V}_{ne} \tag{1.14}$$

$$\varepsilon = \varepsilon_{el} + V_{nn} \tag{1.15}$$

The BO approximation fails for example when two electronic states are not separated enough and the intersystem crossing may occur or when tunnelling effects become important [25]

According to the HF approximation the many-electron wave function Ψ is a product of one-electron wave functions ψ (spinorbitals – the product of spatial wave functions – orbitals and the spin function: α or β) that satisfies the Pauli exclusion principle. Such an antisymmetrized product for a system of N electrons is called a Slater determinant [26]:

$$\Psi_{HF} = \frac{1}{\sqrt{N!}}\begin{vmatrix} \psi_1(1) & \cdots & \psi_1(N) \\ \vdots & \ddots & \vdots \\ \psi_N(1) & \cdots & \psi_N(N) \end{vmatrix} \tag{1.16}$$

In the LCAO approximation an orbital of a molecule, as the name suggests, can be approximated as a linear combination of atomic orbitals (AOs). Atomic orbitals are also referred to as basis functions φ which can be any mathematical construct that is easy

to handle by the computer program calculating the linear combination. Usually the suitable functions are Slater-type orbitals (STOs) or Gaussian-type orbitals (GTOs). The more basis functions there are to approximate the shape of an orbital the more accurately a molecular orbital (MO) can be described. A set of functions used to represent the orbital is called a basis set $\{\varphi_S\}$ which serves to create an orbital occupied by the i-th electron ψ_i:

$$\psi_i = \sum_{s=1}^{m} c_{si}\varphi_s \tag{1.17}$$

By varying the c_{si} coefficients the best single determinant which minimizes the energy of the system can be found as according to variational principle the real ground state energy is equal or lower than the approximated Hartree-Fock energy:

$$E_{ground} \leq E_{HF} = \langle \Psi_{HF} | \boldsymbol{H} | \Psi_{HF} \rangle \tag{1.18}$$

There are constraints imposed on the possible variations of c_{si}. Firstly the orbitals have to be orthogonal and secondly their associated electron-density function must be normalized to the number of electrons.

For closed-shell systems (singlets) it is generally recommended to pose restrictions on MOs and force two electrons of opposite α and β spins to occupy the same spatial orbital. This approach is called Restricted Hartree-Fock (RHF) method. While dealing with open-shell systems (doublets, singlet diradicals, triplets etc.) one or more electrons are unpaired. Then the choice has to be made whether to pose the double occupancy restrictions for paired electrons, while leaving the unpaired electrons to occupy separate orbitals or to treat all α and β MOs separately allowing all of them to adopt different shapes and energies resulting in treatment of all orbitals as singly occupied. The first approach is called Restricted Open-shell Hartree-Fock (ROHF) while the latter is known as Unrestricted Hartree-Fock (UHF). Typically the UHF treatment gives a better description of energies of open-shell

systems yielding equal or lower energies compared to ROHF. For example in a doublet state the interactions between the unpaired α electron and α or β electrons would be different resulting in different MOs for the opposite spin electrons and same-spin electrons. This effect could not be taken into account if α electron interacts with a doubly occupied orbital in a restricted treatment. However the UHF wave function suffers from spin contamination which means that it contains the contributions from higher-lying states. The graphical representation of RHF, ROHF and UHF orbitals is shown in Figure 1.2 [27]

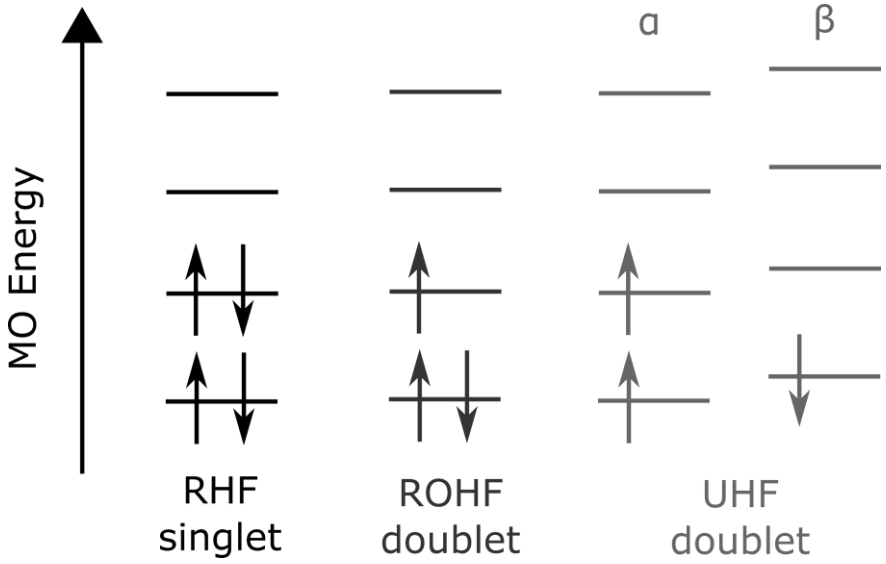

Figure 1.2 Orbital energies in RHF singlet, ROHF doublet and UHF doublet states.

The Hartree-Fock method although quite sophisticated already, does not take into account the electron correlation phenomenon. This simplifies the solution and speeds up the calculations however the electron-electron interactions are treated wrongly. For long-range correlations (non-dynamical) a single Slater determinant is not enough to describe correctly the wave function of the system. The multireference approach can account for that. On the other hand the incorrect treatment of short-range (dynamical) correlations is due to the fact that in HF method an

electron interacts with the mean electron cloud composed of all other electrons rather than interacting with each other electron separately, the latter approach being the correct one. In the methods that tackle this problem a single-reference wave function is expanded. All the approaches dealing with the imperfections of HF solution are called post-Hartree-Fock approaches. The theories dealing predominantly with the dynamical correlation are Møller–Plesset perturbation theory (MP2, MP3, MP4), configuration interaction (e.g. CIS, CISD, Full CI) and coupled-cluster methods (e.g. CCD, CCSD, CCSD(T), CCSDT).

In this PhD project a coupled cluster (CC) method was used to yield better energies of the studied systems. The CC approach borrows some concepts from both perturbation and configuration interaction theories [28]. The CC exact wave function based on the HF ground-state Slater determinant is given as

$$\Psi_{CC} = e^{\boldsymbol{T}} \Psi_{HF} \tag{1.19}$$

where $e^{\boldsymbol{T}}$ can be written as a power series expansion of the cluster operator $\boldsymbol{T}$:

$$e^{\boldsymbol{T}} = 1 + \boldsymbol{T} + \frac{1}{2!}\boldsymbol{T}^2 + \frac{1}{3!}\boldsymbol{T^3} + \ \ldots = \sum_{k=0}^{\infty} \frac{1}{k!}\boldsymbol{T}^k \tag{1.20}$$

The operator $\boldsymbol{T}$ is a sum of single, double, triple and so on excitation operators

$$\boldsymbol{T} = \boldsymbol{T}_1 + \boldsymbol{T}_2 + \boldsymbol{T}_3 + \ \ldots + \boldsymbol{T}_N = \sum_{i=1}^{N} \boldsymbol{T}_i \tag{1.21}$$

Upon acting on HF wave function with this operator, excited determinants are generated by promoting one, two, three and so on electrons from all of the possible occupied orbitals to all possible non-occupied orbitals (Figure 1.3) [29].

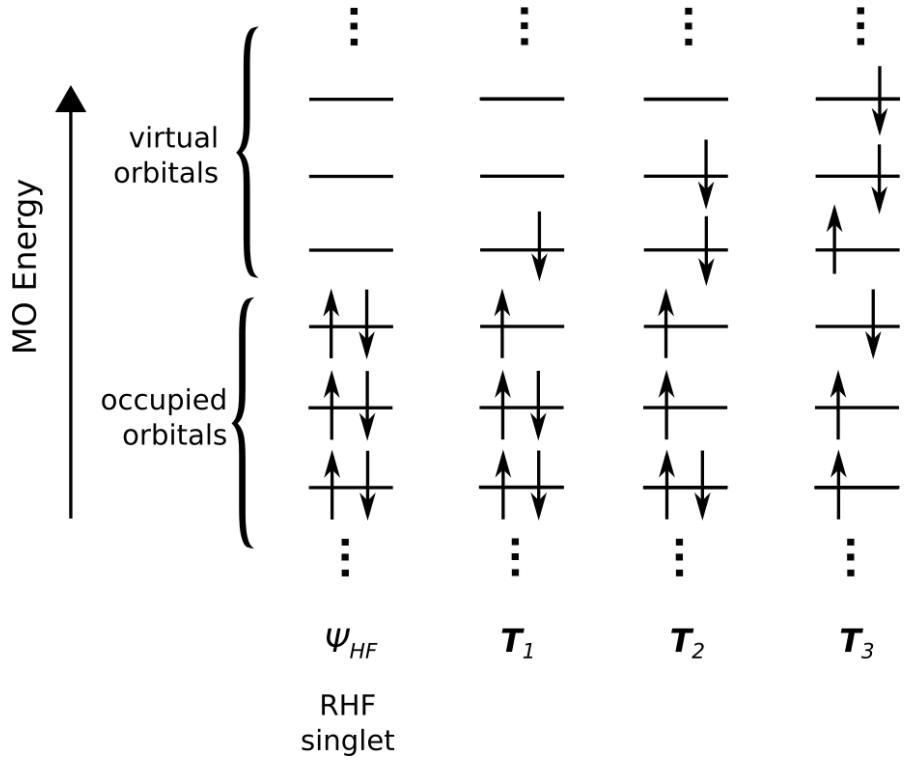

Figure 1.3 Examples of excitations generated by T_1, T_2 and T_3 operators from the RHF wave function.

It has been shown that the biggest contribution to the correlation energy is due to the interaction of the pairs of electrons. For this reason $\boldsymbol{T}$ operator may be truncated and only approximated by $\boldsymbol{T}_2$ operator (generating all doubly excited Slater determinants) giving the coupled cluster doubles (CCD) method.

$$\Psi_{CCD} = e^{\boldsymbol{T}_2}\Psi_{HF} = \left(1 + T_2 + \frac{T_2^2}{2!} + \frac{T_2^3}{3!} + \ldots\right)\Psi_{HF} \qquad (1.22)$$

The inclusion of single excitations on top of doubles ($\boldsymbol{T} = \boldsymbol{T}_1 + \boldsymbol{T}_2$) does not improve the yielded energies significantly however it is only slightly more computationally demanding. This is why coupled cluster singles and doubles (CCSD) is more often used than CCD. The method scales as M^6, where M is the number of basis functions. The next level, coupled cluster singles and doubles and triples (CCSDT), scales already as M^8, which makes the calculations

substantially slower. The examples of single, double and triple excitations are depicted in Figure 1.3. Thus often the triple excitations are included in a perturbative way leading to coupled cluster singles and doubles with perturbative triples (CCSD(T)), scaling as M^7 [30]. The last method became so successful that it is frequently called a *gold standard* for single-reference *ab initio* calculations. Other computational chemistry methods are often benchmarked against the CCSD(T) results.

If the exponential operator is truncated, the CC method remains size consistent which means that the calculated energy of infinitely separated moieties is equal to the sum of the energies calculated for each moiety individually. However it is not variationally bounded, which means that in principle the CC method may provide energies that are lower than the exact energy for the system. That however is not likely to happen due to the limited number of functions in a basis set.

The steep scaling of the CCSD(T) method implies that it may be often too expensive to calculate the energies of larger molecules, especially if one would like to use a decent-size basis set for expansion of the molecular orbitals. Treating the system with small basis set results in the basis set truncation error. The explicitly correlated CCSD(T)-F12 method partially passes around this problem. In this procedure an additional (small) auxiliary basis set based on two-particle functions is used to describe properly the interaction in a pair of electrons. Inclusion of these F12 geminals together with some other simplifications permits to conduct calculations of higher accuracy more efficiently [31]. For example the standard CCSD(T) method using some medium-sized basis set leads to root mean square errors for more than one hundred reaction energies of 7 kJ mol^{-1} and 19 kJ mol^{-1} for closed-shell and open-shell reactions respectively, while the CCSD(T)-F12 energy calculations with a similar size basis set were characterized by a root mean square error of only 1 kJ mol^{-1} for both reaction types, as compared to the complete basis set limit [32].

The main advantage of the family of *ab initio* methods is that they converge systematically to the exact solutions upon reduction of approximations and enlargement of the basis set. However still their application is limited to quite small systems (typically tens or maybe hundreds of atoms) and the more accurate level of theory the smaller the system that can be treated. Only relatively small systems composed of tens of atoms can be subjected to CC calculations, except for local correlation methods that try to overcome the problem of high scaling with system's size by utilizing localized forms of molecular orbitals. A modified Pople diagram [33], presenting a concept that the calculated energies tend to be closer to the exact solution with the level of electron correlation included and the size of basis set, is illustrated in Figure 1.4.

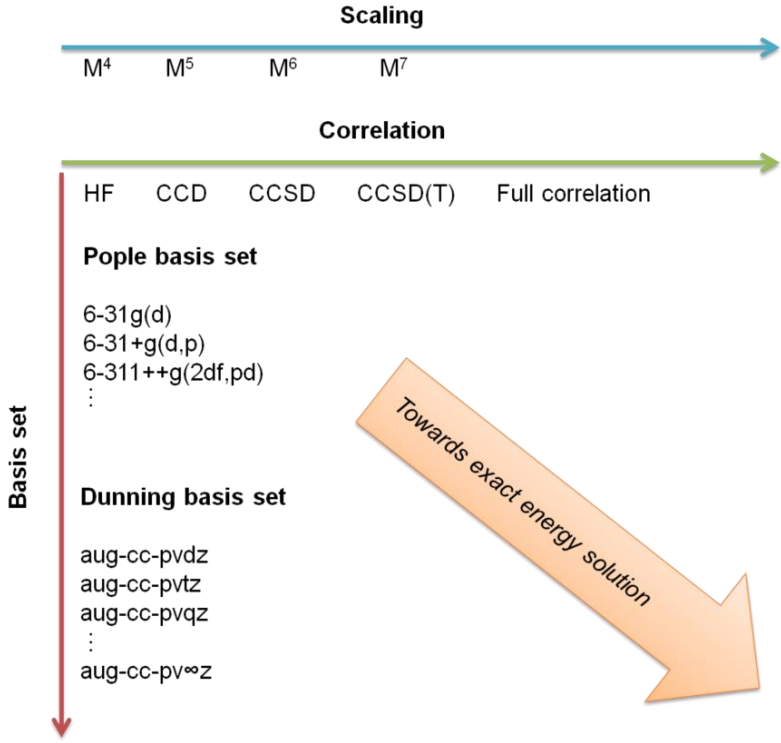

Figure 1.4 Systemic convergence of a single reference wave function energy to the exact solution with the increase of electron correlation inclusion and the number of basis functions.

1.3.2 Density Functional Theory

The fundamental idea of density functional theory (DFT) is that all properties of the ground state of a system containing electrons can be described by its electron density [34]. The validity of this concept was demonstrated by Pierre Hohenberg and Walter Kohn in 1964.

$$\rho_0(x, y, z) \rightarrow \varepsilon_0 \tag{1.23}$$

They proved that in order to elucidate the electronic energy one can use only a functional F of the electron density function ρ_0 depending on three coordinates x, y and z instead of a wave function of 4N variables (three spatial coordinates and one spin for each electron, where N is the number of all electrons). The equation below represents this first Hohenberg-Kohn theorem.

$$\varepsilon_0 = F(\rho_0) = E[\rho_0] \tag{1.24}$$

The proof established that a functional $F(\rho_0)$ exists but its form remained unknown. The second theory of Hohenberg and Kohn provided some practical information for solving Equation 1.24. It implies that when dealing with the electronic ground state of the system, the energy calculated using any trial electronic density will be higher or equal (only if the exact functional is used) to the true ground state energy. This means that the energy is variational just like in HF method. Thus it can be calculated using iterative procedures in a manner similar to the ones used in wave function methods.

The DFT approach was not used in computational chemistry until the implementation of Kohn-Sham equations took place which made DFT practical for describing molecules. Their idea was that the system can be described by non-interacting electrons. Because of that the terms used for energy calculations could be split into the terms that can be calculated exactly which give information about the majority of the energy of a system and a small term requiring the unrevealed exchange-correlation energy

functional E_{xc} [35]. The electronic energy within BO approximation is given as

$$E_{DFT} = T_S[\rho] + E_{ne}[\rho] + J[\rho] + E_{xc}[\rho] \qquad (1.25)$$

where $T_S[\rho]$ is the approximate kinetic energy of the electrons (calculated based on the non-interacting system), $E_{ne}[\rho]$ is the attraction energy acting between nuclei and electrons, $J[\rho]$ is the classical repulsion energy acting between the electrons. $E_{ne}[\rho]$ and $J[\rho]$ can be calculated exactly. Kohn and Sham have shown that single Slater determinant of Kohn-Sham (KS) orbitals may accurately approximate $T[\rho]$ in the form of $T_S[\rho]$. KS orbitals are calculated in a similar manner to MOs in the HF method. Even the same basis functions are employed. Because of the reintroduction of the orbitals the scaling of DFT methods deteriorates compared to what it might possible be if only the electron density was used. Depending on the exact functional form used for E_{xc}, it scales in roughly the same way as the HF method while giving most often much better results. Still the exchange-correlation $E_{xc}[\rho]$ remains elusive. The main purpose of the research in the field of chemically applied DFT is to design the functional that correctly describes the relationship between the electron density and the energy of a system.

Up to date a great number of exchange-correlation functionals have been developed [36]. Two main pathways in their development have been followed: non-empirical and semi-empirical, for which the respective contributions of John Perdew and Axel Becke should be acknowledged. Also Stefan Grimme ought to be praised for the development of the empirical dispersion that accurately describes *van der Waals* forces [37]. In order to somehow categorize non-empirical functionals John Perdew proposed a concept known as the DFT Jacob's Ladder [38] (Figure 1.5) to express the increasing sophistication of E_{xc}.

The main problem of DFT is that the solution cannot be systematically improved like in the case of wave function methods. Nonetheless DFT methods have been immensely successful in the

field of computational chemistry, transition metal chemistry especially, because of their often nearly-right results, cancellation of error for the relative energies and fast convergence to the solution enabling the treatment of the bigger systems. The mean average error of relative reaction energies calculated with DFT methods may vary from around 10 kJ mol^{-1} to 30 kJ mol^{-1} depending on the functional used [39]. However for each system under study the errors can differ. For this reason it is often advisable to benchmark the yielded energies against experimental or high-level *ab initio* calculation results.

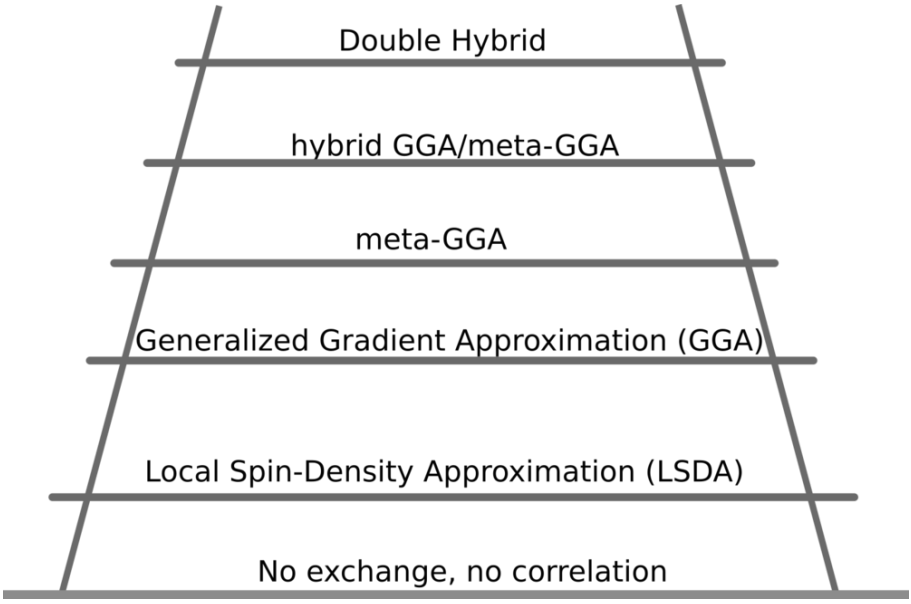

Figure 1.5 The DFT Jacob's Ladder arranging the exchange-correlation functionals from most simple (down) to most sophisticated (up).

1.3.3 Potential Energy Surface

Microscopically the chemical reaction is about the reorganization of the atoms forming reacting species. Geometrically reactants differ from intermediates which differ from products. The energy of each geometry may be calculated employing HF, CC, DFT and other methods hence creating

a landscape of potential energies as a function of atomic positions called the potential energy surface (PES). This is a multidimensional surface of 3N variables as for each of the N atoms constituting the system, three Cartesian coordinates *x, y* and *z* are needed [40]. Fortunately computational chemists may focus only on the most relevant parts of the studied PES. These are the stationary points of the function: minima and saddle points. For both of them the first derivative of PES with respect to atomic coordinates is equal to zero. However the matrix of the second derivatives (associated with vibrational frequencies) called the Hessian Matrix has only positive eigenvalues for the minima while for the saddle points one eigenvalue is negative. By following the intrinsic reaction coordinate (IRC) it is possible to locate the two minima connected by the transition state. The IRC is the path of steepest descent leading from a particular TS structure to the two minima that it connects, and can be located by an optimization process initiated from the TS structure and following initially the eigenvector corresponding to the imaginary frequency of the TS [41]. Such a potential energy profile may be an indication of an elementary transformation and a collection of consecutive transformations from reactants to products can represent a reaction pathway. The most plausible reaction mechanism is chosen based on energy differences, the smaller they are the higher is the probability of a reaction to happen, and the experimental data available.

For studying gas reactions under single-collision conditions it may be enough to calculate only potential energy profile of ground state energies. However for reactions in solution in which the energy may be easily dissipated and exchanged with the surrounding molecules a Gibbs free energy surface provides more accurate information about the course of the reaction. Thermochemical values can be computed using the statistical mechanical partition function, by taking into account the contributions from electronic, translational, rotational and

vibrational motion [42]. The free energy surface may be explored as well with dynamic methods, allowing to examine its larger portions and follow the evolution of a system in time. However the treatment of a phase space constituting 6N coordinates (three coordinates for each atom position a three for each atom momentum) may be often too expensive for quantum mechanical calculations.

1.4 Reaction Mechanism and Kinetic Modelling

The mechanism of a chemical process is a sequence of elementary reactions that occur during the chemical transformation. It can be very simple, described by just one step or very complicated, comprising of a number of elementary reactions. One way to extract some information about the mechanism is to monitor the speed of a reaction by measuring the change of the concentration of reacting species in time. This velocity is defined as reaction rate and usually has a unit of mol dm^{-3} s^{-1}. The rate of reactant consumption is given by the equation below

$$r = -\frac{\mathrm{d[reactant]}}{\mathrm{d}t} \tag{1.26}$$

while the rate of product formation is given by the following expression

$$r = \frac{\mathrm{d[product]}}{\mathrm{d}t} \tag{1.27}$$

For a general reaction

$$a\mathrm{A} + b\mathrm{B} + \ \ldots \rightarrow c\mathrm{C} + d\mathrm{D} + \ \ldots \tag{1.28}$$

in which A, B etc. are reactants and C, D etc. are products while a, b, c, d are their corresponding stoichiometric coefficients the rate of reaction is given as

$$r = -\frac{1}{a}\frac{\mathrm{d[A]}}{\mathrm{d}t} = -\frac{1}{b}\frac{\mathrm{d[B]}}{\mathrm{d}t} = \frac{1}{c}\frac{\mathrm{d[C]}}{\mathrm{d}t} = \frac{1}{d}\frac{\mathrm{d[D]}}{\mathrm{d}t} \tag{1.29}$$

By plotting the rate as a function of the concentration of reactants (A, B, etc.) (or of their partial pressures) an experimental rate law may be found for given reaction conditions

$$r = k\,[\mathrm{A}]^{\alpha}[\mathrm{B}]^{\beta} \ldots \qquad (1.30)$$

Such a reaction is of αth order with respect to species A, βth order with respect to species B etc. and the overall order of the reaction is the sum of the exponents, while k is the rate constant, whose units depend on the molecularity of the reaction [43]. For some processes the rate law is a simple function that provides an easy explanation of the reaction mechanism. The rate may be of zeroth order with respect to a substance, which means that the reaction is independent from the substance's concentration. For S_N1 (unimolecular nucleophilic substitution) reactions, first order kinetics is observed, while for S_N2 type (bimolecular nucleophilic substitution) the reaction is of the second order, indicating that two molecules must be brought together to react [44]. However frequently, especially for catalytic reactions, a rate law is a very complicated function of reactants' concentrations and is described by the fractional order with more than one rate constants (that are often pressure and temperature dependent). A complex form of the rate equation suggests a cumbersome multistep reaction mechanism. In such cases a theoretically derived potential energy profile may be very helpful in localizing the bottlenecks and competing reactions of catalytic processes.

1.4.1 Collision Theory

A simple theory that relates the molecular behaviour to the observed reaction rates is collision theory [45]. It assumes, as the name suggests, that for the chemical transformation to happen the atoms or molecules involved need to collide. For example for an elementary bimolecular reaction happening under low concentration conditions in a gas phase between substrates A and B yielding products C:

$$A + B \rightarrow C \tag{1.31}$$

the speed of the reaction is related to the collision frequency given by the expression

$$Z = \sigma \sqrt{\frac{8k_B T}{\pi \mu}} (N_A)^2 [A][B] \tag{1.32}$$

where σ is the collision cross section, k_B is the Boltzmann constant, T is the temperature, μ is the reduced mass, N_A is the Avogadro constant. The theory treats the colliding molecules A and B as hard spheres of radii r_A and r_B respectively used to calculate the collision cross-section area

$$\sigma = \pi(r_A + r_B)^2 \tag{1.33}$$

While their masses m_A and m_B are employed to calculate the reduced mass

$$\mu = \frac{m_A m_B}{m_A + m_B} \tag{1.34}$$

However not all molecules hold sufficient energy to react. Svante Arrhenius proposed that the excess energy possessed by the reacting molecules is the activation energy E_a. He realized that the number of molecules having an energy equal of higher than E_a is given by the Boltzmann distribution. Thus the successful number of collisions Z^* is smaller than the number of all collisions Z

$$Z^* = \sigma \sqrt{\frac{8k_B T}{\pi \mu}} (N_A)^2 [A][B] e^{\frac{-E_a}{RT}} \tag{1.35}$$

where R is the gas constant. According to the collision theory the rate of reaction r is proportional to the number of successful collisions Z^*. For a bimolecular reaction in Equation 1.24

$$r = \frac{Z^*}{N_A} \tag{1.36}$$

Thus the rate constant for this step may be defined as

$$k = \sigma \sqrt{\frac{8k_B T}{\pi\mu}} (N_A) \mathrm{e}^{\frac{-E_a}{RT}} \tag{1.37}$$

and the rate law as

$$r = k\,[\mathrm{A}][\mathrm{B}] \tag{1.38}$$

Still the observed kinetics of many of the studied reactions diverged from the collision theory approach. It was deduced that not only the molecules have to approach each other, but also at a proper orientation. For this reason an empirical *steric factor P* was introduced. Thus in a general Arrhenius equation [46] a pre-exponential factor *A* for the rate constant was introduced

$$k = P\sigma \sqrt{\frac{8k_B T}{\pi\mu}} e^{\frac{-E_a}{RT}} = A e^{\frac{-E_a}{RT}} \tag{1.39}$$

Collision theory explains pretty well the temperature and the concentration dependence of simple bimolecular reactions. The higher the temperature the more energy the colliding reactants possess and the more concentrated they are the smaller the distances they have to travel to get into the vicinity of another molecule. However, collision theory fails to derive theoretically the values of steric factor and activation energy [47].

1.4.2 Transition State Theory

A more sophisticated rate theory was developed almost simultaneously by Henry Eyring and Michael Polanyi and is known as transition state theory (TST) [48]. It treats the molecules as having specific geometries and introduces the probability of the reaction to progress. According to TST the reaction proceeds through an activated complex and Equation 1.31 should be rather written as

$$\mathrm{A} + \mathrm{B} \leftrightarrow \mathrm{AB}^{\ddagger} \rightarrow \mathrm{C} \tag{1.40}$$

The activated complex, also called transition state (TS) is at the centre of the theory, which assumes a quasi-equilibrium between the TS and reactants. The term "quasi" appears because the nature of the "equilibrium" between reactants and TS is obviously very different from that between two sets of stable species. The transition state usually sits on a maximum energy point on a pathway connecting reactants and product. The energy profile of the considered reaction is presented in Figure 1.6.

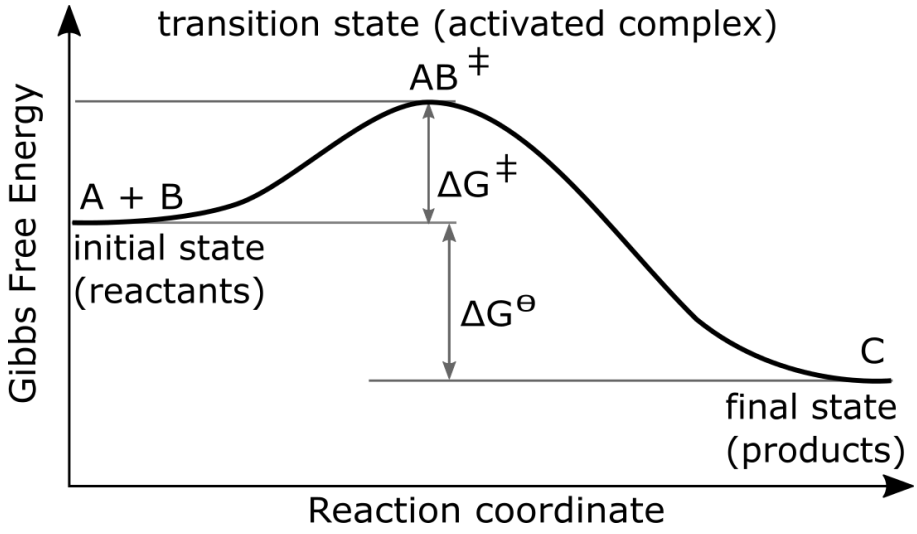

Figure 1.6 The cartoon representation of an energy pathway leading from the reactants A and B through the transition state AB‡ to the product C.

The general equation linking the height of the barrier $\Delta G^{\ddagger}$ and the value of the rate constant is given below.

$$k = \frac{k_B T}{h} e^{-\frac{\Delta G^{\ddagger}}{RT}} \tag{1.41}$$

where k_B is the Boltzmann constant, T is the temperature, h is Planck constant. Here the standard free energy $\Delta G^{\ddagger}$ change between the reactants and the TS is calculated by omitting the contribution of the reaction coordinate to the partition function of the TS. Motion along the reaction coordinate is treated instead indirectly through the pre-factor $k_B T/h$.

For sufficiently long reaction times a canonical system will reach an equilibrium state in which the rates of products and reactants formation are the same. The reversible reaction of the form

$$\mathrm{A} + \mathrm{B} \rightleftharpoons \mathrm{C} \tag{1.42}$$

is characterized by the equilibrium constant K

$$K = \frac{[\mathrm{C}]}{[\mathrm{A}][\mathrm{B}]} = e^{-\frac{\Delta G^{\theta}}{RT}} = \frac{k_f}{k_b} \tag{1.43}$$

where k_f is the forward rate constant given by Equation 1.34 and k_b is the backward rate constant of the reverse reaction.

$$k_b = \frac{k_B T}{h} e^{-\frac{(\Delta G^{\ddagger} + \Delta G^{\theta})}{RT}} \tag{1.44}$$

In a multistep process the reaction rate depends on the rate determining step. It is an elementary reaction characterized by the highest barrier localized on the free energy profile for the specific conditions. Often it can be assumed that the transformations involving smaller barriers are much faster so they do not limit the overall speed of the reaction. The rate constant for a process could be in principle calculated from the difference of the Gibbs free energy of the highest lying saddle point and the Gibbs free energy of the lowest lying minimum. Computationally resolved mechanism of a process may give invaluable information referring to the kinetics. However the accuracy of calculations is pivotal for modelling of the reaction rates, as the rate constants (and the errors) depend exponentially on the Gibbs free energies.

1.4.3 Microkinetic Modelling

In a case of a very complicated process consisting of many elementary steps it can be problematic to localize the rate and selectivity determining steps. Moreover there can be more than one bottleneck of the reaction. Depending on reaction conditions different steps can become more dominant in rate determination.

This is why the experimentally found rate laws can be so complex as different steps play a smaller or larger role throughout the course of the reaction depending on temperature, pressure, reactant concentrations, and solvent effects. The big picture of the reaction is further complicated by competing and side reactions, mixed inhibiting and assisting effect of some reactants etc. Therefore microkinetic modelling [49] gains more and more attention for resolving the reaction rates. In this technique all important elementary steps included in catalytic cycle can be taken into account. For each of them the k_f and k_b has to be specified. The change in concentration or pressure of each species can be calculated by integration of coupled differential rate equations. Thus the time evolution of the values of concentration or partial pressure of reacting or produced substance may be tracked. These changes in time represent the rate of reactant consumption or product formation (Equation 1.21 and 1.22). In this way a detailed kinetics of the process can be specified employing theoretically calculated free energy profile and equations of transition state theory.

However in order to simplify the procedure, microkinetic modelling may be combined with kinetic mechanism reduction [50]. The latter is based most importantly on the quasi steady-state approximation, whereby reaction steps characterized by small free energy barriers can be considered to lead to equilibrium between their reactant and product species much faster than the overall system reaches equilibrium. Thus these rapid steps do not have to be treated explicitly in the model and can be merged with other steps. A second procedure used in kinetic mechanism reduction is that reaction steps that are clearly not at all probable reactions (because they have very high free energy barriers) are omitted as they should not contribute to the final outcome.

1.4 Hydroformylation

1.4.1 Introduction

The process of conversion of alkenes and syngas (a mixture of molecular hydrogen H_2 and carbon monoxide CO) into aldehydes is known as hydroformylation. The reaction was discovered in the German company Ruhrchemie in 1938 by Otto Roelen. Before that he was a part of the team of Fischer and Tropsch investigating the *Synthol* synthesis or Fischer-Tropsch synthesis. Indeed it was while working on the industrial applications of the Fischer-Tropsch process, that he found that oxygen-containing compounds were formed during the plant operation. Insightfully he proposed that these compounds were not produced as intermediates or as a result of a side-reaction of the Fischer-Tropsch process but were yielded through an independent chemical transformation [51]. The originally observed reaction of ethene with syngas, depicted in Scheme 1.1, was called, after the discoverer, the Roelen reaction or the oxo-synthesis (because not only propionaldehyde but also diethylketone was produced) [52]. Later on it appeared that ketones were not formed readily if longer alkenes served as the substrates and the name *hydroformylation* was proposed, which remained the most commonly used term. Moreover it was proved that the catalysis was homogenous. Among all investigated metals firstly cobalt and subsequently rhodium were found to be most applicable for catalyzing the process due to their superior activity.

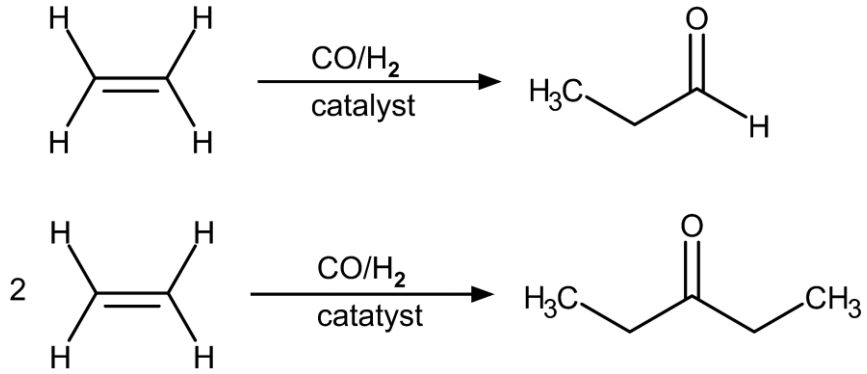

Scheme 1.1 The Roelen reaction producing propionaldehyde and diethylketone from ethylene and syngas. The catalyst used was the heterogenous catalyst for the Fischer-Tropsch process (silica: 66%, cobalt: 30%, thorium oxide: 2%, magnesium oxide: 2%).

If cobalt is used as a catalyst, cobalt carbonyl compounds are formed under the reaction conditions. The active catalyst in the hydroformylation process is cobalt hydrocarbonyl, as was already proposed by Otto Roelen and proved by other studies [53], while dicobalt carbonyl serves as the precursor. Both species are in equilibrium under the oxo-reaction conditions. Additionally, for longer-chain alkenes in which the carbon atoms forming the double bond are non-equivalent, isomers are produced, just like in the case of propene hydroformylation. The cartoon of the aforementioned reaction is depicted in Figure 1.7. Historically there was a clear preference for production of n-butyraldehyde, which after subsequent chemical transformation is used to synthesize plasticizers. Hence the trend has been that industrial development has pursued a route of seeking to develop not only more active but also more n-selective catalysts. Nowadays, however, this trend is no longer quite as strong as hydroformylation may be applied for synthesis of fine chemicals that require a branched aldehyde substrate.

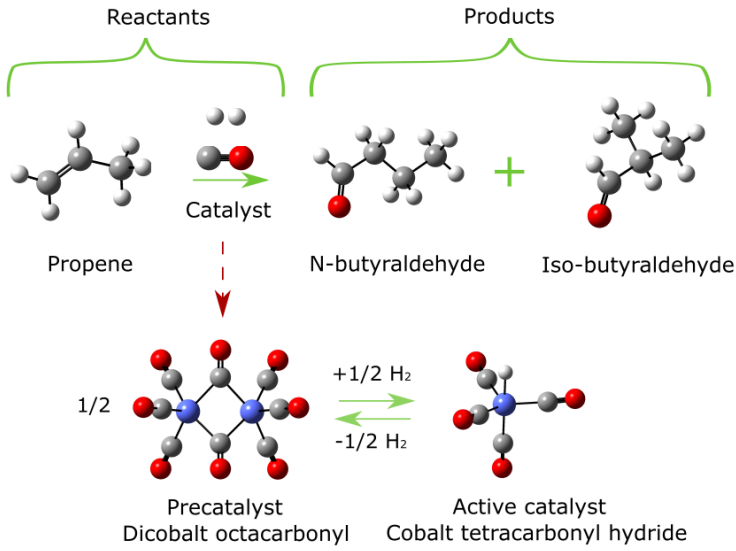

Figure 1.7 Schematic representation of propene hydroformylation catalyzed by unmodified cobalt carbonyl.

1.4.2 Industrial applications

The hydroformylation process transforms cheaper alkenes into higher-value commodities, aldehydes. They can be subsequently hydrogenated to alcohols or serve as substrates for production of amines and esters. A small spectrum of reactions for which an aldehyde is a starting material is presented in Figure 1.8 [54]. Later on a variety of chemical commodities may be produced like detergents, plasticizers and drugs. The annual world production of the oxo-process approached ten million tonnes by 2006 [55]. It is one of the most successful examples of homogenous catalysis.

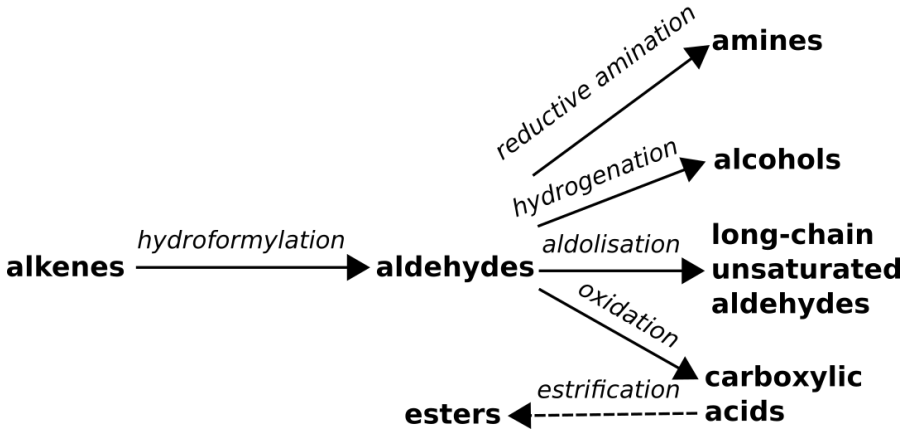

Figure 1.8 Compounds produced as a result of alkene hydroformylation to aldehydes.

The industrial applications matured since the first hydroformylation plant was built. The characteristics of the main operating industrial processes of propene hydroformylation are summarized in Table 1.1.

Table 1.1 Industrial propene hydroformylation processes [56]

Year	**~1950**	**~1960**	**~1974**	**~1984**
Process	*BASF*	*Shell*	*UCC*	*RCH-RP*
Active complex	$HCo(CO)_4$	$HCo(CO)_3(PR_3)$	$HRh(CO)(PPh_3)_3$	$HRh(CO)(TPPTS)_3$
Pressure (bar)	270-300	40-80	15-18	40-60
Temp. (^oC)	120-180	150-190	85-95	110-130
[Catalyst] (%)	0.1-1.0	0.6	0.01-0.1	0.001-0.1
n/iso ratio	80 : 20	88 : 12	92 : 8	95 : 5

The first catalyst to be used commercially was unmodified cobalt catalyst in a high-pressure, high-temperature process implemented in *BASF*. Typically the production of linear butyraldehyde was favoured. A high syngas pressure was required for stabilization of cobalt carbonyl catalysts, while higher

operating temperatures favoured faster conversion of propene. In the *Shell* process phosphine ligands (PR_3) were added in order to stabilize the cobalt catalyst. Because of that the pressure could be reduced to around 100 bar, however the phosphine-modified catalyst favours direct conversion to alcohols. The selectivity towards the linear product was slightly improved. Finally cobalt was replaced by much more active rhodium metal for propene hydroformylation. The process was developed specifically by *Union Carbide Corporation* (*UCC*) and the major advantage was the operation at pretty low pressures. Again, the n/iso ratio was improved although small amounts of propane were produced through unwanted hydrogenation of propene. The last *Ruhrchemie/Rhône-Polulenc* (*RCH/RP*) process referred here employed triphenylphosphine trisulphonic ligands that enable the catalyst to stay in aqueous phase which could be continuously recycled. The two rhodium-based processes are restricted to hydroformylation of short-chain hydrocarbons and cobalt catalyzed hydroformylation is still used [56]. The lower price and the lower toxicity of cobalt are also advantageous when compared to rhodium. Thus both industrial and scientific investigations are being continued in the field of cobalt-catalyzed hydroformylation.

1.4.3 Reaction Mechanism

The mechanism of hydroformylation has been the subject of extensive studies [52] so that the elementary steps involved in the catalyzed alkene transformation could be postulated. Nowadays it is commonly accepted that under oxo-conditions the main reaction pathway follows the mechanism proposed by Heck and Breslow [57]. Cobalt can be fed to the reactor either as the pure metal or in various other forms to subsequently yield cobalt carbonyls.

Dicobalt octarbonyl, $Co_2(CO)_8$, is usually used as a precatalyst in cobalt-catalyzed hydroformylation. The experimental studies brought evidence that there are at least three distinct stable isomers of $Co_2(CO)_8$ [58] of C2v, D3h and D2h symmetries, and this

has also been confirmed by theoretical calculations [59]. The geometries of these structures are presented in Figure 1.9.

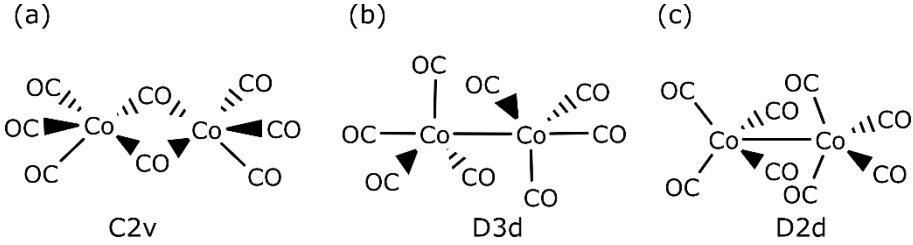

Figure 1.9 Dicobalt octacarbonyl isomers.

The most electronically stable isomer is the one of C2v geometry, and is characterized by two bridging CO ligands and a lack of direct Co-Co bond [60]. We here adopt the description in terms of the MLX approach of Green [61]. In order to draw correctly the Lewis structure of this species in such a way that it satisfies the 18-electron rule, it was proposed to treat one bridging CO ligand as μ-L ligand that contributes two electrons to the first cobalt centre and also two electrons to the second cobalt centre (thereby forming a three-centre two-electron bond) while the other bridging CO ligand should be treated as μ-X_2 ligand contributing one electron to the bond with first cobalt atom and another electron to the bond with second cobalt atom. The remaining six carbonyl ligands are considered to behave as 'normal' 2-electron ligands L (Figure 1.10).

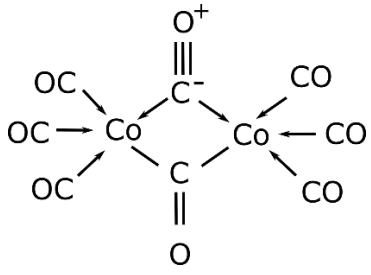

Figure 1.10 Bonding structure of $Co_2(CO)_8$. The 18-electron rule for the metal center is preserved (ML_4X). Cobalt is at the first oxidation state.

The first very important step of the hydroformylation process is the hydrogenation of dicobalt octacarbonyl producing the active catalyst – cobalt tetracarbonyl hydride

$$Co_2(CO)_8 + H_2 \leftrightarrows 2\,HCo(CO)_4 \qquad (1.45)$$

The thermochemical parameters of the reaction have been identified experimentally by independent studies giving similar results for three of them (Table 1.2). Both cobalt species are considered to interconvert fairly rapidly.

Table 1.2 Experimentally obtained enthalpies and entropies of dicobalt octacarbonyl hydrogenation.

Authors [62]	Medium	ΔH [kcal mol^{-1}]	ΔS [cal mol^{-1} K^{-1}]
Ungvary, 1972	n-heptane	4.3	-2.6
Rathke et al., 1992	Supercritical CO_2	4.0	-4.2
Tannenbaum et al., 1998	n-hexane	4.1	-3.1

Presented values are for the mixed standard state of 1 M for solutes and 1 atm for H_2

The second major step is the incorporation of alkene into metal centre. The reaction could occur following an S_N2-like concerted displacement mechanism. However, the associative substitution of carbonyl ligand with ethene seems to be less plausible than a dissociative S_N1 pathway due to the well-known inhibition of the speed of hydroformylation by CO pressure. Thus, the dissociation of one carbonyl ligand yields an unsaturated intermediate cobalt $HCoCO_3$ complex which in a second step accommodates the olefin forming the π-complex with the alkene. In the following steps alkene is inserted into hydrogen-cobalt bond forming an unsaturated alkyl-cobalt complex, which can accommodate a carbon monoxide to fulfil the 18-electron rule. The alkene insertion step is quite important in the context of isomerisation because here hydrogen can be transferred to one of the non-equivalent carbons forming the C=C bond yielding afterwards different isomers of the aldehyde. To continue with the reaction mechanism the alkyl cobalt complex undergoes the

migratory insertion of carbon monoxide into Co-alkyl bond becoming an acyl cobalt complex. The formed unsaturated acyl cobalt species may add CO (forming a saturated acylcobalt carbonyl species, which can reversibly lose the CO ligand) or H_2 at the cobalt centre. In the case of dihydrogen addition, and after oxidative addition and reductive elimination of H and the acyl group, the aldehyde is formed and catalyst regenerated. The corresponding catalytic cycle for propene hydroformylation by unmodified cobalt catalyst is depicted in Scheme 1.2. Some of species involved in hydroformylation have been detected experimentally using high pressure infrared and ultraviolet spectroscopy [63]. These and the non-detectable species have been as well the subject of extensive theoretical studies [64] in which the geometries and bonding patterns of intermediates and transition states as well as the analysis of the elementary steps of the catalytic cycle have been presented.

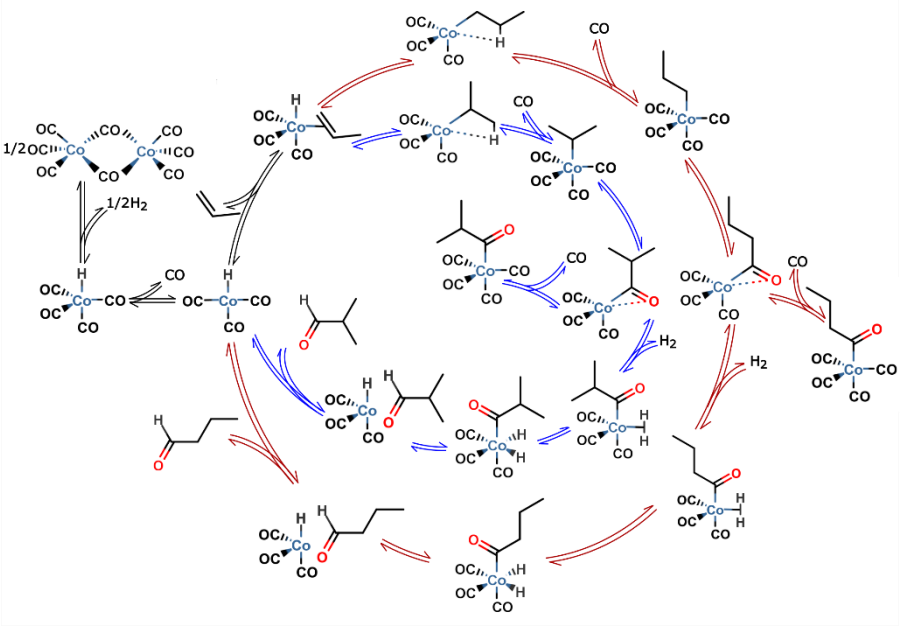

Scheme 1.2 Catalytic cycle of propene hydroformylation. The red cycle is leading to the formation of linear n-butyraldehyde, while a blue cycle to branched iso-butyraldehyde.

However the mechanism postulated in the article by Heck and Breslow [57] did not exclude the possibility that the source of hydrogen in the final step of hydroformylation is the catalyst $HCo(CO)_4$ yielding the aldehyde and cobalt heptacarbonyl hydride In fact it could be also possible that the saturated acylcobalt tetracarbonyl reacts with hydrogen or catalyst to produce the aldehyde although it is stated in the paper that an inhibiting effect of CO pressure was observed for the reduction of acylcobalt carbonyl to aldehyde. These results were confirmed by yet another study where the formation of linear and branched butyraldehydes directly from butyrylcobalt tetracarbonyls by either H_2 or $HCo(CO)_4$ cleavage was investigated [65]. The proposed mechanism of the investigated reactions is presented in Scheme 1.3. It was reported there that an increase of the CO pressure resulted in the decrease of the rates off products formation. Moreover, it was concluded that the reaction with cobalt tetracarbonyl hydride, $HCo(CO)_4$, was faster for n-species while the reaction with H_2 was favouring iso species thus presenting some important insight into the selectivity of propene hydroformylation. It was suggested that depending on the reaction conditions the reductive elimination of acylcobalt carbonyl complex is performed by H_2 and/or $HCo(CO)_4$. The first was suggested to be predominant in the industrial process when high pressures, high temperatures and low catalyst concentrations are applied

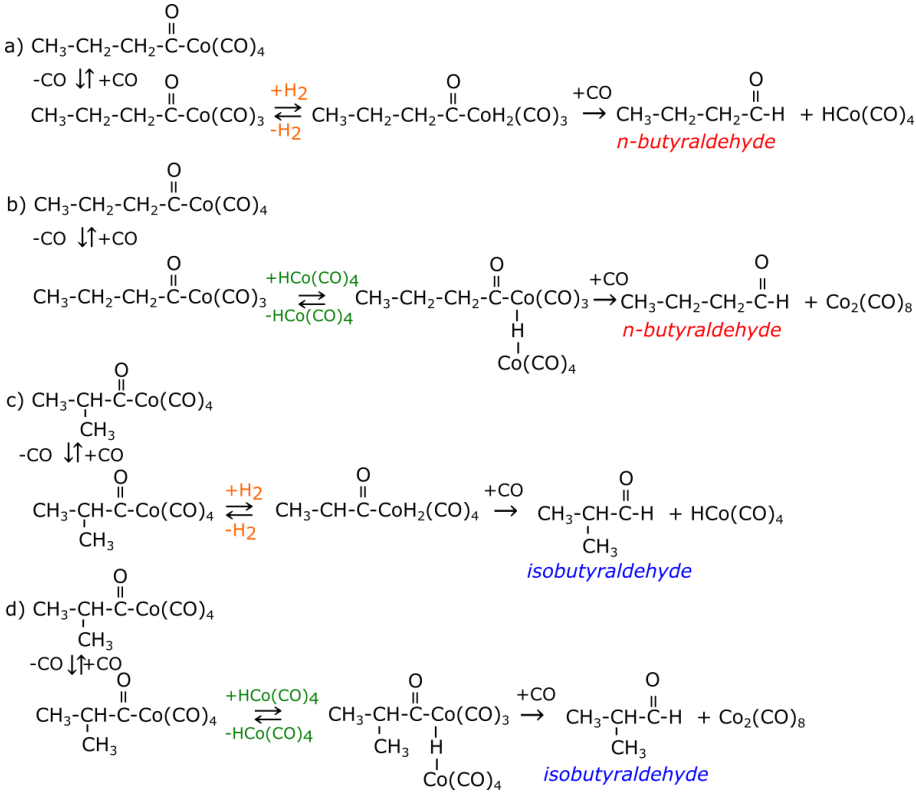

Scheme 1.3 a) H_2 cleavage of n-butyrylcobalt tetracarbonyl; b) Catalyst cleavage of n-butyrylcobalt tetracarbonyl; c) H_2 cleavage of isobutyrylcobalt tetracarbonyl; d) Catalyst cleavage of isobutyrylcobalt tetracarbonyl [65].

Experimental studies of the reaction kinetics and selectivity may contribute to the deeper understanding of the reaction mechanism and may be used to optimize the conditions of the process. However, the yielded empirical rate equations suggest a complex dependence on reactant concentrations in this many-step organometallic reaction. For example, in the detailed studies of Gholap et al [66] the rate of propene hydroformylation was measured as a function of carbon monoxide pressure, hydrogen pressure and initial concentrations of dicobalt octacarbonyl and propene. The applied pressures and temperatures were chosen so that the industrial conditions would be partially mimicked. The syngas consumption as well as the concentration of formed n- and

isobutyraldehydes were measured. A consistent picture was obtained as the overall rate of propene hydroformylation (r_h) was about the same as the sum of the rates of linear (r_n) and branched (r_{iso}) aldehyde formation. This yielded empirical rate equations for these rates, based on fitting to values observed under approximately 30 different experimental conditions are given below.

$$r_h = \frac{k[H_2]^{0.6}[CO][Co_2(CO)_8]^{0.8}[C_3H_6]}{(1 + K_B[CO])^2} \tag{1.46}$$

$$r_n = \frac{k_n[H_2]^{0.55}[CO][Co_2(CO)_8]^{0.75}[C_3H_6]^{0.87}}{(1 + K_{nB}[CO])^2} \tag{1.47}$$

$$r_{iso} = \frac{k_{iso}[H_2]^{0.32}[CO][Co_2(CO)_8]^{0.62}[C_3H_6]}{(1 + K_{isoB}[CO])^2} \tag{1.48}$$

The partial orders with respect to the substrates' concentration in the rate equations suggest a complex nature of this organometallic reaction.

1.4.4 Computational Studies

Many aspects of organometallic reactions including hydroformylation may be studied using the tools of computational chemistry. Nowadays it is quite common that the experimental investigation of novel catalysts is accompanied by the electronic structure calculations that provide an additional scientific insight. In the case of hydroformylation which was shown by experimental studies to have a complicated pathway a computational approach may assist with resolution of the reaction mechanism and determination of rate and selectivity determining steps. This knowledge might be essential in order to be able to design more sustainable catalyst in the future.

In general, most of the computational studies for complex reactions employ DFT calculations, especially if compounds of transition metals are involved, as in the present case. This is due to

a trade-off between the accuracy and computation time, especially if geometry optimization and frequency calculations are conducted. Some post-HF methods have been used as well but only for refinement of energies of structures that have been obtained from geometry optimization at the lower DFT level of theory. When treating the systems with first-row transition metal a special care must be taken as there can be some near-degeneracy effects and multiconfigurational approach should be used [67].

Cobalt catalyzed hydroformylation has received somehow less attention from theoreticians than rhodium systems however still a number of studies have been done. A pivotal contribution of computational chemistry is always its ability to provide information about the energy, geometry and spectra of transient species that are difficult to measure experimentally. Such a compound is for example the 16-electron cobalt tricarbonyl hydride complex $HCo(CO)_3$, postulated for dissociative mechanism of alkene insertion. It was suggested by Versulius et al [68] that the most stable form should be a singlet complex of Cs butterfly geometry resulting from the loss of a carbonyl ligand at equatorial position. The C3v-symmetric structure that is generated by instead removing the axial ligand was higher in energy by 38 kJ mol^{-1}.

When it comes to the resolving of the reaction mechanism of propene hydroformylation a very detailed study was published by Huo et al [69]. The reactants, intermediates and transition states structures were localized on the potential energy surface using the B3LYP functional. Their results led to a different prediction concerning the geometry and energy of $HCo(CO)_3$ complex. The lowest structure they found was a C2v-symmetric (i.e. planar) butterfly geometry which still confirmed the dissociation of equatorial CO from $HCo(CO)_4$. Moreover, it was concluded that the saturated propyl carbonyl complexes, $Co(CO)_4$-C_3H_7, were the key intermediates responsible for the observed selectivity as the n species were more stable than iso species.

A computational kinetic model was proposed by Rush et al. [70] for the very same reaction employing DFT geometry optimization and frequency calculations and CCSD(T)-F12 single-point energy calculations for refinement of the ground state energy values. Furthermore transition state theory was employed for kinetic modelling. A quite close agreement with the experimental rates measured by Gholap et al. [66] have been achieved for one temperature, 423 K. It was concluded that the rate determining step was the binding of propene to the unsaturated cobalt hydride carbonyl $HCo(CO)_3$ species which is present in a very low concentration in the reaction mixture.

Recently automated methods have been used for studying alkene hydroformylation. They present an appealing alternative to the tiresome refinement of compound geometries "by hand" while localizing a global minimum among all possible conformations. Important models include the artificial force induced reaction method [71], graph-based reaction path sampling [72] and transition state search using chemical dynamics simulations [73]. All of the aforementioned techniques have been applied to alkene hydroformylation research as a useful test case of a complex reaction, but they have not led to substantially new insight into the potential energy surface, instead confirming the results obtained by Rush et al [70].

1.5 Methane Activation

1.5.1. Introduction

Methane, mainly exploited for heating and electricity generation, has the potential to become a pivotal feedstock for the synthesis of fuels and chemical commodities, as the reserves of petroleum are shrinking. This smallest hydrocarbon is the main component of natural gas and biogas. There is still an abundance of conventional natural gas resources and the technology of shale gas

recovery is maturing, while renewable biogas is also entering the scene. However a main challenge of methane utilization by the chemical industry remains the economic synthesis of value-added substances from this species. Methane is a very challenging molecule for synthetic chemists due to its four strong, localized and equivalent C-H bonds. Most often high temperatures are required for the initiation of the methane reaction and the radical nature of them leads to poor selectivity. Thus catalytic processes that would enable the conversion of methane into higher-value molecules in ambient temperature and pressure conditions are being at the centre of many research endeavours.

Currently methane is already used in the production of chemicals in large-scale processes but this is done following an indirect route in which CH_4 is firstly transformed into *syngas* through methane reforming process. *Syngas* is one of the main substrates for a wide variety of essential catalytic processes, like the Haber-Bosch reaction for the production of ammonia, the Fischer-Tropsch synthesis of hydrocarbons and alkene hydroformylation - the processes mentioned earlier in this thesis. Other investigated reactions employed for methane valorisation are the production of pure hydrogen and solid carbon, the direct synthesis of hydrocarbons, the aromatization of methane and the direct functionalization of methane [74].

1.5.2 Methane Reforming

Nowadays the predominant way in which methane can be further on used for the synthesis of bulk chemicals is *syngas* production following the reforming processes. There are three of them: reforming techniques employing water, carbon dioxide or oxygen for the reaction with methane (Table 1.3). The syngas production processes require high temperatures, atmospheric pressures and suitable catalysts to achieve good methane conversions and selectivity towards carbon monoxide and hydrogen. Due to the very high temperatures applied (T>1000 K)

the processes generate high costs. Other technological problems include formation of coke, catalyst deactivation and safety issues. Still syngas production, both catalytic and non-catalytic, is a well-established industrial process used for methane chemical transformation [75].

Table 1.3 Methane reforming processes.

Process	Reaction	ΔH (298 K) [kJ mol^{-1}]
Steam reforming	$CH_4 + H_2O \rightarrow CO + 3H_2$	206
Dry (CO_2) reforming	$CH_4 + CO_2 \rightarrow 2CO + 2H_2$	247
Partial oxidation	$CH_4 + ½\ O_2 \rightarrow CO + 2H_2$	-36

1.5.3 Production of Carbon, Hydrogen, Aliphatic and Aromatic Hydrocarbons

The different routes exploiting methane for production of hydrogen and carbonaceous materials in high temperatures have been investigated. The possible reactions are summarized in Table 1.4. Until now the novel processes stay in the domain of research.

Table 1.4 Investigated processes for methane conversion

Process	Reaction	ΔH (298 K) [kJ mol^{-1}]
TCD	$CH_4 \rightarrow C + 2H_2$	75.6 kJ mol^{-1}
OCM	$2CH_4 + ½O_2 \rightarrow C_2H_6 + H_2O$	-177 kJ mol^{-1}
	$2CH_4 + O_2 \rightarrow C_2H_4 + 2H_2O$	-282 kJ mol^{-1}
NOCM	$2CH_4 \rightarrow C_2H_6 + H_2$	64.4 kJ mol^{-1}
	$2CH_4 \rightarrow C_2H_4 + 2H_2$	201.5 kJ mol^{-1}
MA	$6CH_4 \rightarrow C_6H_6 + 9H_2$	531 kJ mol^{-1}
	$6CH_4 + n\text{-}C_4H_{10} \rightarrow C_6H_6 + 6H_2$	396 kJ mol^{-1}*
	$6CH_4 + 4½O_2 \rightarrow C_6H_6 + 9H_2O$	-1846 kJ mol^{-1}

* ΔH (427 K)

One of the methane transformation pathways is the thermocatalytic decomposition (TCD) serving for the production of

hydrogen and solid carbon [76]. The main advantage of such a reaction is that the pure hydrogen produced does not have to be separated from other gases. The technology for the production of hydrogen lacking impurities may be essential for some applications, for example fuel cells. Another interesting aspect of TCD is that various types of carbon material may be obtained, such as amorphous carbon, nanofibers, nanotubes, graphene multilayers, attracting a lot of attention from scientists working in the area of sensors, semiconductors or gas-selective separation materials. Heterogenous catalysts for TCD are mainly metals (cobalt, ruthenium, nickel and rhodium are the most active) or carbon material itself, leading to the cases of autocatalysis.

Aliphatic hydrocarbons can be produced from methane following either an oxidative (exothermic) route, or a direct route (endothermic). In oxidative coupling of methane (OCM), ethane and ethene can be produced, however for the existing processes the selectivity and the maximum observed methane conversion are rather poor, due to higher activity of products compared to methane, [77]. The non-oxidative coupling of methane (NOCM) is characterized by a better selectivity and lower operating temperatures, but is very slow [78]. However with the progress in design of the catalysts and engineering some feasible processes may emerge.

The direct transformation of methane into benzene and hydrogen is called methane aromatization (MA) [79]. This endothermic reaction could again be very fruitful owing to the value of the final products. The use of alkenes or oxygen may improve the thermodynamics although under oxidizing conditions water instead of more valuable hydrogen is produced. The reaction may be catalysed by certain zeolites. Along the process always a solid carbon is a side-product of the reaction while in higher temperatures (>1000 K) needed for the improved conversion even much more coke is obtained in favour of benzene. The coke deposits on the catalyst causing premature its

deactivation. The addition of certain gases (CO, CO_2, H_2, NO, H_2O) during reactor operation can limit coke formation.

1.5.4 Direct Functionalization of Methane

The reactions of direct functionalization of methane with heteroatoms are in majority exothermic (Table 1.5). However the toxic and corrosive nature of the reactants impedes the application of the processes [80]. This is why the introduction of the functional group i.e. hydroxyl, carboxylic, amine etc. under mild conditions would be more desirable.

Table 1.5 Methane direct functionalization reactions.

Reaction	ΔH (298 K) [kJ mol^{-1}]
$CH_4 + F_2 \rightarrow CH_3F + HF$	-453
$CH_4 + Cl_2 \rightarrow CH_3Cl + HCl$	-99
$CH_4 + Br_2 \rightarrow CH_3Br + HBr$	-29.0
$CH_4 + I_2 \rightarrow CH_3I + HI$	52.9
$CH_4 + ½\ O_2 + HBr \rightarrow CH_3Br + H_2O$	-166
$CH_4 + ½\ O_2 + HCl \rightarrow CH_3Cl + H_2O$	-104
$CH_4 + ½\ O_2 \rightarrow CH_3OH$	-126.4

In fact, the direct partial oxidation of CH_4 is sometimes called the "Holy Grail" of catalysis [81]. There is a lot of research devoted to the field, in spite the difficulties in activation posed by the stable methane molecule. Furthermore, the catalyst should act efficiently throughout all reactions in the catalytic cycle: activation, functionalization and regeneration. The *modus operandi* of a catalyst used for methane conversion is presented in Figure 1.11.

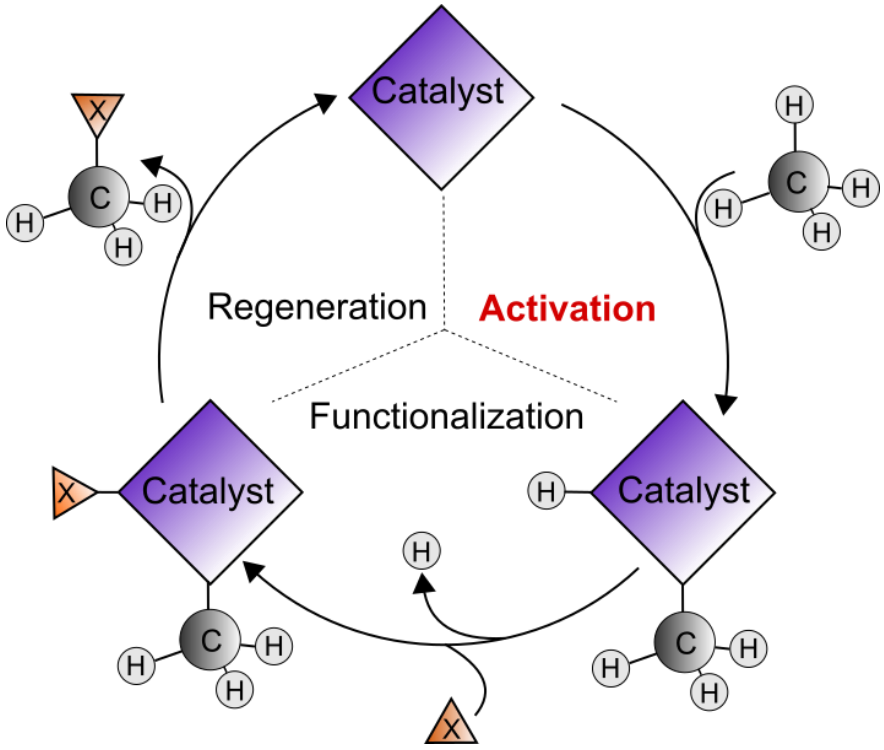

Figure 1.11 Cartoon of a methane direct functionalization catalytic cycle.

Still the most famous catalyst remains to be the platinum complex developed by Periana et al. [82], which is characterized by a *yield* reaching 72% and *selectivity* of 81% under modest pressures and temperatures of 35 bar and 493 K. In oleum methyl bisulphate is the product of the reaction.

1.5.5 Gas Phase Methane Activation Reactions

The reaction mechanisms of methane activation by metal-based catalyst can be divided into three general types, described previously by Shilov [83]. These are the *true activation* following mainly proton coupled electron transfer (PCET) mechanism, *fake activation* displaying the characteristics of hydrogen atom transfer (HAT) and the *Fenton-type mechanism* in which the catalyst activates hydrogen peroxide which in turn reacts with methane

forming water and methyl radical. All three mechanism types are illustrated in Figure 1.12.

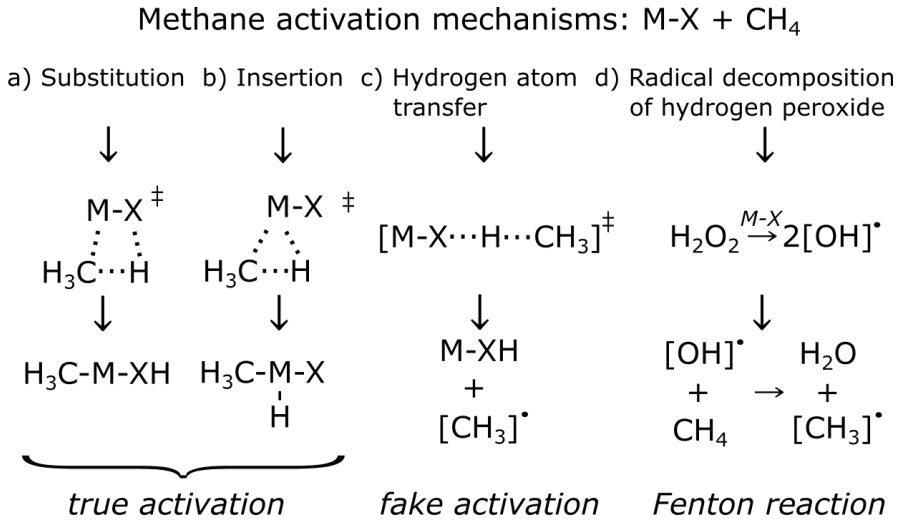

Figure 1.12 Types of methane activation mechanism

Still, unravelling of the mechanism of a broad spectrum of methane activation reactions can be a Sisyphean task. The processes studied are in majority performed by heterogenous catalysts of complicated structure, the catalytic cycle involves multiple steps and often radical reactions take place. The clear picture is disturbed by the abundance of side-reactions, fast deactivation of the catalyst and harsh operating conditions. This thought-provoking problem of how to acquire more information on a microscopic molecular level may be tackled by proposing a simplified model which in turn could be studied very accurately. Such endeavours have been undertaken. For many years the research group of Helmut Schwarz has been executing the gas-phase experiments under single collision conditions [84]. Coupling these with mass spectrometry enables to gather detailed information about reactants and products. The studied "catalysts" of methane activation reaction, small metal-oxide cluster cations and metal-carbide cations may serve as a model of the active sites of the "real" heterogenous catalyst. The experiments are

accompanied by exhaustive electronic structure calculations employed to obtain the relevant PES of the reaction. Hence the mechanism of methane activation may be specified and reasoned based on the molecular electronic effects.

1.6 Motivation and Objectives of the PhD Project

The production of chemical commodities is mostly dominated by catalytic reactions. Without the catalysts it would be highly difficult or even impossible to obtain many materials essential in the daily life of modern society. Although the industrial application of catalysis is rather mature in terms of production technology, optimization of the processes conditions and elaboration of employed catalysts, the necessity of further research and development in the area has been recognized. The awareness of the harmful impact of the toxic substances, greenhouse gases emission and overconsumption of thermal energy is growing. One of the possible solutions is the development of catalysts that would support the sustainable, more environmentally friendly and safer production technologies.

In order to design more sensible chemical processes the deeper understanding at all levels of catalysis is invaluable, from the molecular structure of the catalyst species to the manufacturing plant operation. Basic research may be of great importance for studying the fundamentals of chemistry, especially the reaction mechanism. The progress in the supercomputers power, informatics and applications of quantum mechanical calculations enable the development of computational chemistry methods that are becoming more and more reliable. The results obtained from calculations based on theoretical, physical and quantum chemistry may be complementary to the performed experiments. In this thesis some perspectives of the role of the computational chemistry in the immense field of catalysis are addressed.

The first purpose of this research is to evaluate whether it is feasible to predict the course of a complex catalytic reaction with available theoretical methods. The case study is propene hydroformylation by organometallic cobalt carbonyl catalyst. In this investigation we address mainly the selectivity and temperature dependence of the reaction, continuing the work previously done in our group [70] in which the computational protocol for quite accurate predictions of the main product formation at a single temperature was presented.

The second aim of this doctorate project is to assess the possibilities of the application of novel molecules and materials in catalysis. We focus on the putative methane activation by small clusters of a $[X_2Y_2]^{\bullet+}$ form where X is a pnictogen atom and Y is a chalcogen atom. The electronic structure of these molecules in their neutral form have been the subject of extensive research in our group previously [85]. Moreover the resemblance of the studied clusters to the $[Al_2O_2]^{\bullet+}$ cations, that have been reported to carry out methane activation [86], have stimulated us to explore the potential energy surface of $[X_2Y_2]^{\bullet+} + CH_4$ reaction.

Overall through this research contribution we would like to demonstrate the usefulness of theoretical chemistry approaches and widen the available knowledge of two important catalyzed processes, namely propene hydroformylation and methane activation. The stress is put on the determination and explanation of reaction mechanism employing available methods of computational chemistry.

1.7 References

[1] B. Lindström, L. J. Pettersson, *CATTECH* **2003**, 7, 130-138.
[2] A. Cornish-Bowden, *J. Biosci.* **1998**, 23, 87-92.
[3] K. J. Laidler, A. Cornish-Bowden in *New Beer in an Old Bottle: Eduard Buchner and the Growth of Biochemical Knowledge* (Ed.: A. Cornish-Bowden) Universitat de València, València **1997**, pp 123-126.

[4] E. Fulhame, *An Essay on Combustion, with a View to a New Art of Dying and Painting, wherein the Phlogistic and Antiphlogistic Hypotheses are Proved Erroneous*, The first American Edition, Printed and sold by James Humphreys, Philadelphia, **1810**, pp 229-232. <https://archive.org/details/2554047R.nlm.nih.gov/>
[5] A. J. B. Robertson, *Platinum Metals Rev.* **1975** 19, 64-69.
[6] H. Davy, *Phil. Trans.* **1817** 107, 77-85.
[7] E. Mitscherlich, *Pogg. Ann.* **1834**, 31, 273 after B. Lindström, L. J. Pettersson, *CATTECH* **2003**, 7, 130-138.
[8] J. Wisniak*, Educ. quím.* **2010**, 21, 60-69.
[9] Wilhelm Ostwald – Nobel Lecture. NobelPrize.org. Nobel Media AB 2018. Mon. 27 Aug 2018. <https://www.nobelprize.org/prizes/chemistry/1909/ostwald/lecture/>
[10] Paul Sabatier – Nobel Lecture. NobelPrize.org. Nobel Media AB 2018. Tue. 11 Sep 2018. <https://www.nobelprize.org/prizes/chemistry/1912/sabatier/lecture/>
[11] J. N. Armor, *Catal. Today* **2011**, 163, 3–9.
[12] L. Lloyd, *Handbook of Industrial Catalysts*, New York, Springer, **2011**, pp 23-39.
[13] L. Lloyd, *Handbook of Industrial Catalysts*, New York, Springer, **2011**, pp 48-55.
[14] J. L. Casci, C. M. Lok, M. D. Shannon, *Catal. Today* **2009**, 145, 38-44.
[15] J. R. Ludwig, C. S. Schindler, *Chem* **2017**, 2, 313-316.
[16] G. W. Parshall, R. E. Putscher, *J. Chem. Educ* **1986**, 63, 189-191.
[17] X. Lim, *Nature* **2016**, 537, 156-158.
[18] IUPAC Compendium of Chemical Terminology, Electronic version, http://goldbook.iupac.org/C00876.html
[19] L. Lloyd, *Handbook of Industrial Catalysts*, New York, Springer, **2011**, pp 1-22.

[20] D. Astruc, *Organometallic Chemistry and Catalysis*, Berlin Heidelberg, springer, 2007, pp 351-355.
[21] J. W. Thybaut, G. B. Marin, *Catalysis – Testing of Catalytic Properties*, Encyclopedia of Life Support Systems (EOLSS).
[22] G. Centi, P. Ciambelli, S. Perathoner, P. Russo, *Catal. Today* 2002, 75, 3-15.
[23] a) C. Poree, F. Schoenebeck, *Acc. Chem. Res.* **2017**, 50, 605−608; b) Z. Wang, P. Hu, *Phil. Trans. R. Soc.* **2016**, 374, 1-12.
[24] J.M. Mercero, J.M. Matxain, X. Lopez, D.M. York, A. Largo, L.A. Eriksson, J.M. Ugalde, *Int. J. Mass Spectrom.* **2005**, 240 37–42.
[25] B. K. Carpenter, *Science* **2011**, 332, 1269-1270.
[26] F. Jensen, *Introduction to Computational Chemistry*, John Wiley & Sons, Chichister **2002**, pp 57-59.
[27] F. Jensen, *Introduction to Computational Chemistry*, John Wiley & Sons, Chichister **2002**, pp 70-71.
[28] E. G. Lewars, *Computational Chemistry*, Springer, **2016**, pp 291-300.
[29] R. J. Bartlett, M. Musiał, *Rev. Mod. Phys.* **2007** 79, 291-299.
[30] J.M. Mercero, J.M. Matxain, X. Lopez, D.M. York, A. Largo, L.A. Eriksson, J.M. Ugalde, *Int. J. Mass Spectrom.* **2005**, 240 47–48.
[31] D. P. Tew, C. Hättig, R A. Bachorz, W. Klopper in *Recent Progress in Coupled Cluster Methods* (Eds.: P. Čársky, J. Paldus, J. Pittner), Springer Netherlands, Dordrecht, **2010**, pp 535-539.
[32] G. Knizia, T. B. Adler, H.-J. Werner, *J. Chem. Phys.* **2009**, 130, 054104, 1-20.
[33] J. A. Pople, *J. Chem. Phys* **1965**, 43, 229-230.
[34] E. G. Lewars, *Computational Chemistry*, Springer, **2016**, pp 483-489.
[35] F. Jensen, *Introduction to Computational Chemistry*, John Wiley & Sons, Chichister **2002**, pp 177-182.
[36] N. Mardirossian, M. Head-Gordon, *Mol. Phys.* **2017**, 115, 2315-2370.

[37] a) S. Grimme, *J. Comput. Chem.* **2004**, 25, 1463-1473; b) S. Grimme, S. Ehrlich, L. Goerik, *J. Comput. Chem.* **2011**, 32, 1456–1465.
[38] J. P. Perdew, K. Schmidt, *AIP Conf. Proc.* **2001**, 577, 1-20.
[39] See for example: G. N. Simm, M. Reiher, *J. Chem. Theory Comput.* **2016**, 12, 2762−2773.
[40] J. N. Harvey in *Physical Inorganic Chemistry: Principles, Methods, and Models* (Ed. A. Bakac), John Wiley & Son, New Jersey, **2010**, pp 459-501.
[41] S. Maeda, Y. Harabuchi, Y. Ono, T. Taketsugu, K. Morokuma, *Int. J. Quantum Chem* **2015**, 115, 258–269.
[42] J. W. Ochterski, *Thermochemistry in Gaussian*, **2000**, 1-19.
[43] K. J. Laidler, S. Glasstone, *J. Chem. Educ.* **1948**, 383-387.
[44] S. Aŝperger, *Chemical Kinetics and Inorganic Reaction Mechanisms Second Edition*, Springer, New York, **2003**, pp 33-38.
[45] S. Aŝperger, *Chemical Kinetics and Inorganic Reaction Mechanisms Second Edition*, Springer, New York, **2003**, pp 11-13.
[46] K, J. Laidler, *J. Chem. Educ* **1984**, 61, 494-498.
[47] S. Aŝperger, *Chemical Kinetics and Inorganic Reaction Mechanisms Second Edition*, Springer, New York, **2003**, pp 14-15.
[48] K. J. Laidler, M. C. King, *J. Phys. Chem.* **1983**, 87, 2657-2664.
[49] M. Besora, F. Maseras, *WIREs Comput Mol Sci.* **2018**, e1372, 1-13.
[50] S. Zhang, I. P. Androulakis, M. G. Ierapetritou, *Chem. Eng. Sci.* **2013**, 93, 150-162.
[51] B. Cornils, W. A. Hermann, M. Rash, *Angew. Chem.* **1994**, 33, 2144-2163.
[52] J. Falbe, *The Hydroformylation Reaction Oxo Reaction /Roelen Reaction* in *Carbon Monoxide in Organic Synthesis*, Springer-Verlag, Berlin, Heidelberg **1970**, pp. 3.
[53] M. Orchin, L. Kirch, J. Goldfarb, *J. Am. Chem. Soc.* **1956**, 78, 5450-5451.
[54] B. Cornils, W. A. Herrmann, M. Beller, R. Paciello, *Applied Homogeneous Catalysis with Organometallic Compounds: A*

Comprehensive Handbook in Four Volumes. Third Edition. Volume 4, Wiley-VCH, Weinheim **2018**, pp. 26-29.
[55] S. Bizzari, M. Blagoev, A. Kishi, in *Chemical Economics Handbook Report: Oxo Chemicals*, SRI International **2006**, Report No. 682.7000 in F. Hebrard, P. Kalck, *Chem. Rev.* **2009**, 109, 4272–4282.
[56] A. Behr, P. Neubert, *Applied Homogeneous Catalysis*, Wiley-VCH Verlag & Co. KGaA, Weinheim **2012**, pp. 273-284.
[57] R. F. Heck, D. S. Breslow, *J. Am. Chem. Soc.* **1961**, 83, 4023 – 4027.
[58] R. L. Sweany, T. L. Brown, *Inorg. Chem* **1977**, 16, 415-421.
[59] D. Karakaş, S. E. Kariper. *J. Mol. Struct* **2014**, 1062, 77-81.
[60] A. A. Low, K. L. Kunze, P. J. Machugall, M. B. Hall, *Inorg. Chem* **1991**, 30, 1079-1086.
[61] J. C. Green, M. L. H. Green, G. Parkin, *Chem. Commun.* **2012**, 48, 11481–11503.
[62] a) F. Ungváry, *J.Organomet. Chem*. **1972**, 36, 363-370; b) J. W. Rathke, R. J. Klingler, T. R. Krause, *Organometallics* **1992**, 11, 585-588; c) R. Tannenbaum, U. K. Dietler, G. Bor, F. Ungváry, *J. Organomet. Chem.* **1998**, 570, 39–47.
[63] a) M. F. Mirbach, *J. Organomet. Chem.* **1984**, 26, 205-213; b) M. Caporali, P. Frediani, A. Salvini, G. Laurenczy, *Inorg. Chim. Acta.* **2004**, 357, 4537–4543.
[64] M. Torrent, M. Solà, G. Frenking, *Chem. Rev.* **2000**, 100, 439-450.
[65] I. Kovács, F. Ungváry, L. Markó, *Organometallics* **1986**, 5, 209-215.
[66] a) R. V. Gholap, O. M. Kut, J. R. Bourne, *Ind. Eng. Chem. Res.* **1992**, 31, 1597-1601; b) R. V. Gholap, O. M. Kut, J. R. Bourne, *Ind. Eng. Chem. Res.* **1992**, 31, 2446-2450.
[67] T. Kégl, *RSC Adv.* **2015**, 5, 4304–4327.
[68] L. Versluis, T. Ziegler, E. J. Baerends, W. J. Ravenek, *Am. Chem. Soc.* **1989**, 111, 2018-2025 ; b) L. Versluis, T. Ziegler, L. Fan, *Inorg. Chem.* **1990**, 29, 4530-4536.

[69] C.-F. Huo, Y.-W. Li, M. Beller, H. Jiao, *Organometallics* **2003**, 22, 4665-4677,
[70] L. E. Rush, P. G. Pringle, J. N. Harvey, *Angew. Chem.* **2014**, 126, 8816 –8820.
[71] a) S. Maeda, K. Morokuma, *J. Chem. Theory Comput.* **2012**, 8, 380–385; b) S. Maeda, T. Taketsugu, K. Morokuma, *J. Comput. Chem.* **2014**, 35, 166–173.
[72] a) S. Habershon, *J. Chem. Phys.* **2015**, 143, 094106; b) S. Habershon, *J. Chem. Theory Comput.* **2016**, 12, 1786–1798.
[73] J. A. Varela, S. A. Vázquez, E. Martínez-Núñez, *Chem. Sci.* **2017**, 8, 3843-3851.
[74] P. Tang, Q. Zhu, Z. Wu, D. Ma, *Energy Environ. Sci.* **2014**, 7, 2580.
[75] P. Tang, Q. Zhu, Z. Wu, D. Ma, *Energy Environ. Sci.* **2014**, 7, 2581-2582.
[76] Ahmed Aidid Ibrahim, Ahmed Sadeq Al-Fatesh, Wasim Ullah Khan, Mostafa Ali Soliman, Raja Lafi AL Otaibi, Anis Hamza Fakeeha, *J.Chem.Soc.Pak.* **2015**, 37, 1280-1308
[77] A. Galadima, O. Muraza, *J. Ind. Eng. Chem.* **2016**, 37 1–13.
[78] M. Belgued, P. Pareja, A. Amariglio, H. Amariglio, *Nature* **1991**, 352, 789–790.
[79] J. J. Spivey, G. Hutchings, *Chem. Soc. Rev.* **2014**, 43, 792-803.
[80] P. Tang, Q. Zhu, Z. Wu, D. Ma, *Energy Environ. Sci.* **2014**, 7, 2585-2586.
[81] R. Horn, R. Schlögl, *Catal. Lett.* **2015**, 145, 23–39.
[82] R. A. Periana, D. J. Taube, S. Gamble, H. Taube, T. Satoh, H. Fujii, *Science* **1998**, 280, 560-564.
[83] A. E. Shilov, G. B. Shul'pin, *Chem. Rev.* **1997**, 97, 2879-2932 after A. I. Olivos-Suarez, À. Szécsényi, E. J. M. Hensen, J. Ruiz-Martinez, E. A. Pidko, J. Gascon, *ACS Catal.* **2016**, 6, 2965–2969.
[84] H. Schwarz, S. Shaik, J. Li, *J. Am. Chem. Soc.* **2017**, 139, 17201–17212.

[85] J. M. Mercero, X. Lopez, J. E. Fowler, J. M. Ugalde*, J. Phys. Chem. A*, 1997, 101, 5574-5579.
[86] J. Li, S. Zhou, J. Zhang, M. Schlangen, T. Weiske, D. Usharani, S. Shaik, H. Schwarz, *J. Am. Chem. Soc.* **2016**, 138, 7973–7981.

Chapter 2

Computational Modelling of Selectivity in Cobalt-Catalyzed Propene Hydroformylation

The content of this chapter was published as:
E. N. Szlapa, J. N. Harvey, "Computational Modelling of Selectivity in Cobalt-Catalyzed Propene Hydroformylation", Chem. Eur. J. 2018.
DOI: 10.1002/chem.201803490
The version presented here is the pre-print manuscript. The page layout, the table and the numbering of tables and figures have been modified to fit to the style and the format of this thesis. Some additional information concerning bonding and structure have also been added.

My contribution to the work presented involved theoretical calculations, data analysis, discussion of the results, preparation of the first version of the manuscript. Kinetic modelling, discussion of the results and writing of the final manuscript were done together with the co-author, Jeremy Harvey.

Abstract: A mechanistic model for the cobalt-catalyzed hydroformylation of propene, based on density functional theory and coupled cluster electronic structure calculations and transition state theory, is proposed to explain the experimentally observed reactivity and selectivity. The electronic structure calculations provide very accurate energies which are used with transition state theory to compute rate constants, and the kinetics of the network of coupled reactions is then modelled numerically for this organometallic reaction. The model accounts well for the dependence of rate on concentration of catalysts and reagents, and also on temperature, and the agreement with experiment is

improved still further upon making small adjustments to the ab initio calculated free energy values. The calculations provide detailed kinetic insight into the mechanism of hydroformylation, and the role of various elementary steps in defining reactivity and selectivity.

2.1 Introduction

Hydroformylation, also known as the "oxo" reaction, is a catalytic reaction exploited for transformation of an alkene into an aldehyde through the addition of synthesis gas (1:1 mixture of molecular hydrogen [H_2] and carbon monoxide [CO]). The process was discovered by chance by Otto Roelen at Ruhrchemie in 1938 [1] and it is one of the first examples of homogenous organometallic catalysis. It is a well-established industrial process with an annual world production of several million tonnes per year, from which still at least one million are produced with cobalt catalysts [2]. Although nowadays the majority of the process uses rhodium catalysts due to their higher selectivity and less harsh operating conditions, cobalt catalysts that are less toxic, much cheaper and which provide a different selectivity pattern remain of significant use and hence remain a major topic of study [3].

Hydroformylation of alkenes, except for ethene, leads to production of a mixture of aldehyde isomers. Formation of an unwanted isomer, historically the branched aldehyde, generates undesirable costs, especially for industrial-scale processes. Thus there is a considerable effort continuously being done, devoted to investigation of modern catalysts [4]. However in a pursuit of developing more selective and active catalysts it is essential to explore the mechanistic reasons behind the observed kinetics and the selectivity of known and established catalytic processes. These reasons, in the case of the unmodified cobalt-catalyzed propene hydroformylation, are still not fully understood. The aim of this paper is to employ the tools of computational and theoretical

chemistry in order to better understand the reasons behind the observed kinetics and selectivity of this reaction.

Cobalt and rhodium catalyzed alkene hydroformylation have been already extensively studied computationally [5]. There have been also many computational endeavours to explore the potential energy surface (PES) of this catalytic reaction [6], even with automated methods [7]. The present contribution builds on a previous investigation from our group in which a catalytic pathway leading to the main linear product as well as competing alkene hydrogenation was explored [8], based on the mechanism proposed by Heck and Breslow [9]. Because the developed protocol for investigation of kinetics in propene hydroformylation proved to be almost quantitatively correct, it is employed also, albeit in a modified and expanded way, in this study. This computational protocol includes electronic structure calculations of species involved in catalytic cycle followed by kinetic modelling based on transition state theory (TST).

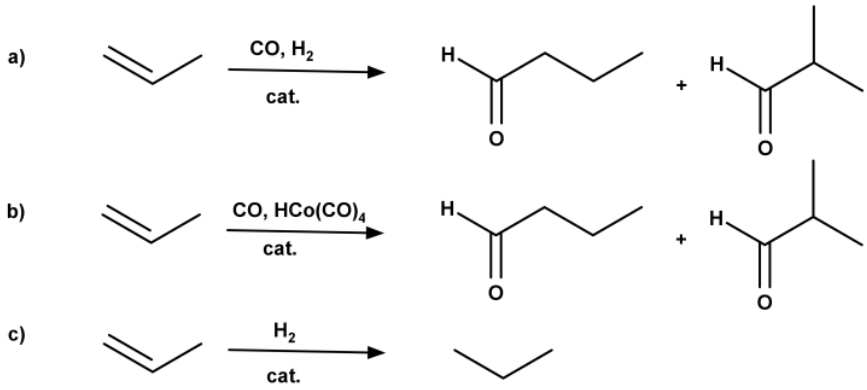

Scheme 2.1 Competing reactions that can occur during the process of propene hydroformylation.

As shown in Scheme 2.1 some reactions may be competing during the industrial hydroformylation process leading to different ratios of products depending on the reaction conditions. As the aim of this paper is to investigate selectivity, the pathway of branched iso-butyraldehyde formation (i-cycle) was explored in addition to

the linear n-butyraldehyde formation (n-cycle). Moreover in this work it was taken into account that the aldehyde production may be enabled by the transfer of hydrogen not only from H_2 molecule (Scheme 2.1a) but also from the catalyst – $HCo(CO)_4$ (Scheme 2.1b). The latter reaction – catalyst cleavage is one of the proposed mechanisms for the hydroformylation process [10] and is believed to be predominant at lower temperatures, lower pressures and higher concentration of catalyst [11]. The side reaction of unwanted propene hydrogenation producing propane (Scheme 2.1c) was also considered in this study.

2.2 Results and Discussion

The starting point for this study was a careful exploration of the relevant parts of the PESs for the hydroformylation process using Density Functional Theory (DFT) together with the B3LYP functional and the empirical D3BJ dispersion correction. An exhaustive search for relevant minima and transition states (TSs) was performed at this level of theory. In the text, we will focus only on the conformations of the minima and TSs that are lowest in energy. Except for the bimetallic systems, for which significant multi-reference character was observed, energies were then refined using single-point energies computed at the coupled cluster singles and doubles with perturbative triples (CCSD(T)) level of theory, using the F12 approach in order to get near-basis-set-limit results and also taking into account scalar relativistic effects.

The structures and calculated energies for the species and reactions steps predicted to be important based on these electronic structures calculations are summarised in Scheme 2.2 and Table 2.1.

Table 2.1 Relative energies of the key species in propene hydroformylation process, units: [kJ mol^{-1}].

Species	ΔE CCSD(T)		ΔG CCSD(T) (423 K)	
	n	iso	n	iso
1-**2**+C_3H_6+2H_2 + CO	-33.2[a]		-27.0[a]	
2 + C_3H_6 + H_2 + CO	0.0		0.0	
3 + C_3H_6 + H_2 + 2 CO	152.8		78.6	
4 + H_2 + 2 CO	33.7		33.5	
TS5 + H_2 + 2 CO	65.1	66.0	60.4	61.7
6 + H_2 + 2 CO	28.3	26.8	32.4	30.5
7 + H_2 + CO	-66.7	-65.7	6.4	10.1
TS8 + H_2 + CO	-7.4	-8.7	65.0	65.2
9 + H_2 + CO	-25.9	-33.9	48.4	41.2
TS10 + H_2	-24.2	-28.4	104.6	104.1
11 + H_2	-118.6	-124.7	25.3	21.8
TS12 + CO	-9.4	-15.5	126.8	122.3
13 + **3** + CO	5.3	0.8	81.7	77.5
13 + **2**	-147.5	-152.0	3.1	-1.1
TS14 + 2 CO	62.4	65.3	123.6	129.5
15 + **3** + 2 CO	-0.5		8.4	
15 + **2** + CO	-153.3		-70.2	
TS16 - **2** + H_2 + CO	-41.8[b]	-47.2[b]	99.1[b]	102.2[b]
17 - **2** + H_2 + CO	-100.8[b]	-103.8[b]	48.3[b]	39.2[b]

[a] Value for Co_2CO_8 from DFT calculations [b] Values for bimetallic species obtained from equation $\Delta E = \Delta E_{DFT} + (\Delta E_{9CCSDT} - \Delta E_{9DFT})$

Even though many previous studies have used quantum chemical methods to study the mechanism of cobalt-catalyzed hydroformylation, there are some new features obtained here which we wish to underline, so we will briefly describe the whole mechanism as emerging from the calculations.

The starting form of the catalyst in hydroformylation is dicobalt octacarbonyl **1** [$Co_2(CO)_8$], which under catalytic conditions can convert rapidly with addition of molecular

hydrogen [H_2] into two equivalents of cobalt tetracarbonyl hydride **2** [$HCo(CO)_4$]. Experimental studies have shown [12] that this reaction and its reverse reach rapid equilibrium under the conditions used for catalysis. Next, upon loss of one carbonyl [CO] ligand, **2** forms the 16-electron cobalt tricarbonyl hydride **3** [$HCo(CO)_3$], which in turn can be coordinated by propene [C_3H_6] through its carbon-carbon double bond to yield species **4**. Careful energy scans showed that there is no potential energy barrier along the routes for addition of CO or C_3H_6 to **3**, suggesting that both steps should be very rapid – we have assumed them to be diffusion-limited and used an empirical expression based on the solvent viscosity to predict their rate constants, as discussed below. In our previous work [8], we noted that **3** can also form a complex **3•toluene** with a typical solvent, toluene. We also speculated that concerted dissociative substitution pathways could lead directly from **2** to **4**, from **2** to **3•toluene**, and/or from **3•toluene** to **4**, thereby side-stepping the formation of unsolvated **3**. In the present study, we have indeed located TSs for these processes, but find that their free energy is markedly higher than that implied for the diffusion-limited addition barriers by the use of the viscosity-dependent expression for the rate constant, so they appear not to play a kinetically important role.

The propene ligand can rotate around the metal-ligand axis with a relatively low barrier (less than 30 kJ mol^{-1} at 423K), leading to four conformers: in two of them the C=C bond of propene is perpendicular to Co-H bond while in other two it is parallel. From the latter conformeric species in which either the $=CH_2$ or =CHMe end is closer to the cobalt hydride. there are also regioisomeric TSs for insertion into the Co-H bond (methylene group up **TS5n** or down **TS5i**). This is the branching point leading to either catalysis of the formation of linear n-butyraldehyde (n-cycle) or of branched iso-butyraldehyde (i-cycle). This is the only bifurcation point we could locate in the mechanism; we assume that interconversion

between n and iso species can happen only by reversion to the alkene complex **4** and passage over **TS5n** or **TS5i**.

The insertion of alkene into Co-H yields the propyl complex cobalt tricarbonyl **6n/6i** [$Co(CO)_3$-C_3H_7] which is formally a 16-electron species but is stabilized by an agostic interaction between the cobalt centre and one of the β-hydrogen atoms. These species may in turn coordinate an additional ligand to the metal centre. Addition of carbon monoxide to **6n/6i** leads to the low-energy cobalt tetracarbonyl propyl complexes **7n/7i** [$Co(CO)_4$-C_3H_7]. Transition states corresponding to an associative CO ligand approach combined with breaking of the agostic interaction were located on the PES. However, species **6n** and **6i** can also exist as slightly higher-energy conformers in which the agostic interaction is absent. Scans along the CO-addition coordinate for these non-agostic conformers show no potential energy barrier. This means that a dissociative pathway in which initial loss of the agostic interaction is followed by barrierless ligand addition is a viable route for ligand addition, and it has an activation free energy that is lower than the straightforward associative addition mechanism. Accordingly, we retain the two-step mechanism in our model.

The insertion of CO into the Co-propyl bond through **TS8n**/**TS8i** yields the butyryl complexes [$Co(CO)_3$-C_3H_7CO] **9n/9i**, which again are formally 16-electron species and again are stabilized by additional interactions in their lowest-energy forms. They can coordinate another CO molecule through **TS10n**/**TS10i** to yield a saturated butyryl cobalt tetracarbonyl complexes [$Co(CO)_4$-C_3H_7CO] **11n/11i**. These are off-cycle species that must revert to **9n/9i** in order to form products.

Production of the propene hydroformylation end-products **13** can occur through coordination of an H_2 molecule to **9**. During this stage of the aldehyde production process, H_2 first coordinates to the cobalt centre then oxidative addition yields a Co(III) dihydride. This is followed by reductive elimination of aldehyde over **TS12n** or **TS12i**. These steps yield the aldehyde product **13n/13i** (n-

butyraldehyde/iso-butyraldehyde) leaving the active catalyst **3** to further catalyse the hydroformylation reaction.

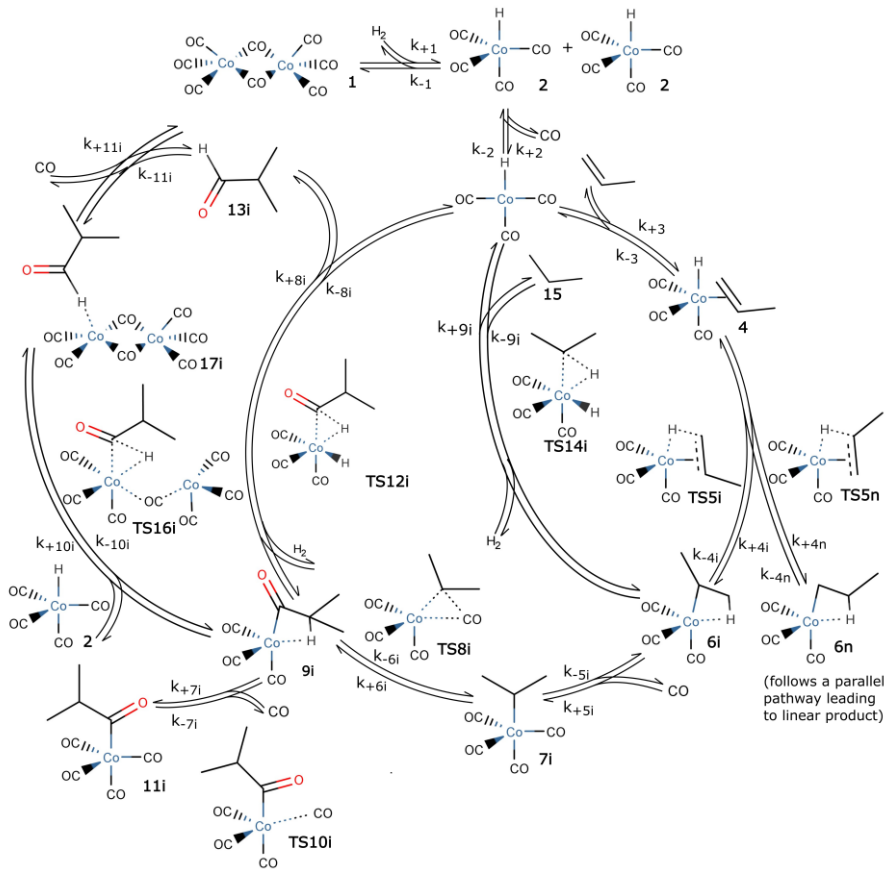

Scheme 2.2 Propene hydroformylation cycle.

The hydrogenation of propene can occur in competition to hydroformylation if a hydrogen molecule is added to **6n**/**6i**. This process follows hydrogen insertion, oxidative addition and reductive elimination through **TS14n**/**TS14i** which is the rate limiting TS in the hydrogenation process. For both the n and iso cycles propane **15** is produced and catalyst revived.

Though **TS12n** and **TS12i** are usually considered to be the main routes to aldehyde formation, we have also considered a

possible competing route in which the species **9** are instead cleaved by $HCo(CO)_4$ **2**. This step has been suggested in experimental studies and indeed there is strong evidence for its importance at lower temperatures [11]. Species **2** can interact with the coordinatively unsaturated **9**, forming initially a complex with a bridging hydride, which can then cross through **TS16n**/**TS16i** to yield complex **17n**/**17i** which is essentially a weakly bound complex between the aldehyde product and dicobalt heptacarbonyl [$Co_2(CO)_7$]. The cycle is completed after releasing the product and addition of CO forming the catalyst **1**. Similar routes involving coordinatively saturated species **11** were also explored but no low-energy barrier was found. This agrees with experimental studies in which an inverse dependence of the rate of this process on CO pressure was observed [11].

These TSs **TS16n** and **TS16i** are lower both in relative potential energy and in relative Gibbs free energy (G) than **TS12n** and **TS12i**. It is also noteworthy that unlike the pattern observed for all other species on the potential energy surface after the bifurcation induced by insertion of alkene into the Co-H bond, the linear isomer **TS16n** lies lower than the branched **TS16i**. This can be attributed to the significant steric congestion in this TS. The lower standard Gibbs free energy for **TS16** does not however entail that it dominates the kinetics, especially as it requires reaction with relatively low-abundance **3**, whereas **TS12** involves reaction with H_2, which is present at high pressure. The competition between the two routes will be considered again below.

All of the aforementioned minimum-energy species together with transition structures corresponding to the transformation of one species into another have been located on the PES except for the case of TSs corresponding to diffusion-limited processes. Also, we have been very careful to locate for each intermediate and TS the structure that was lowest in energy. Moreover intrinsic reaction coordinate calculations were conducted to confirm that a particular TS corresponds to the assigned elementary step in

catalytic cycle. For the steps reported here as having no barrier on the potential energy surface, scans were carried out to ensure that this was indeed the case, justifying the decision to treat the corresponding steps as diffusion-limited in the kinetic modelling.

We now turn to a description of our kinetic modelling. As in our previous work [8], the motivation for performing kinetic modelling is that the identity of the rate-limiting or selectivity-determining steps is not clear based on the free energies alone. Indeed, kinetic modelling has become much more heavily used in the area of organometallic mechanistic modelling in recent years [13]. The procedure we have used for kinetic simulation involves four aspects: 'bunching' of kinetic steps; calculation of the individual rate constants based on the *ab initio* results; actual kinetic simulation; and fitting of the calculated free energies to improve the level of agreement between theory and experiment for the kinetics. Concerning the first aspect, as in our previous work [8], we have relied on the fact that some of the elementary steps in the overall mechanism of the propene hydroformylation catalytic cycle have low barriers in both the forward and reverse directions and can therefore be assumed to reach quasi-equilibrium with respect to other transformations. We therefore combine the corresponding species into one single 'species', effectively applying the Curtin-Hammett principle.

For the second aspect, we need to obtain rate constants k for all the steps in the thus reduced mechanism. This is done based on the calculated free energies as described above. This has mainly been done using the simplest form of transition state theory, in the form of the standard Eyring equation of transition state theory:

$$k = \frac{k_B T}{h} e^{-\frac{\Delta G^{\ddagger}}{RT}} \tag{2.1}$$

While the value of equilibrium constants K was calculated from the standard relation:

$$K = e^{-\frac{\Delta G^{\theta}}{RT}} \tag{2.2}$$

In these equations k_B is Boltzmann's constant, T is the temperature, h is Planck's constant, and R is the gas constant. In Equation (2.1), $\Delta G^{\ddagger}$ is the Gibbs energy of activation - the difference in free energy between the relevant transition state and the corresponding reactant state, while in Equation (2.2), ΔG^{θ} is the standard Gibbs free energy change from reactants to products for the step considered. In many cases, we use the detailed balance condition to compute the rate constant for the reverse reaction, k_{-}, based on the forward rate constant k and the equilibrium constant K.

A number of the bimolecular reactions studied are barrierless, that is, there is no barrier on the potential energy surface as the two species approach and go on to form products. There is however a free energy barrier for such steps, which could in principle be characterized by using more sophisticated versions of TST, such as the various forms of variational TST. Here, however, these reactions have been assumed to be diffusion-limited and their rate constant has been assumed to follow a simple relation depending only on the temperature of reaction and the solvent viscosity η given by the following equation [14]:

$$k = \frac{8k_B T}{3\eta} \tag{2.3}$$

The value of viscosity η for toluene – the solvent used in the experiment – is around 2.07×10^{-4} kg m^{-1} s^{-1} for temperature of 423 K and pressure of 100 atm according to the fit to experimental values [15].

In principle, hydroformylation can be reversible, since the standard free energy for products **13** is roughly the same as that of reactants, see Table 2.1. Formation of the by-product propane is much more exoergic and should therefore be irreversible. We tested the extent of reversibility in exploratory kinetic simulations, but it was found to be very low, basically due to the fact that the high pressure of CO and H_2 under the simulated conditions shifts the equilibrium firmly towards products. Accordingly, all the final kinetic simulations used the simplifying approximation that any

step leading to formation of n-butyraldehyde, iso-butyraldehyde or propane was irreversible.

One final important factor concerning the rate constants plays a significant role for the selectivity of catalysis: the symmetry numbers σ [16] associated with each reaction step, which enters the expression for the rate constant k in the following revised version of Equation 2.1:

$$k = \sigma \frac{k_B T}{h} e^{-\frac{\Delta G^{\ddagger}}{RT}} \tag{2.4}$$

The standard rotational symmetry numbers σ_r are already included in the Gibbs free energy corrections calculated from the partition function for relevant symmetric species (for example σ_r = 2 for H_2) where the symmetry is implied by the point group corresponding to the minimum energy structure. However for flexible molecules possessing low-frequency vibrations that could be almost assumed to be free rotations, the *effective* symmetry may be higher than the point-group symmetry. This can also be the case if there are multiple reaction paths corresponding to different permutations of the atoms involved. We note that this is a different issue to the treatment of low frequency modes, as suggested by Truhlar et al. [17]. Furthermore, for some species, a different number of permutational isomers can be reached through low-barrier processes that can lead to exchange of position of selected atoms. We have found that it is crucial to include a consideration of the permutational symmetry numbers σ_p that arise from these effects for one particular step in order to obtain a qualitatively correct prediction of the ratio of linear to branched aldehyde produced. This is because the key **TS12i** leading to branched aldehyde is slightly *lower* in free energy than the **TS12n** leading to linear aldehyde in the absence of consideration of such factors, so that hydroformylation will always be predicted to favour branched aldehydes without taking these aspects into account. The key elementary reaction to be considered from the symmetry point of view is propene insertion into the Co-H bond (Figure 2.1). For the

forward reaction there is only one hydrogen atom $H_{(1)}$ that can be transferred to the carbon atom of propene to yield species **6n**/**6i**. In case of species **6n**, although the minimum-energy structure has one β-agostic C-H bond and one non-agostic C-H bond, the barrier to exchange these hydrogen atoms is low, so the effective symmetry is higher. This is why for calculating the rate constant of the reverse reaction a symmetry number of *two* has to be taken into account. For species **6i** there are *six* hydrogen atoms to take into account when calculating the reverse rate constant. This analysis of symmetry is somehow similar to the treatment of free internal rotations [16], although we do not introduce the free rotor partition function to account for them but explicitly include a higher symmetry number for the whole molecule for this reaction step which takes into account the possible permutations of hydrogen atom at the position of agostic hydrogen. Furthermore it should be noted that the torsion of a methyl group about C(1)-C(2) bond leading to an exchange of a hydrogen interacting with a metal centre in **6i** recreates the same isomer, while the oscillatory movement that leads to the exchange of β-hydrogens in **6n** or β-hydrogens belonging to another methyl group in **6i** results in forming a stereoisomer of the analysed species, although equivalent in energy. There are other steps where symmetry numbers play a role, but these do not affect the selectivity for branched and linear isomers, hence are not considered in detail here – the hypothetical correction can in any case be assumed to be smaller than other errors in the computational protocol.

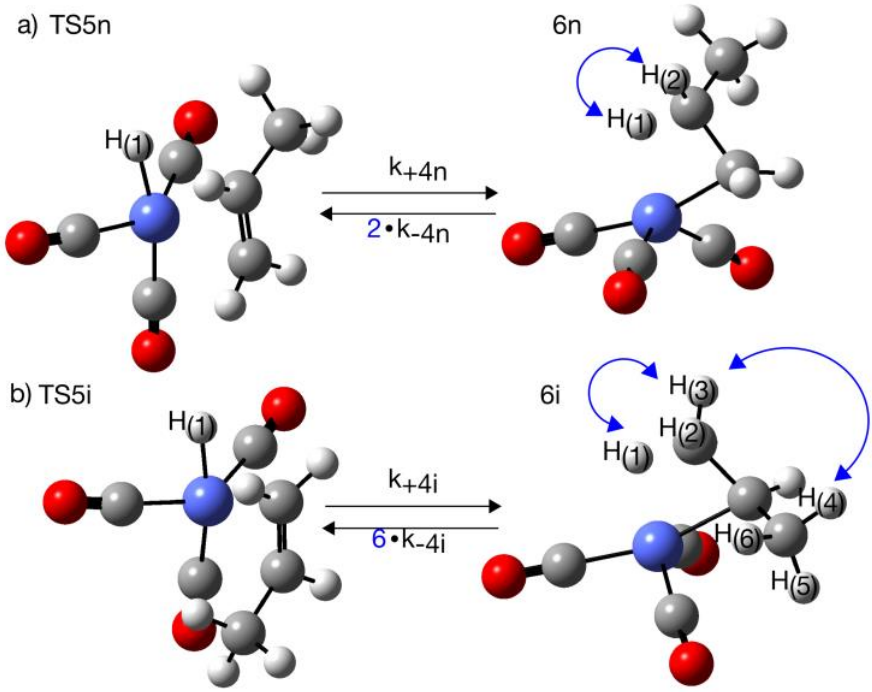

Figure 2.1 Propene insertion into Co-H bond in (a) n-cycle and (b) i-cycle.

The detailed expressions used to evaluate each individual rate constant *k* are described in the Appendix A. Due to the fact that all *ab initio* calculations have been repeated for this work, using a slightly different methodology, the rate constants are very slightly different from those reported in an earlier study [8], but usually with only rather small differences.

We then performed simulations, initially using the kinetics package Tenua [18]. Explicit integration over time of the rate equations is more flexible for the more complex mechanism studied here, compared to the steady-state approximation approach we used previously [8]. We have however tested that it gives exactly the same predicted kinetics when using the same rate constants and concentrations. The simulated n-butyraldehyde and iso-butyraldehyde formation rates were compared with experimentally measured rates reported in papers by Gholap et al. [19]. In these studies, rates were measured at relatively low

conversion, and with a fixed pressure of CO and H_2. Accordingly, in our simulations, the concentration of alkene, and the pressures of the gases were held fixed. The integration in time is carried out for a period of time amply sufficient to reach steady-state (typically a few seconds), and the rates obtained from the slope of the concentration curves at that point.

We first show the modelled rates for n-butyraldehyde and iso-butyraldehyde formation ($R_{calc,n}$ and $R_{calc,i}$ respectively) for specific experimental conditions and compare them to those obtained experimentally [19], at the temperature used in our earlier study [8], 423 K (Figure 2.2). As can be seen, our 'ab initio' model, based purely on quantum mechanical calculations and TST, gives already quite reasonable agreement with the experimental results for rates of products formation as well as for their dependence on experimental conditions without any need for fitting. The rate of formation of n-butyraldehyde is somewhat underestimated, as is the selectivity, but the errors are relatively small. Agreement within much better than a factor of ten as well as reproduction of the broad features of the dependence of rates on reaction parameters confirms our earlier conclusion [8] that this type of modelling can semi-quantitatively reproduce the observed kinetics of this complex organometallic transformation. It should be noted that if we omit the symmetry factor mentioned above, the predicted selectivity is much less good.

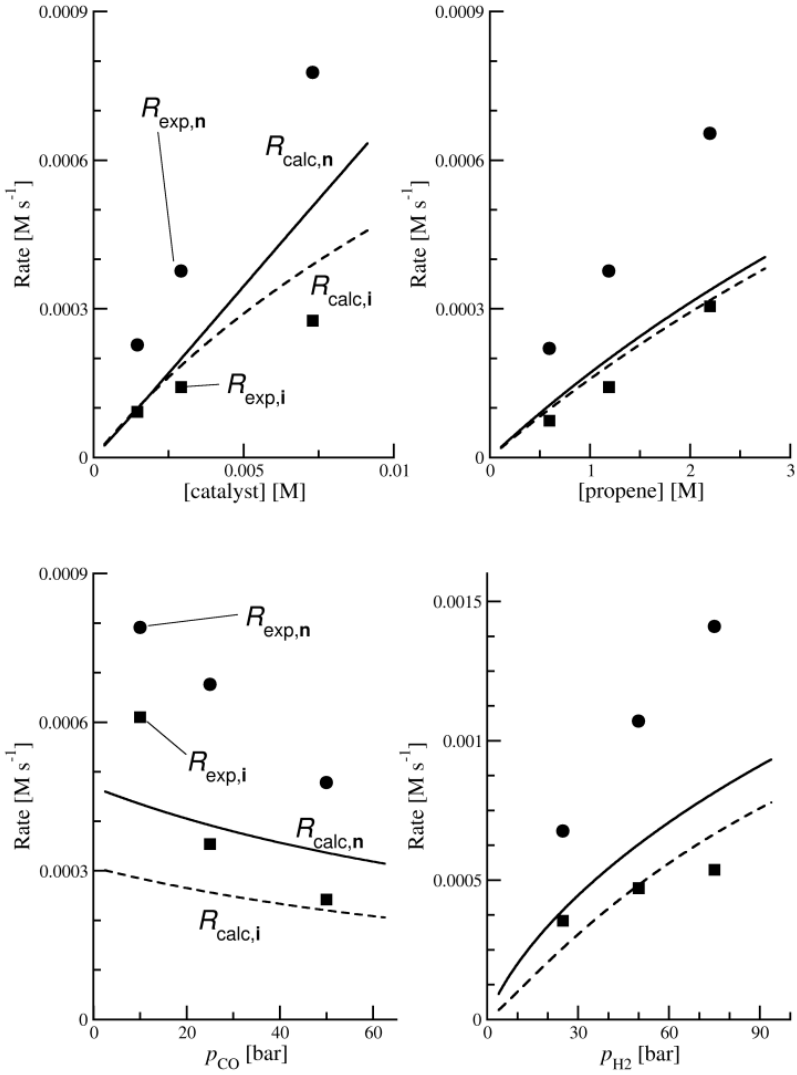

Figure 2.2 Comparison between experimental (points) and calculated (lines) rates of n-butyraldehyde (R_n) and iso-butyraldehyde (R_i) production at 423 K. Experimental conditions: Top left: Rate as a function of catalyst [$Co_2(CO)_8$] concentration [catalyst]; p_{CO} = p_{H2} = 50 bar, [alkene] = 1.19 M. Top right: Rate as a function of propene concentration [alkene]; p_{CO} = p_{H2} = 50 bar, [catalyst] = 0.00292 M. Bottom left: Rate as a function of carbon monoxide pressure p_{CO}; p_{H2} = 25 bar, [catalyst] = 0.0073 M, [alkene] = 1.19 M. Bottom right: Rate as a function of hydrogen pressure p_{H2}; p_{CO} = 25 bar, [catalyst] = 0.0073 M, [alkene] = 1.19 M. Experimental data for n isomer as round dots, for iso isomer are squares. Calculated rates for n isomer as black lines, for iso isomer as dashed lines.

The agreement with experiment for the unmodified model deteriorates upon switching to the other two temperatures studied experimentally, 403 K and 383 K. As an example, the calculated rates for forming **13n** at these temperatures are compared to experiment in Figure 2.3. The calculated rates fall off too fast with temperature, suggesting that our model has a too high activation enthalpy. This seems at first to be a serious issue: the experiment suggests an activation enthalpy of the order of 80 kJ mol^{-1} [17a], whereas our calculated energy for a key intermediate, $[HCo(CO)_3]$ **3**, compared to $[HCo(CO)_4]$ **2**, lies much higher, at roughly 150 kJ mol^{-1} (see Table 2.1). The TS for addition of alkene to **3**, which we argued [8] was the main turnover-limiting point in the cycle, has an energy very similar to that of **3**.

Closer investigation reveals that this conclusion needs to be tempered: in fact, both addition of alkene to **3**, and reductive elimination through **TS12** and **TS16**, appear to contribute to limiting turnover. Very small changes in the free energies used to calculate the rate constants can shift the balance between these two steps. If reductive elimination becomes partly turnover-limiting, then given that the corresponding TSs are barely higher in energy than the reservoir species such as **7** (**TS16n** lies 57.3 kJ mol^{-1} above **7n**, e.g., see Table 2.1), the overall apparent activation energy that emerges from the kinetic model becomes much smaller.

Indeed, upon allowing a small number of calculated free energies to change by a few kJ mol^{-1} with respect to the *ab initio* values, within the uncertainty range associated with the computational values, we obtain much better agreement with experiment. Specifically, we have written our own kinetic simulation code, using the same robust stiff integrator as is used in Tenua [18], and included a Monte Carlo procedure for modifying the rates, and for minimizing the *overall* root-mean-square (RMS) deviation χ between the calculated and experimental rates for all

the experimental conditions in which experimental data was reported [19]. The χ is defined by Equation 2.5.

$$\chi^2 = \sum_{i}^{n_{exp}} \left(\frac{R_{calc,i}}{R_{exp,i}} - 1 \right)^2 \quad (2.5)$$

The *ab initio* Gibbs free energies for each species and TS were obtained at each of the three values of *T*, a linear fit was made to extract corresponding enthalpy (*H)* and entropy (*S)* values, and for a selected set of species, random changes to these *H* and *S* values were then made, and the kinetic equations integrated again. Changes leading to a lower overall RMS error were kept, until an optimum fit was found. The *H* and *S* values were constrained to change with respect to the initial ab initio values by a maximum of respectively 4 kJ mol^{-1} and 0.035 kJ mol^{-1} K^{-1}, respectively. The resulting 'best fit' is also shown in Figure 2.3 for the same set of experimental conditions, and it can be seen that the predicted temperature dependence is hugely improved.

The species for which the enthalpy and entropy values were modified included **1**, **TS16n** and **TS16i**, because for bimetallic species CCSD(T) calculations could not be performed so these values arguably had a higher uncertainty. Also, given the uncertainty in assigning rate constants for diffusion-limited reactions, the enthalpy and entropy of the corresponding transition states were also allowed to change: diffusion of CO to **3**, diffusion of propene to **3** and CO diffusion to **6n** and **6i**. By carrying out such fitting, we reduce the overall RMS error of the rates for forming *n*- and *iso*-butyraldehyde under 34 different experimental conditions from 69% (as obtained with the raw CCSD(T) rate constants) to 22% (after fitting). Details of the raw and fitted kinetics are included in the Appendix A.

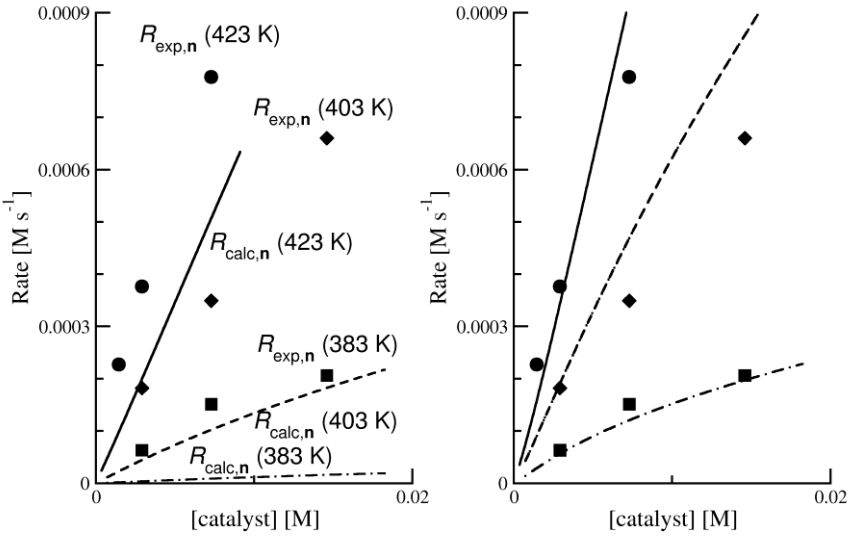

Figure 2.3 Calculated (lines) and experimental (dots) rates for forming *n*-butyraldehyde, as a function of overall catalyst concentration [Co], with the raw ab initio rate constants (left) and the fitted values (right). In each case, $p_{CO} = p_{H2} = 50$ bar, and [alkene] = 1.19 M. The circles and the solid line are for $T = 423$ K, The diamonds and dashed line are for $T = 403$ K, and the squares and dot-dashed line are for $T = 383$ K.

Inspecting the nature of the adjustments confirms the interpretation suggested above. The diffusion-limited step for addition of alkene to [$HCoCO_3$] **3** has its entropy adjusted upwards by 0.033 kJ mol^{-1} K^{-1} (equivalent to a drop in G at 423 K of 14 kJ mol^{-1}). Despite a slight compensating increase in its enthalpy, by 1 kJ mol^{-1}, this leads to the corresponding rate constant becoming larger by a factor of about 35 at all temperatures. The effect of this is that this alkene addition step changes from becoming almost entirely turnover-limiting at the lower T when using the raw *ab initio* free energies (shown by the rate of the *forward* reaction being much larger than that of the *reverse* reaction, $R_f/R_r = 48$ at 383 K, with typical values of [catalyst] = 2.92×10^{-3} M, [propene] = 1.19 M, $p_{CO} = p_{H2} = 50$ bar) to being only partly rate-limiting with the

adjusted values (the forward and reverse rates are now more similar, R_f/R_r = 1.5 at the same T and concentrations). The turnover-limiting step with the adjusted free energies shifts to being mainly the reductive elimination steps through the transitions states **TS12** and **TS16**. These three bottlenecks are in fact quite finely balanced in terms of their impact on the rate of turnover, with the role of each of them varying quite strongly depending on the temperature, the concentrations of the different reagents, and of course the assumed H and S values. Additional comparisons between experimental and calculated (raw and fitted) rates are shown in the Appendix A.

The purpose of carrying out the fitting is not to claim that the fitted values and the associated kinetic model are necessarily correct, but merely to show that the relatively small deviations between the raw calculated rates and the experimental values can be accounted for by very small adjustments to the calculated free energies, well within the expected error bars of the computational approach.

As in our previous study, the calculated kinetics provides extensive insight into various aspects of the mechanism. We report some such values here for the ab initio (not fitted) model For example, the speciation of the cobalt-containing species can be considered. For $p_{CO} = p_{H2}$ = 50 bar, [propene] = 1.19 M, [catalyst] = 2.92×10^{-3} M, and T = 423 K, most of the cobalt is predicted to be present as $HCo(CO)_4$ (4.85×10^{-3} M) , with just 0.29×10^{-3} M of $Co_2(CO)_8$, 0.29×10^{-3} M of **7n** and **7i**, 0.11×10^{-3} M of **11n** and **11i**, and tiny amounts of all other species. The rate of formation of the propane by-product can also be predicted: it is quite strongly T-dependent, being just 2×10^{-8} M s^{-1} at 383 K, only 0.3% of the rate of hydroformylation, but rising to 8×10^{-6} M s^{-1} at 423 K, or about 2.5 % of the rate of hydroformylation (very similar to the value we reported previously [8]).

Another interesting aspect is the relative contribution of the 'standard', H_2-induced cleavage of the Co-C bond via **TS12**, and the

bimetallic cleavage through **TS16**. We find that our model predicts that both can contribute, with the raw model predicting a total (n+i) rate through **TS12** of 3.4×10^{-4} M s^{-1} (same conditions as above), and through **TS16** of 4.6×10^{-5} M s^{-1}, just over 10%. This rises to roughly 30 % upon dropping the temperature to 383 K, and is also somewhat higher in the fitted model. While the accuracy of the calculations cannot allow us to make a firm conclusion about the role of this mechanism, especially as we have only used DFT to study **TS16**, it does appear likely that it plays a role, especially at lower temperatures, in agreement with experiment [11]. This is important because it is much more *n*-selective than the mechanism through **TS12**.

2.3 Conclusions

In this study, we have used accurate DFT and CCSD(T) electronic structure calculations to explore the potential energy surfaces for hydroformylation of propene by $Co_2(CO)_8$. We also used transition state theory and kinetic modelling to assess the emerging kinetics arising from our calculated energies, and compared them to experimental data for this important industrial transformation. Our raw kinetic model, based entirely on the *ab initio* free energies, provides a good agreement with experiment, with a RMS error on calculated rates of 69 %. This means that the ratio of the calculated and experimental rates is on average between 0.3 and 1.7, i.e. the calculated rates are in error by less than a factor of 3 (this is an average – the worst rate differs from experiment by a factor of 15). This confirms that the calculations can provide quantitative insight into the mechanism of the reaction, and implies that the errors on the key free energies in our calculations are approaching chemical accuracy: an error by a factor of 3 at 423 K corresponds to an error of less than 4 kJ mol^{-1}.

Nevertheless, the model is not by any means perfect, and in particular the consideration of the predicted temperature dependence of the rate, and of the predicted *n*/*i* selectivity (both of

which were not included in our previous study [8]) highlighted some issues. First, we found that a pathway degeneracy or symmetry factor [16] most likely plays a key role in leading to the experimentally well-known *n* selectivity of hydroformylation. Omitting this factor leads to very low or inverse selectivity. Next, we find that our raw model apparently overestimates the free energy of the diffusional barrier for addition of alkene to the 16-electron unsaturated **3** $HCo(CO)_3$ species. As a consequence, this step becomes wholly turnover-limiting, and this in turn leads to an exaggerated magnitude for the predicted temperature dependence of the rate. A very slight adjustment of the calculated free energies leads to much improved agreement with the experimental temperature dependence which can be traced back to a role for the lower-energy reductive elimination transition states **TS12** and **TS16** in determining the turnover rate.

Our model also suggests that a bimetallic mechanism for formation of aldehyde, through reaction of **1** $HCo(CO)_4$ with **9** $RCO\text{-}Co(CO)_3$ over **TS16**, can play a role even at the temperatures typically used for catalysis. This reaction had already been shown to contribute at lower temperature [11].

2.4 Computational Details

For all presented structures geometry optimizations were carried out at the DFT level of theory with the B3LYP (Becke, three-parameter, Lee-Yang-Parr) [20] functional including Grimme's dispersion correction with Becke-Johnson damping [21] as implemented in Gaussian09 [22] using ultrafine grid and the standard 6-311G(d) basis set [23] for all atoms. In the paper only species and conformers relevant for the kinetic simulations are shown and discussed. However many more structures were explored and more information on all structures can be found in the Appendix A. Single-point energy calculations were performed on the optimized structures at the CCSD(T) level of theory, with the Molpro quantum chemistry software [24], using a flexible basis set

(Co - aug-cc-pwcvtz, H, O and C - cc-pvdz) and an approach involving explicit treatment of interelectronic correlation – the CCSD(T)-F12 approach [25]. Separate CCSD(T) calculations without F12 treatment were carried out with and without using the 2nd order Douglas Kroll method [26] to compute the one-electron integrals, and the difference in the energies obtained was used to generate a correction for relativistic effects. Unfortunately the species that contain two cobalt atoms are characterized by a multireference behaviour and are also too large for coupled cluster calculations to be performed, hence for these species only DFT values are available. For the precatalyst **1** the presented relative energy is based on the DFT energies of **1**, **2** and H_2. A different approach was taken for the species involved in a pathway leading to butyraldehyde production by catalyst cleavage. These are the species in which there is an interaction between species **9** and the catalyst **2** itself. As these species ultimately derive from **9**, we have assumed that DFT describes their energy relative to **9** correctly. Hence their final relative energy values are calculated from the following equation: $\Delta E_{final} = \Delta E_{DFT} + (\Delta E_{9CCSDT} - \Delta E_{9DFT})$, which means that to the DFT stationary point energy of a species the CCSD(T) correction was added. That correction was assumed to be the difference between the CCSD(T) energy and the DFT energy of species **9n** and **9i** for aldehyde production by catalyst in the n-cycle and i-cycle respectively. No similar correction for the catalyst species **2** is need as it is the reference species, so its relative energy is zero in both levels of theory.

The presented ΔG values are for a mixed standard state of 1 atm for gases (H_2 and CO) and 1 M = 1 mol dm^{-3} for the rest of molecules (solutes) and a temperature of 423 K. Care was taken to symmetrise all symmetric species so the rotational symmetry number is already included in the G values. The values of G were calculated using the simple quasiharmonic correction, similar to the one proposed before by Truhlar et al [17], however in this paper the boundary value for low frequency vibrations was set to

50 cm^{-1}. The presented ΔG is obtained by combining the single point relative energies ΔE values calculated at the CCSD(T) level of theory and the Gibbs free energy correction calculated using frequencies and structures from DFT.

For simulation of rates we used numerical integration of the kinetic equations, holding the concentration of propene and the pressures of CO and H_2 fixed in time; rates were obtained upon reaching steady-state. For this purpose, we have used the Tenua program [18] as well as our own code; this latter has the ability to minimize the overall difference between calculated and experimental rate constants for a number of different reaction conditions using a least-squares approach while allowing adjustment of the underlying free energies and free energies of activation.

2.5 References

[1] a) O. Roelen. German Patent., DE 849548, **1938**; b) O. Roelen, U.S. Patent. 2,327,066 **1943**; c) B. Cornils, W. A. Hermann, M. Rash, *Angew. Chem*. **1994**, 33, 2144-2163.

[2] A. Behr, P. Neubert, *Applied Homogeneous Catalysis*, Bergstr Wiley-VCH, Weinheim **2012**, pp. 281.

[3] F. Hebrard, P. Kalck, *Chem. Rev.* **2009**, 109, 4272–4282.

[4] R. Franke, D. Selent, A. Börner, *Chem. Rev.* **2012**, 112, 5675–5732.

[5] T. Kégl, *RSC Adv*. **2015**, 5, 4304–4327.

[6] C.-F. Huo, Y.-W. Li, M. Beller, H. Jiao, *Organometallics* **2003**, 22, 4665-4677;

[7] a) S. Maeda, K. Morokuma, *J. Chem. Theory Comput.* **2012**, 8, 380–385; b) S. Maeda, T. Taketsugu, K. Morokuma, *J. Comput. Chem.* **2014**, 35, 166–173; c) S. Habershon, *J. Chem. Phys.* **2015**, 143, 094106; d) J. A. Varela, S. A. Vázquez, E. Martínez-Núñez, *Chem. Sci.* **2017**,8, 3843-3851.

[8] L. E. Rush, P. G. Pringle, J. N. Harvey, *Angew. Chem.* **2014**, 126, 8816 –8820.

[9] a) R. F. Heck, D. S. Breslow, *J. Am. Chem. Soc.* **1961**, 83, 4023 – 4027; b) R. F. Heck, *Acc. Chem. Res.* **1969**, 2, 10 – 16.
[10] N. H. Alemdaroğlu, J. M. L. Penninger, E. Oltay, *Mh. Chem.* **1976**, 107, 1153-1165.
[11] I. Kovács, F. Ungváry, L. Markó, *Organometallics* **1986**, 5, 209-215.
[12] a) F. Ungváry, J.Organomet. Chem 1972, 36, 363-370; b) J. W. Rathke, R. J. Klingler, T. R. Krause, Organometallics 1992, 11, 585-588.
[13] M. Kalek, F. Himo, *J. Am. Chem. Soc.* **2017**, *139*, 10250-10266; M. Jaraiz, L. Enriquez, R. Pinacho, J. E. Rubio, A. Lesarri, J. L. Lopez-Perez, *J. Org. Chem.* **2017**, 82, 3760-3766; M. Besora, F. Maseras, *WIREs Comp. Mol. Sci.* **2018**, e1372.
[14] K. J. Laidler, *Chemical Kinetics, 3rd ed.,* Harper & Row, New York, **1987**.
[15] A. H. Krall, J. V. Sengers, J. Kestin, *J. Chem. Eng. Data* **1992**, 37, 349 – 355.
[16] a) A. Fernández-Ramos, B. A. Ellingson, R. Meana-Pañeda, J. M. C. Marques, D. G. Truhlar, *Theor. Chem. Account* **2007**, 118, 813-826; b) M. K. Gilson, K. K. Irikura, *J. Phys. Chem. B* **2010**, 114, 16304–16317.
[17] a) R. F. Ribeiro, A. V. Marenich, C. J. Cramer, D. G. Truhlar, *J. Phys. Chem. B* **2011**, 115, 14556–14562; b) Y. Zhao, D. G. Truhlar, *Phys. Chem. Chem. Phys.* **2008**, 10, 2813–2818.
[18] D. Wachsstock*, Tenua 2.1—the kinetics simulator for Java, by Daniel Wachsstock, MD*. http://bililite.com/tenua/.
[19] a) R. V. Gholap, O. M. Kut, J. R. Bourne, *Ind. Eng. Chem. Res*. **1992**, 31, 1597-1601; b) R. V. Gholap, O. M. Kut, J. R. Bourne, *Ind. Eng. Chem. Res*. **1992**, 31, 2446-2450.
[20] A. D. Becke, *J. Chem. Phys.* **1993**, 98, 5648–5652.
[21] S. Grimme, S. Ehrlich, L. Goerigk, *J. Comp. Chem*. 2011, 32, 1456-1465.
[22] Gaussian 09, Revision E.01, M. J. Frisch, G. W. Trucks, H. B. Schlegel, G. E. Scuseria, M. A. Robb, J. R. Cheeseman, G. Scalmani,

V. Barone, B. Mennucci, G. A. Petersson, H. Nakatsuji, M. Caricato, X. Li, H. P. Hratchian, A. F. Izmaylov, J. Bloino, G. Zheng, J. L. Sonnenberg, M. Hada, M. Ehara, K. Toyota, R. Fukuda, J. Hasegawa, M. Ishida, T. Nakajima, Y. Honda, O. Kitao, H. Nakai, T. Vreven, J. A. Montgomery, Jr., J. E. Peralta, F. Ogliaro, M. Bearpark, J. J. Heyd, E. Brothers, K. N. Kudin, V. N. Staroverov, T. Keith, R. Kobayashi, J. Normand, K. Raghavachari, A. Rendell, J. C. Burant, S. S. Iyengar, J. Tomasi, M. Cossi, N. Rega, J. M. Millam, M. Klene, J. E. Knox, J. B. Cross, V. Bakken, C. Adamo, J. Jaramillo, R. Gomperts, R. E. Stratmann, O. Yazyev, A. J. Austin, R. Cammi, C. Pomelli, J. W. Ochterski, R. L. Martin, K. Morokuma, V. G. Zakrzewski, G. A. Voth, P. Salvador, J. J. Dannenberg, S. Dapprich, A. D. Daniels, O. Farkas, J. B. Foresman, J. V. Ortiz, J. Cioslowski, and D. J. Fox, Gaussian, Inc., Wallingford CT, **2013**.

[23] a) K. Raghavachari, J. S. Binkley, R. Seeger, J. A. Pople, *J. Chem. Phys.* **1980**, 72, 650-654; b) A. D. McLean, G. S. Chandler, *J. Chem. Phys.* **1980**, 72, 5639-5648

[24] a) H.-J. Werner, P. J. Knowles, G. Knizia, F. R. Manby, M. Schütz, *WIREs Comput. Mol. Sci.* **2012**, 2, 242-253; MOLPRO, version 2012.1, a package of ab initio programs, H.-J. Werner, P. J. Knowles, G. Knizia, F. R. Manby, M. Schütz, P. Celani, T. Korona, R. Lindh, A. Mitrushenkov, G. Rauhut, K. R. Shamasundar, T. B. Adler, R. D. Amos, A. Bernhardsson, A. Berning, D. L. Cooper, M. J. O. Deegan, A. J. Dobbyn, F. Eckert, E. Goll, C. Hampel, A. Hesselmann, G. Hetzer, T. Hrenar, G. Jansen, C. Köppl, Y. Liu, A. W. Lloyd, R. A. Mata, A. J. May, S. J. McNicholas, W. Meyer, M. E. Mura, A. Nicklass, D. P. O'Neill, P. Palmieri, D. Peng, K. Pflüger, R. Pitzer, M. Reiher, T. Shiozaki, H. Stoll, A. J. Stone, R. Tarroni, T. Thorsteinsson, and M. Wang, , see http://www.molpro.net.

[25] a) T. B. Adler, G. Knizia, H.-J. Werner, *J. Chem. Phys*. **2007**, 127, 221106; b) H.-J. Werner, G. Knizia, F. R. Manby, *Mol. Phys.* **2011**, 109, 407-417.

[26] a) M. Reiher, A. Wolf, *J. Chem. Phys.* **2004**, 121, 2037-2047; b) M. Reiher, A. Wolf, *J. Chem. Phys.* **2004**, 121, 10945-10956; c) A. Wolf, M. Reiher, B. A. Hess, *J. Chem. Phys.* **2002**, 117, 9215-9226.

Chapter 3

Predictive Methane Activation by Alternant N_2O_2 and N_2S_2 Cluster Radical Cations

The content of this chapter is a reproduction of the manuscript submitted for publication in *International Journal of Mass Spectrometry*.

The changes compared to the submitted manuscript include the page layout and the numbering of tables and figures that have been modified in order to match the style and the format of this thesis. Figure 3.1 has been modified and extended to present four instead of one molecular orbitals of each discussed radical species. Additional discussion concerning future work possibilities has been added to conclusions.

My contribution to the work presented involved theoretical calculations, data analysis, preparation of the first version of the manuscript. The discussion of the results was done together with the co-authors, Xabier Lopez and Jesus Ugalde. Writing of the final manuscript was conducted together with Jesus Ugalde.

Abstract: Methane activation reaction by small alternant N_2Y_2 (Y = O, S) radical cation rings is predicted by the methods of computational chemistry. Approximate density functional theory and coupled cluster singles and doubles with perturbative triples calculations are employed to investigate the potential energy surface of this putative reaction. On the contrary to previously reported methane activation processes by square planar four-membered rings following the proton coupled electron transfer

mechanism, the $[N_2O_2]^{\bullet+}$ and $[N_2S_2]^{\bullet+}$ clusters according to our results may activate methane but with a hydrogen atom transfer mechanism.

3.1 Introduction

Methane is nowadays indicated as one of the potential sustainable substrates for chemical commodities such as polymers, plasticizers or solvents. This compound is a main component of natural gas, of which there are still abundant resources (both conventional and of technically recoverable shale gas) and of biogas – a renewable alternative to fossil fuels. As a matter of fact methane is already indirectly used by industry as a source of carbon in synthetic chemistry, though it has to be firstly transformed into syngas ($CO + H_2$) through high temperature energy intensive steam reforming process. One of the challenges of modern catalysis would be to functionalize methane directly into higher value products, in controlled mild temperature processes [1]. This goal has been found to be very challenging due in particular to the significant stability of non-polar CH_4 molecule [2].

Schwarz et al. have developed a protocol for the precise study of methane activation by small molecules and clusters. Their extensive studies have provided both key experimental and theoretical insight into the catalytic methane activation [3]. In this vein, relevant to the purpose of the present investigation is the recent communication regarding the activation of methane by the square planar aluminium oxide radical cationic cluster $[Al_2O_2]^{\bullet+}$ [4] and, the oxidation to methanol by $Si_2O_4^{\bullet+}$ [5].

In general, the activation of methane by oxide clusters may proceed following two major mechanisms [6], see Scheme 3.1. The first one refers to the hydrogen atom transfer (HAT) mechanism, for which it is agreed that the spin density of the open-shell species localized on the atom abstracting the hydrogen plays the crucial role in facilitating the hydrogen abstraction from methane. When

the spin density is not localized on the atom forming the new bond with the methane's hydrogen, the system would have to undergo an additional electronic reorganization resulting in higher HAT barriers. Conversely, CH_4 may be also activated by heterolytic cleavage of C-H bond through the so-called proton-coupled electron transfer (PCET) mechanism, which was proved to be the preferred mechanism when $Al_2O_2^{\bullet+}$ acts as the catalyst [4].

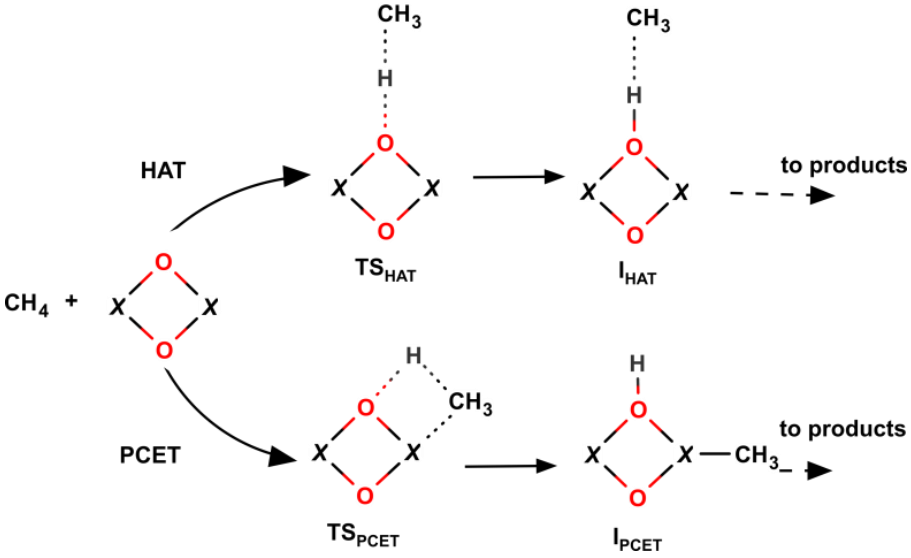

Scheme 3.1 The simplified HAT and PCET mechanisms of methane activation by oxide clusters.

In our group we have studied similar four member alternant ring clusters of the X_2Y_2 form, in which X is a pnictogen atom (N, P, As and Sb) and Y is a chalcogen atom (O, S, Se and Te) [7]. These ring compounds in their neutral form could adopt either butterfly or planar geometry. According to the previously conducted multireference calculations the clusters containing oxygen and/or nitrogen were more stable as the planar isomers, and most of them possessed significant biradicaloid character. Consequently, their corresponding cations should have a radical character similar to the one of $Al_2O_2^{\bullet+}$. Based on this circumstance it seems worth exploring whether the $X_2Y_2^{\bullet+}$ cationic radical clusters could carry the CH_4 activation as well. In this paper we present a theoretical

mechanistic investigation of the catalysis of methane by these species. This investigation is focused on three smallest chalcogen pnictogen rings, namely $N_2O_2^{\bullet+}$, $N_2S_2^{\bullet+}$ and $P_2O_2^{\bullet+}$, whose corresponding neutral species have been characterized earlier. Thus, a number of low lying N_2O_2 isomers have been studied theoretically, and the planar ring isomer was located at 43.9 kcal mol^{-1} above the lowest lying NO + NO species [8]. However, it was suggested that higher energy isomers could also be prepared [9]. Indeed, some of them have been detected experimentally [10]. On the other hand, P_2O_2 isomers were detected in a matrix environment reaction [11] and the accompanying theoretical study showed that on the contrary to N_2O_2, the cyclic isomer lies below PO + PO dissociation products [12] with the alternant square-ring planar geometry being the most stable isomer [13]. The N_2S_2 alternant ring cluster is the most intensively studied species among the rings investigated in this paper. Its crystal X-ray structure has been analyzed [14] pointing to the nearly square planar geometry. These results were confirmed for the isolated molecule in solid gas matrices [15]. It polymerizes at room temperature to a metallic polymer, exhibiting superconducting properties at very low temperatures [16]. The electronic structure of N_2S_2 has been under fierce debate [17], with latest calculations suggesting that it possesses an open-shell singlet spin-state diradical character with the radical electrons located on nitrogen atoms.

3.2 Computational methods

In order to study the putative methane activation reaction by alternant $X_2Y_2^{\bullet+}$ clusters, the potential energy surface (PES) of the process was explored at the DFT level of theory. The calculations were done using B2-PLYP functional [18] combined with Grimme's dispersion with Becke-Johnson damping (D3BJ) [19]. For all atoms the standard 6-311g(d) [20] basis set was used. On top of the geometry optimizations, the frequency calculations were conducted in order to confirm the nature of each optimized

stationary point – only positive frequency values for minima on PES, and one imaginary frequency for transition states (TS). Subsequently the intrinsic reaction coordinate (IRC) calculations were conducted for each TS in order to check which minima are connected by the particular TS. For some of the bimolecular reactions no barrier was found – for these processes a number of geometry relaxed scans were performed to confirm that the reaction proceeds without a TS. Furthermore, to confirm the validity of the results obtained employing DFT calculations, some of the structures were again optimized with two more functionals, namely M06-2X [21] with D3 dispersion correction [22] and ωB97X-D [23] which includes empirical dispersion, in both cases with 6-311g(d)+ basis set on all atoms. All DFT methods gave consistent information of reaction PES (see the Appendix B). As it is commonly accepted, the geometries of molecular structures are less dependent on the level of theory than their energies, so coupled cluster singles and doubles with perturbative triples (CCSD(T)) single-point energy calculations with Dunning aug-cc-pvtz [24] basis set were performed on the structures optimized with B2-PLYP functional, resulting in a very good agreement of DFT and CCSD(T) energies for the majority of the structures. The T1 diagnostic for all structures was smaller than 0.044, so it was assumed that CCSD(T) may reliably describe the investigated system [25]. The Mulliken spin densities presented are calculated at Hartree-Fock level of theory while the atomic polar tensor (APT) charges are calculated at DFT level of theory. All calculations have been conducted using Gaussian16 program [26]. Further information regarding the theoretical protocols that could be used for study of the reactivity of gas phase ions may be found in ref. [27]. Additional details of the calculations carried out together with Cartesian coordinates of all optimized structures are included in Appendix B.

3.3 Results and Discussion

In our investigation we have focused on the exploration of the doublet PES for the reaction of the radical cation rings with methane. The study of the catalytic activity of these radical cations is motivated by previously reported results [4] in which methane activation by oxide cations $[XYO_2]^{\bullet+}$ (X, Y = Al, Si, Mg) was investigated and it was shown both experimentally, and theoretically, that $[Al_2O_2]^{\bullet+}$ was indeed able to cleave C-H bond of methane. It is worth recalling that the computational mechanistic study of the latter reaction suggested that it follows the PCET pathway rather than HAT.

In Figure 3.1 the structures of three pnictogen chalcogen radical ring cations, namely $N_2O_2^{\bullet+}$, $P_2O_2^{\bullet+}$ and $N_2S_2^{\bullet+}$ studied in this paper as potential catalysts in methane activation, are depicted along with their corresponding singly occupied molecular orbitals (SOMO), in which the unpaired electron is localized according to the conducted DFT calculations. Both of the oxide clusters that were found to be the lowest energy structures possessed the planar D2h geometries. The spin density is distributed equally between the two nitrogen or phosphorous atoms and the radical electron is located on the highest occupied molecular orbital (HOMO), a π orbital localized on the pnictogen atoms. Surprisingly for the $N_2S_2^{\bullet+}$ species the D2h planar structure was not found to be the minimum species. Instead, the lowest energy ring-like structure possesses C2v symmetry, with a small dihedral angle of 163 degrees in which spin density is equally shared by the nitrogen atoms. The analysis of the canonical orbitals of this structure revealed that the SOMO was a π-type molecular orbital localized on both nitrogen atoms. This orbital was found to be lower in energy than the HOMO located in this species on sulphur atoms. Conventionally SOMO and HOMO for radical species should be the same orbital, however it is not always the case [28]. Additionally the stability of the DFT solution for this C2v electronic structure of

$N_2S_2^{\bullet+}$ was checked in a separate calculation and no internal instabilities were detected.

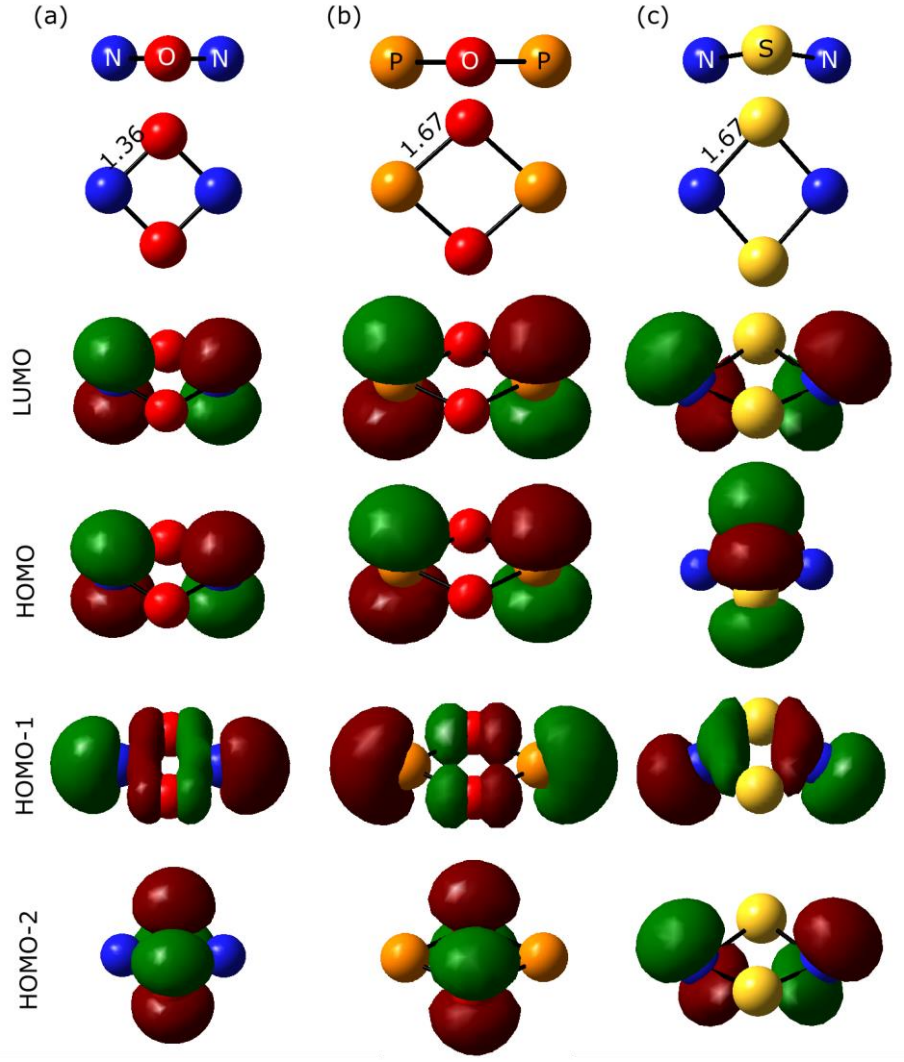

Figure 3.1 Geometries and orbitals of the studied radical cationic clusters: (a) $N_2O_2^{\bullet+}$, (b) $P_2O_2^{\bullet+}$, (c) $N_2S_2^{\bullet+}$. The presented occupied orbitals correspond to α orbitals, while the unoccupied orbitals shown here correspond to β orbitals. The SOMO for the oxygen containing species is labelled "HOMO" while for $N_2S_2^{\bullet+}$ it is the HOMO-2.

The smallest cluster investigated in this paper in the context of the σ-bond C-H bond activation of methane, was $N_2O_2^{\bullet+}$. For the

reaction with CH_4, no TS was located. The relaxed scan for the distance between the H atom of methane and the N atom of alternant $N_2O_2^{\bullet+}$ ring showed that the energy of the system was continuously getting smaller as both of the atoms were getting closer, leading to the minimum on the potential energy surface $\mathbf{I_{NO}}$ located at –55.4 kJ mol^{-1} relative to the entrance channel. The methane molecule approached the ring from above of the ring's plane, the reason being that in $N_2O_2^{\bullet+}$ cluster the unpaired electron is located on the π orbital on a nitrogen atoms. In $\mathbf{I_{NO}}$ species the N-H bond is formed and the radical is transferred to the carbon atom. The process ends with the formation of the $\mathbf{I_{NO}}$ complex between methyl $CH_3^{\bullet}$ and the hydride $[HN_2O_2]^+$ cationic ring. From this point, the reaction may proceed by separation of both moieties, yielding the methyl radical $CH_3^{\bullet}$ and hydride ring cation $[HN_2O_2]^+$ of Cs geometry. Observe, nonetheless that the products of such reaction lay +5.8 kJ mol^{-1} higher in energy than the reactants. The PES of this transformation is depicted in Figure 3.2.

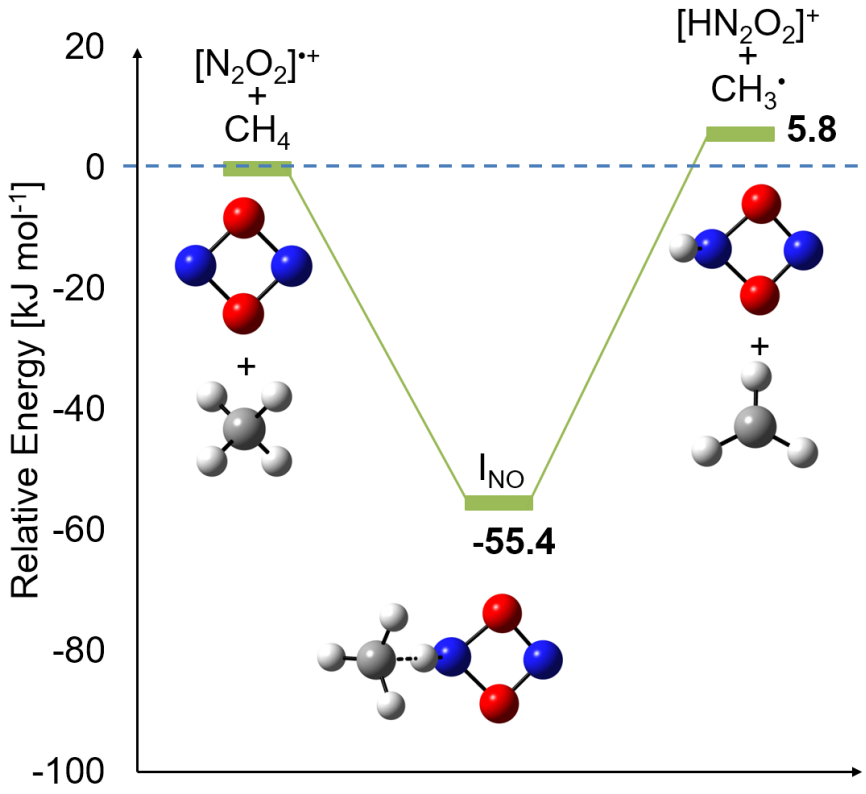

Figure 3.2 PES of CH_4 reaction with $N_2O_2^{\bullet+}$. The energies are calculated at the CCSD(T)/aug-cc-pvtz//B2-PLYP/6-311g(d) level of theory.

The reaction mechanism of the $N_2S_2^{\bullet+}$ cluster radical is more complex because in this case an initial encounter complex, **EC_{NS}**, is formed, stabilized by 23.3 kJ mol^{-1} with respect to the reactants. The interaction of the hydrogen of methane with the nitrogen atom of the cluster, see Figure 3.3, provides the stabilization energy for these feeble complex, which rearranges easily through **TS_{NS}** into the lowest energy species on the potential energy surface, the stable intermediate **I_{NS}**, localized at -82.8 kJ mol^{-1} below the reactants level. Inspection of the geometry and chemical bonding patterns of **TS_{NS}**, is very suggestive of a hydrogen atom abstraction like mechanism for this transformation. Finally, $CH_3^{\bullet}$ could diffuse

away from the produced $CH_3^{\bullet}$ ···$HN_2S_2^+$, complex **I_{NS}**, to yield $HN_2S_2^+$ (C2v geometry), and the methyl radical, which lie 40.0 kJ mol^{-1} below reactants level. This reaction is predicted to be thermodynamically favourable.

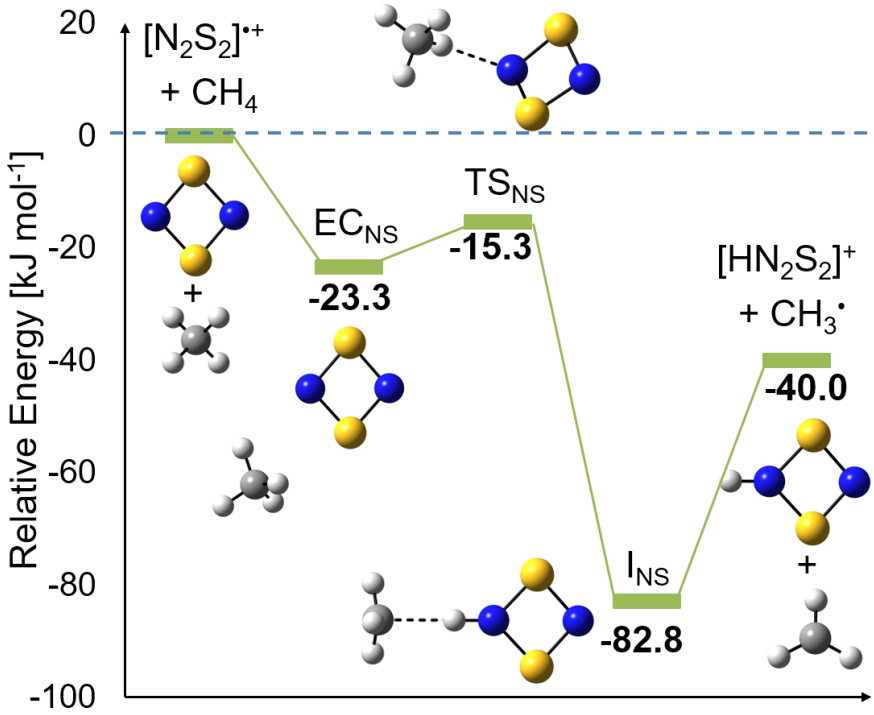

Figure 3.3 PES of CH_4 reaction with $N_2S_2^{\bullet+}$. The energies are calculated at the CCSD(T)/aug-cc-pvtz//B2-PLYP/6-311g(d) level of theory.

The mechanisms of the methane activation reactions just described for the $N_2O_2^{\bullet+}$ and $N_2S_2^{\bullet+}$ clusters show characteristics which differ markedly with respect to those of oxide clusters reported before by Schwarz et al. [4,5]. Thus, for the $N_2O_2^{\bullet+}$ and $N_2S_2^{\bullet+}$ clusters the activation of the C-H σ-bond of methane, follows a HAT type mechanism. However, it is worth mentioning that in these cases, it is not the oxygen atom (or sulphur atom) that

abstracts the hydrogen atom from methane, but it is the nitrogen atom. Since the unpaired electron of these radical cationic clusters is already located on the N atoms, the system does not have to undergo an electronic reorganization and the HAT is not burdened with an energy penalty. The mechanism for the CH_4 cleavage for studied systems differs from the one put forward in the introduction (See Scheme 3.1). The new HAT mechanism is sketched in Scheme 3.2.

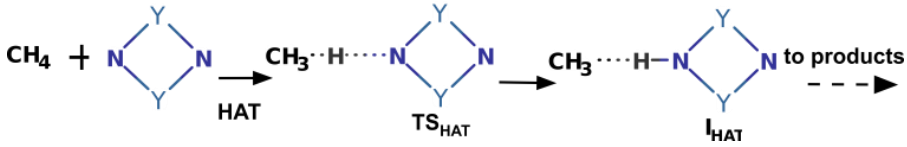

Scheme 3.2 Mechanism of HAT from methane by the $N_2Y_2^{\bullet+}$ (Y = O, S) clusters.

However, neither of the two reactions described so far, namely $N_2O_2^{\bullet+} + CH_4 \rightarrow HN_2O_2^{+} + CH_3^{\bullet}$ and $N_2S_2^{\bullet+} + CH_4 \rightarrow HN_2S_2^{+} + CH_3^{\bullet}$, will hardly stop with the hydrogen abstraction from methane, for the methyl radical is detached from the hydrido hydrogen and it could easily bind on the various heteroatomic centres of the hydrido cluster yielding markedly stable structures. Figure 3.4 shows the structures of the six distinct isomeric species resulting from the binding the $CH_3^{\bullet}$ methyl radical to $HN_2S_2^{+}$ and $HN_2O_2^{+}$ clusters. Observe that all such structures are largely stabilized with respect to their corresponding reactants' level. In all cases the positive charge is shared between the two moieties $HN_2Y_2^{\bullet}$ (Y = O, S) and CH_3, while the spin density mostly resides on the $HN_2Y_2^{\bullet}$ (Y = O, S) moiety. Recall that the lowest energy isomer for sulphur containing species, denoted as **Min1$_{NS}$** in Fig. 3.4, corresponds to the trans-$[(H)(CH_3)N_2S_2^{\bullet}]^{+}$, while **Min1$_{NO}$** of the corresponding structure for oxygen containing ring is less stable from the lowest lying **Min3$_{NO}$** isomer but only by 4.5 kJ mol^{-1}. Notice that structures **Min2** and **Min3** presented in Figure 3.4 have a localized unpaired electron at the unfunctionalized nitrogen atoms, as revealed by their

calculated spin densities. It is hypothesized that this nitrogen atom would likely react with a secondary methane molecule.

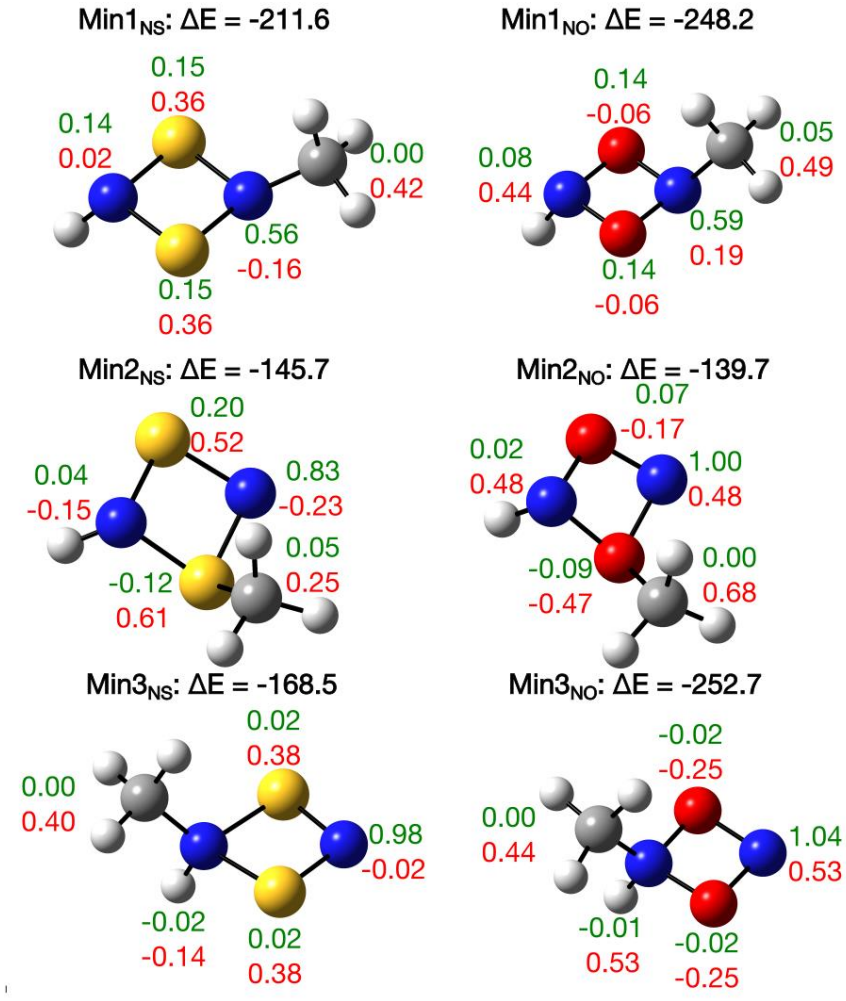

Figure 3.4 The spin densities and APT charges of the optimized structures of $[(CH_3)HN_2Y_2]^{\bullet+}$ (Y=O, S) compounds. Spin densities in green and APT charges in red. The stabilization energies with respect to $HN_2Y_2^+ + CH_3^\bullet$, ΔE, are in kJ mol^{-1}. The energies are calculated at the CCSD(T)/aug-cc-pvtz//B2-PLYP/6-311g(d) level of theory.

Additionally we have found that the structures could open their rings by dissociating homolytically their HN-Y (Y = O, S) bonds to yield low energy structures found in our search of the potential

energies surfaces. These minimum energy structures, **Min4** and **Min5**, sketched in Figure 3.5, possess a radical on the terminal HN group and consequently they could react with secondary methane molecules. In **Min5$_{NS}$** the charge is mainly localized on the sulphur atom adjacent to the HN group, and it is doubly bonded to its adjacent nitrogen, namely its chemical structure can formally be written as HN•-S$^+$=N-S-CH$_3$. The **Min5$_{NO}$** structure has also a localized radical on the HN nitrogen but inspection of the APT charges is suggestive of the following formal chemical structure: HN•-O-N$^+$-O-CH$_3$. Finally it worth mentioning that **Min4** structures could lose a NY$^+$($^1\Sigma$) dimer to yield [HNYCH$_3$]• (Y = O, S) radicals.

Full description of the geometries and vibrational spectra of species shown in Figures 3.4 and 3.5 can be found in the Appendix B together with the located reaction pathways.

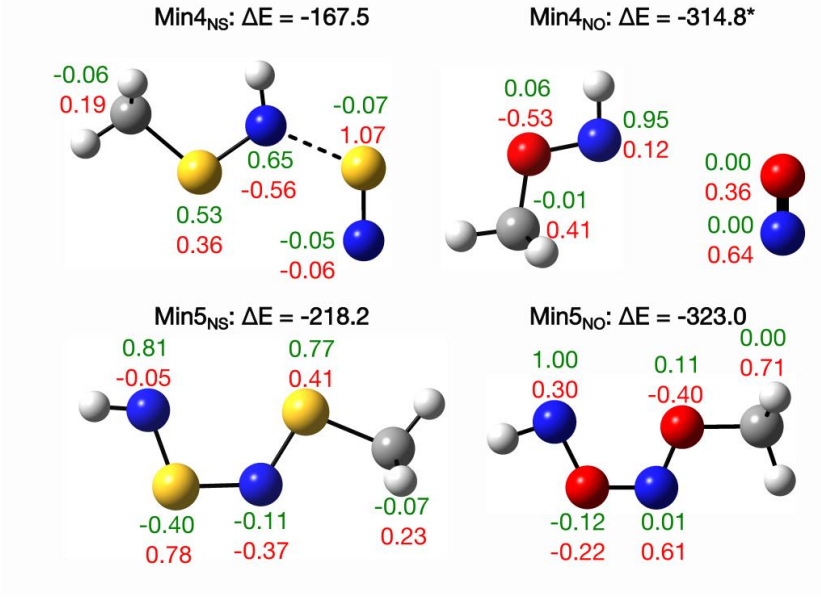

Figure 3.5 The spin densities and APT charges of the optimized open structures of [(CH$_3$)HN$_2$Y$_2$]$^{•+}$ (Y=O, S) compound. Spin densities in green and APT charges in red. The stabilization energies with respect to HN$_2$Y$_2^+$ + CH$_3$•, ΔE, are in kJ mol^{-1}. Data for Min4$_{NO}$ corresponds to the infinitely separated moieties of CH$_3$ONH• + NO$^+$. The energies are calculated at the CCSD(T)/aug-cc-pvtz//B2-PLYP/6-311g(d) level of theory.

In order to get deeper insight into the putative catalysis of methane activation by alternant X_2Y_2 rings it is worth to mention and analyse the cases which do not catalyse the reaction according to the performed calculations. In the third case study of methane activation yet another alternant pnictogen chalcogen cluster was investigated, namely $P_2O_2^{\bullet+}$, the cluster in which nitrogen atoms are replaced by heavier phosphorous homologues. This putative reaction was explored with unrestricted DFT method, employing B2-PLYP functional and 6-311g(d) basis set on all atoms as previously.

The energies of the system according to the performed relaxed scan in which the distance between H atom of methane and P atom of the ring is getting smaller are rising, on the contrary to the $N_2O_2^{\bullet+}$ case. The thermodynamics as well indicates that this reaction is not plausible. The probable products of $CH_4 + P_2O_2^{\bullet+}$ reaction, are less energetically stable than the reactants, $CH_3^{\bullet} + HP_2O_2^{+}$ lying at +155.4 kJ mol^{-1} relatively to $CH_4 + P_2O_2^{\bullet+}$. This theoretical observation is as well in accordance to the chemical intuition. Even though the radical cluster may accommodate the H atom the newly formed P-H bond is much weaker than the C-H bond so the reaction is thermodynamically disfavoured.

To confirm the hypothesis about bond strength importance the silane (SiH_4) activation PES was explored (Figure B.8 in Appendix B). Indeed the relaxed scan between H atom of SiH_4 and P atom of $P_2O_2^{\bullet+}$ showed that hydrogen is abstracted by the ring spontaneously without any corresponding barrier leading to the intermediate lying lower in energies than reactants (ΔE_{DFT} = -40.1 kJ mol^{-1}). The Si-H bond is much weaker so it can be more easily broken compared to the C-H strong bond.

Interestingly the TS corresponding to PCET mechanism for CH_4 activation was located for the phosphorous-oxygen radical (Figure B.7 in Appendix B), again on the contrary to the smaller nitrogen oxygen ring. However it lies very high in relative energies (ΔE_{DFT} = 184.1 kJ mol^{-1}). Due to the very high PCET barrier this

mechanism cannot be an attractive route for methane activation but it points to the possible conclusion that due to the higher electronegativity difference between P and O atoms compared to N and O atoms the charges in the former cluster are more separated and this explains why PCET TS could be located for $P_2O_2^{\bullet+}$ but not for $N_2O_2^{\bullet+}$ reacting with CH_4. PCET mechanism may be more plausible in case of larger charge separation and the Lewis acid-base character of H abstracting ring.

3.4 Conclusions

The present computational study based on the tools of quantum chemistry of the putative CH_4 activation by alternant $N_2Y_2^{\bullet+}$ (Y = O, S) radical cations has been performed employing both approximate DFT and CCSD(T) calculations, revealing that the HAT mechanism of methane activation by these species is plausible. For the sake of completeness, the approximate DFT investigation of the implausible C-H σ-bond activation of methane by $P_2O_2^{\bullet+}$ has also been presented. Both positive and negative results for the methane activation using alternant pnictogen chalcogen rings coming out from the calculations as presented in this paper emphasize the advantages of using computational techniques in rational catalysts' design. The analysis of Mulliken spin densities and APT charges of the low energy structures obtained after the reaction of methyl radical with $HN_2Y_2^+$ (Y = O, S) revealed that in these species the unpaired electron is again mostly localized on the nitrogen atom. This may suggest that this species could in principle activate another methane molecule. However it may be recommended to validate the performed analysis of atomic charges and spin densities with more accurate methods [29] in future. Moreover, the investigation of the PES of the reaction with a second methane molecule could be the subject of subsequent study on the presented system.

The conclusions of this paper are the following. Firstly the radical cluster cations $N_2Y_2^{\bullet+}$ (Y = O, S) should be able to activate

methane. Secondly, as shown for $P_2O_2^{\bullet+}$, the spin density on the atom abstracting hydrogen is not enough for the HAT to happen. The newly formed X-H bond has to be of the relatively same strength as the broken C-H bond, and the reaction thermodynamically plausible. Thirdly, in accordance with the results of our calculations the CH_4 activation by $N_2O_2^{\bullet+}$ and $N_2S_2^{\bullet+}$ clusters should follow the HAT mechanism. In particular, the methane's hydrogen will be transferred to the nitrogen atom of the radical cluster cation. Furthermore, the resulting methyl radical will further attack the so-formed hydrido cluster to yield $NY^+(^1\Sigma)$ and $[HNYCH_3]^\bullet$ and $[HNYNYCH_3]^{\bullet+}$ ($^2A'$), (Y = O, S), species. Fourthly, secondary reactions may occur given the presence of N-radical species as products of the primary reaction. Fifthly, all these considerations await experimental confirmation.

3.5 References

[1] A. I. Olivos-Suarez, À. Szécsényi, E. J. M. Hensen, J. Ruiz-Martinez, E. A. Pidko, J. Gascon, *ACS Catal.* **2016**, 6, 2965–2981.

[2] (a) H. Schwarz, Angew. Chem. Int. Ed. **2011**, 50, 10096 – 10115; (b) P. B. Armentrout, Chem. Eur. J. **2017**, 23, 10 – 18

[3] H. Schwarz, S. Shaik, J. Li, *J. Am. Chem. Soc*. **2017**, 139, 17201–17212.

[4] J. Li, S. Zhou, J. Zhang, M. Schlangen, T. Weiske, D. Usharani, S. Shaik, H. Schwarz, *J. Am. Chem. Soc.* **2016**, 138, 7973–7981.

[5] X. Sun, S. Zhou, M. Schlangen, H. Schwarz, *Chem. Eur. J.* **2017**, 23, 1498 – 1501.

[6] J. Li, S. Zhou, J. Zhang, M. Schlangen, D. Usharani, S. Shaik, H. Schwarz, *J. Am. Chem. Soc.* **2016**, 138, 35, 11368–11377.

[7] J. M. Mercero, X. Lopez, J. E. Fowler, J. M. Ugalde, J. Phys. Chem. A, 1997, 101, 5574-5579.

[8] K. A. Nguyen, M. S. Gordon, J. A. Montgomery, Jr., H. H. Michels, *J. Phys. Chem*. **1994**, 98, 10072-10078.

[9] M. A. Vincent, I. H. Hillier, L. Salsi, *Phys. Chem. Chem. Phys.* **2000**, 2, 707-714.

[10] D. W. Arnold, D. M. Neumark, *J. Chem. Phys.* **1995**, 102, 18, 7035-7045; R. Li, . E. Continetti, *J. Phys. Chem*. A **2002**, 106, 1183-1189.
[11] L. Andrews, M. McCluskey, Z. Mielke, R. Withnall, *J. Mol. Struct.* **1990**, 222, 95-108.
[12] P. J. Bruna, M. Mühlhäuser, S. D. Peyerimhoff, *Chem. Phys. Lett.* **1991**, 180, 6, 606-612.
[13] M. Mühlhäuser, B. Engels, M. Ernzerhof, Ch. M. Marian, S. D. Peyerimhoff, *J. Phys. Chem.* **1996**, 100, 120-122.
[14] C. M. Mikulski, P. J. Russo, M. S. Saran, A. G. MacDiarmid, A. F. Garito, A. J. Heeger, *J. Am. Chem. Soc.* **1975**, 97, 6338.
[15] R. Evans, A. J. Downs, R. Köppe, S. C. Peake, *J. Phys. Chem. A* **2011**, 115, 5127–5137.
[16] A. J. Banister, I. B. Gorrell, *Adv. Mater.* **1998**, 10, 17, 1415-1429.
[17] See, for example, (a) S. Millefiori, A. Millefiori, *Inorganica Chimica Acta* **1980,** 45, L19-L22; (b) J. Gerratt, S. J. McNicholas, P. B. Karadakov, M. Sironi, M. Raimondi, D. L. Cooper, *J. Am. Chem. Soc.* **1996**, 118, 6472-6476; (c) R. D. Harcourt, T. M. Klapötke, A. Schulz, P. Wolynec, *J. Phys. Chem. A* **1998**, 102, 1850-1853; (d) R. C. Mawhinney, J. D. Goddard, *Inorg. Chem.* **2003**, 42, 6323-6337; (e) H. M. Tuononen, R. Suontamo, J. Valkonen, R. S. Laitinen, *J. Phys. Chem. A* **2004**, 108, 5670-5677; (f) F. Breher, *Coordin. Chem. Rev.* **2007**, 251, 1013–1014; (g) Y. Zhang , Y. Xu, Q. S. Li, *Molecular Physics* **2007**, 105, 10, 1883–1889; (g) B. Braïda, A. Lo, P. C. Hiberty, *ChemPhysChem* **2012**, 13, 811 – 819; R. D. Harcourt, *ChemPhysChem* **2013**, 14, 2859 – 2864.
[18] S. Grimme, *Chem. Phys.* **2006**, 124, 034108.
[19] (a) L. Goerigk, S. Grimme, *J. Chem. Theory Comput.* **2011**, 7, 291–309; (b) S. Grimme, S. Ehrlich, L. Goerigk, *J. Comput. Chem.* **2011**, 32, 7, 1456-1465.
[20] (a) K. Raghavachari, J. S. Binkley, R. Seeger, J. A. Pople, J. Chem. Phys. 1980, 72, 650-654; (b) K. Raghavachari, G. W. Trucks, J. Chem. Phys. 1989, 91, 1062-65.

[21] Y. Zhao, D. G. Truhlar, *Theor. Chem. Acc.* **2008**, 120, 215-41.
[22] S. Grimme, J. Antony, S. Ehrlich, H. Krieg, *J. Chem. Phys.* **2010**, 132, 154104.
[23] J. D. Chai, M. Head-Gordon, *Phys. Chem. Chem. Phys.* **2008**, 10, 6615-6620.
[24] R. A. Kendall, T. H. Dunning Jr., R. J. Harrison, *J. Chem. Phys.* **1992**, 96, 6796-6806.
[25] J. C. Rienstra-Kiracofe, W. D. Allen, H. F. Schaefer III, *J. Phys. Chem. A* **2000**, 104, 9823-9840.
[26] M. J. Frisch, G. W. Trucks, H. B. Schlegel, G. E. Scuseria, M. A. Robb, J. R. Cheeseman, G. Scalmani, V. Barone, G. A. Petersson, H. Nakatsuji, X. Li, M. Caricato, A. V. Marenich, J. Bloino, B. G. Janesko, R. Gomperts, B. Mennucci, H. P. Hratchian, J. V. Ortiz, A. F. Izmaylov, J. L. Sonnenberg, D. Williams-Young, F. Ding, F. Lipparini, F. Egidi, J. Goings, B. Peng, A. Petrone, T. Henderson, D. Ranasinghe, V. G. Zakrzewski, J. Gao, N. Rega, G. Zheng, W. Liang, M. Hada, M. Ehara, K. Toyota, R. Fukuda, J. Hasegawa, M. Ishida, T. Nakajima, Y. Honda, O. Kitao, H. Nakai, T. Vreven, K. Throssell, J. A. Montgomery, Jr., J. E. Peralta, F. Ogliaro, M. J. Bearpark, J. J. Heyd, E. N. Brothers, K. N. Kudin, V. N. Staroverov, T. A. Keith, R. Kobayashi, J. Normand, K. Raghavachari, A. P. Rendell, J. C. Burant, S. S. Iyengar, J. Tomasi, M. Cossi, J. M. Millam, M. Klene, C. Adamo, R. Cammi, J. W. Ochterski, R. L. Martin, K. Morokuma, O. Farkas, J. B. Foresman, D. J. Fox, *Gaussian 16, Revision A.03*, **2016**, Gaussian, Inc., Wallingford CT.
[27] J. M. Mercero, J. M. Matxain, X. Lopez, D. M. York, A. Largo, L. A. Eriksson, J. M. Ugalde, *Int. J. Mass Spectrom.* **2005**, 240, 37-99.
[28] See, for example: A.Kumar, M. D. Sevilla, *J. Phys. Chem. B* **2018**, 122, 98-105.
[29] See for example: E. Ramos-Cordoba, P. Salvador, M. Reiher, *Chem. Eur. J.* **2013**, 19, 15267 – 15275.

Chapter 4

Summary and Outlook

The development of scientific ideas and practical applications of catalytic reactions have been conducted in parallel both in academia and in industry. Catalysis has overwhelmingly dominated the field of synthetic chemistry. The perfect catalyst would be environmentally friendly, cheap and easy to recover. It would operate under mild temperature and pressure conditions and be selective towards the desired product hence producing less waste.

In the recent years, due to the massive development of supercomputers, algorithms and theoretical electronic structure methods, computational chemistry has become more and more often utilized for conducting research in the field of catalysis. Theoretical predictions of the course of chemical reactions employing computational methods may aid, for example, during the process of the development of more sustainable catalysts. After all the chemical phenomena are based on the fundamental electromagnetic forces acting between the atoms, and quantum mechanics may be used to understand them. However the information from *in silico* experiments cannot be irrationally time consuming. Because of that the bigger is the system one would like to simulate the less precise method can be employed. Thus the theoretical results may not be good enough to make reliable predictions of the course of chemical reactions. Moreover, in order to make quantitative predictions, the calculations have to approach the chemical accuracy. This means that the errors of calculated relative energies should not be bigger than 4 kJ mol^{-1}.

In this thesis the application of computational chemistry methods in the field of applied catalysis, particularly for resolving reaction mechanism, has been explored. In Chapter 2 a research

devoted to computational modelling of the activity and the selectivity of cobalt carbonyl catalyst in propene hydroformylation has been presented. Although the reaction has been the subject of extensive research before, both experimental and theoretical, some questions remained unanswered. In order to study this complex organometallic reaction we have employed the computational protocol encompassing three major steps:

1. Geometry optimization of key species involved in catalytic cycle of propene hydroformylation at the DFT level of theory. Thermochemical calculations have been performed at this level of theory as well.
2. Refinement of the ground state energies of reactants, intermediates, transition states and products by conducting single-point energy calculations employing CCSD(T)-F12 method.
3. Microkinetic modelling of reaction rates based on transition state theory.

The simulations of the rates of formation of the two major products of the reaction, n-butyraldehyde and iso-butyraldehyde based on calculated free energy profile (Figure 4.1) have been conducted and agreed pretty well with the experimental results. The integration of permutational symmetry numbers in the bifurcation step proved to be important for correct determination of selectivity. Furthermore the addition of a competing pathway of products formation by catalyst [$HCo(CO)_4$] cleavage of acylcobalt species further improved the n/iso ratio, which was in accordance with experimental results too. Last but not least a refinement of the calculated Gibbs free energy barriers was necessary in order to diminish the errors done for the lower temperature conditions and to agree quantitatively with the experiment. However the changes applied did not exceed 4 kJ mol^{-1} for the enthalpies and 0.035 kJ mol^{-1} for the entropies which means that our calculations were approaching chemical accuracy.

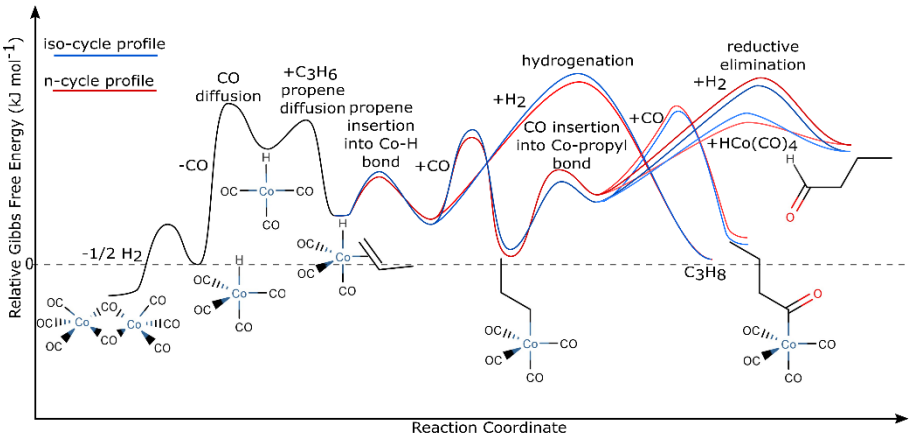

Figure 4.1 Schematic free energy profile of propene hydroformylation calculated for mixed standard state of 1 atm for gases and 1 mol dm^{-1} for solutes.

Although the CCSD(T)-F12 single-point energy calculations have been performed to refine the energies, both geometry optimization and thermochemical calculations were conducted only at the DFT level of theory. Moreover bimetallic species were not subjected to the energy refinement, which might have introduced higher errors than the ones mentioned in the previous paragraph. However, using the DFT relative energies for all the species in the reaction already provided quite a good model for the reaction kinetics. In fact, given that the final Gibbs free energies of key species had to be adjusted in order to agree quantitatively with the experiment for lower temperature conditions, the pure DFT energies could have been treated the same way, perhaps with slightly bigger adjustments allowed, and may well have led to the same conclusions as those obtained based on the model with energies refined at the CCSD(T)-F12 level of theory. This conclusion is especially important for possible future studies on the systems that due to too big size or multireference behaviour cannot be reliably treated with the coupled cluster method.

The project presented in Chapter 2 proves that the problem of too low accuracy of calculations which may impede correct predictions of reaction mechanism, kinetics and selectivity, can be

overcome. Still this is not an easy task and very careful methodology ought to be adapted. Moreover the slight fitting of the relative Gibbs free energies used for rate constant calculations may be necessary even for very reliable *ab initio* results. It may be advantageous to generally employ the microkinetic modelling of reaction rates for the mechanisms derived theoretically in addition to localizing the minimum energy pathway in order to resolve the big picture of the chemical process.

The exploration of untraversed catalytic reaction has been presented in Chapter 3. We have investigated methane activation by alternant ring cations composed of two chalcogen and two pnictogen atoms. The reaction mechanism was studied theoretically under single collision conditions thus only the values of potential energies on the presented energy profiles were reported. The performed calculations, that included DFT geometry optimization and frequency calculations and CCSD(T) single point calculations, determined that the $[N_2O_2]^{\bullet+}$ and $[N_2S_2]^{\bullet+}$ species seemed to be plausible catalysts for methane activation. Moreover the reaction mechanism was found to follow the hydrogen atom transfer route (Figure 4.2), which would proceed without any or a very low barrier. We have also recognized that the secondary reactions of the produced methyl radical and hydrogenated ring could take place leading to species substantially stabilized by around 150-250 kJ mol^{-1} compared to the initial reactants.

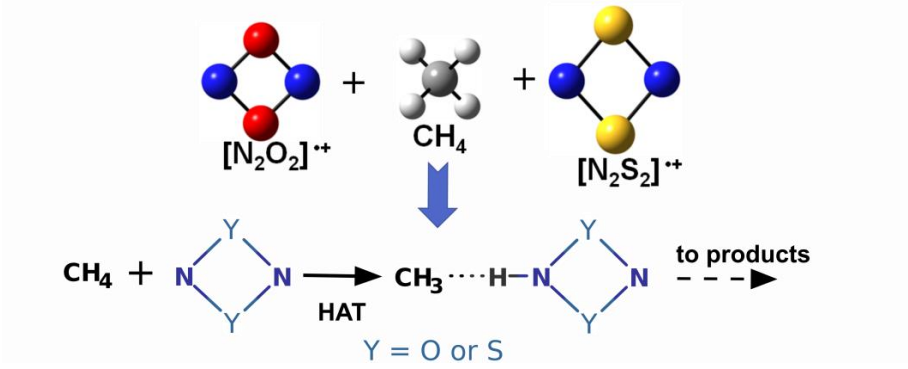

Figure 4.2 Methane activation by $[N_2O_2]^{\bullet+}$ and $[N_2S_2]^{\bullet+}$ following the mechanism of hydrogen atom transfer type.

Even though our computational results suggest that the methane activation performed by $[N_2O_2]^{\bullet+}$ and $[N_2S_2]^{\bullet+}$ is plausible, the reaction may not necessarily find application. Firstly the studied ring clusters may not be easy to synthesize and activate efficiently. Secondly an experiment performed under single collision conditions does not reflect the conditions used for efficient chemical substances production. Last but not least methane activation is just the first step in the catalytic cycle of methane direct functionalization. Certainly, the interesting theoretical results presented in Chapter 3, provide only little information on the putative reaction of chalcogen-pnictogen clusters with methane and need to be experimentally verified. Still the aforementioned issues should not discourage the theoretical chemists from investigating untraversed reaction pathways. After all, the results of conducted quantum chemical calculations may be a good start for subsequent research.

In the case of presented methane activation it might be compelling to continue the studies on the proposed chalcogen pnictogen cluster radicals and evaluate whether consecutive step of methane functionalization could be catalyzed by the $N_2Y_2^{\bullet+}$ (Y = S or O) species. Investigation of the ability of other similar compounds as well as the actual materials like disulfur dinitride (N_2S_2) crystals and $(SN)_x$ polymer to activate methane may be conducted too.

All in all the research presented in this thesis conducted on the two highly important catalytic processes not only contributes to the better comprehension of these systems but also highlights the potential applications of computational methods in the field of catalysis. Still an experiment is considered to be of the utmost importance for determining the properties of chemical transformations. Indeed there are some limitations of computational chemistry research like oversimplification of the studied systems, which can yield a highly unrealistic model having little or no impact on the developments in the field. However

computational chemistry approach may provide an invaluable insight into the understanding of chemical processes and electronic reasons behind the observed reactivity. As the *in silico* methods together with the supporting technology are continuously being developed, it becomes a more and more important tool in scientific research both for validation of the molecular reaction mechanism and for proposing novel catalytic processes.

Appendix A

This appendix is the supplementary information part of Chapter 2

A.1 Computational Methods – Details

The exploration of the PES for the propene hydroformylation process was done at the DFT level of theory, using the Gaussian 09 revision E.01 program [1]. Geometry optimization of all molecular structures was done using the B3LYP functional [2] as implemented in Gaussian and Grimme's dispersion correction with Becke-Johnson damping (D3BJ) [3] together with the 6-311G(d) Pople basis set [4] on all atoms, and an ultrafine DFT integration grid for more accuracy. A lot of care was taken to find the minima and transition states lying lowest in energy among possible conformations of molecular structures, by carrying out optimization starting from multiple manually constructed initial structures.

Computations of vibrational frequencies were performed at the same level of theory as the geometry optimization. Firstly the vibrational calculations revealed the nature of the molecular structures (no imaginary frequencies for minima and one imaginary frequency for TS). Secondly a statistical mechanical analysis could be done in order to evaluate the zero point-energy, enthalpy H, entropy S and Gibbs free energy G of each stationary point structure, used later on in kinetic modelling. For the calculations of entropy we employed the low frequency correction, which means that for all real frequencies computed by DFT to be lower than 50 cm^{-1} their initial value was replaced by 50 cm^{-1} for the statistical mechanical analysis in order to reduce the error that these modes contribute to S. This correction was proposed before by Truhlar et al. [5], with the exception that we use a threshold of 50 cm^{-1}. The reported and used G in case of the gases H_2 and CO are for a standard state of 1 atm while in the case of other species, a

standard state of 1 M concentrations was used because they are modelled as solutes.

Apart from DFT calculations, CCSD(T) single point energy calculations were performed for all suitable structures. The calculations at the CCSD(T)) level of theory were done with the Molpro quantum chemistry software [6], using a flexible basis set and the approach involving explicit treatment of interelectronic correlation – the CCSD(T)-F12 approach [7]. By using explicit correlation, we can minimize basis set truncation error. Separate CCSD(T) calculations using the 2nd order Douglas Kroll method [8] to compute the one-electron integrals were employed so as to take into consideration relativistic effects. In order to account for both explicit correlation and relativistic effects three CCSD(T) single point energy calculations had to be performed for each molecule:

I Non-relativistic CCSD(T) calculations - E_{CC}

II Non-relativistic CCSD(T)-F12 calculations – $E_{CC\text{-}F12}$

III Relativistic CCSD(T) calculations: $E_{CC\text{-}DK}$

The final reported CCSD(T) energy is given by the equation: $E_{CC\text{-}F12\text{-}DK} = E_{CC\text{-}F12} + E_{CC\text{-}DK} - E_{CC}$

A sample input file for CCSD(T) calculations is presented below. It contains the three CCSD(T) single point energy calculations mentioned above and the specific basis sets (normal and auxiliary) used for each atom and calculation. The example is for the molecule **9n**. Note that each CCSD(T) calculation uses a slightly different basis set combination, suited to the specific approach used.

```
memory,3000,m
geomtyp=xyz
geom={
19
CoCO3npr_insH_as
Co 0.665494   0.056981  -0.007426
C  0.722964   0.172040   1.756605
O  0.867255   0.187559   2.890004
C  1.435509   1.651350  -0.424754
O  1.894160   2.657741  -0.697582
C  1.690211  -1.007640  -0.977813
O  2.419966  -1.709453  -1.507504
```

```
C  -0.675912  -1.190406   0.061359
O  -1.022899  -2.264963   0.424025
C  -1.565121  -0.153425  -0.691306
H  -1.064044   0.809110  -0.905590
H  -1.772480  -0.593519  -1.670095
C  -2.848873   0.115122   0.098065
H  -3.322948  -0.847276   0.308596
H  -2.584194   0.549068   1.067412
C  -3.810153   1.037555  -0.647331
H  -4.108113   0.607527  -1.607814
H  -4.719047   1.208549  -0.065346
H  -3.357099   2.013410  -0.847160}
 occ,54,context=hf,ccsd(t) ; wf,108,1,0,context=hf,ccsd(t)
basis=ahlrichs-vdz
{ hf }
basis={ co=aug-cc-pwcvtz ; c=cc-pvdz ; o=cc-pvdz ; h=cc-pvdz }
{ hf }
{ccsd(t) ; core,16 ; maxit,50 ; shift,.5,.5 }
basis={co=aug-cc-pwcvtz ; c=cc-pvdz-f12 ; o=cc-pvdz-f12; h=cc-pvdz-f12
set,df
co=aug-cc-pvtz/mp2fit;  c=aug-cc-pvdz/mp2fit  ;  o=aug-cc-pvdz/mp2fit;  h=aug-cc-
pvdz/mp2fit
set,jk
co=def2-tzvpp/jkfit ; c=aug-cc-pvdz/jkfit ; o=aug-cc-pvdz/jkfit ; h=aug-cc-pvdz/jkfit
set,ri
co=def2-tzvpp/optri ; c=cc-pvdz-f12/optri ; o=cc-pvdz-f12/optri ; h=cc-pvdz-f12/optri}
{ hf }
{ ccsd(t)-f12,scale_trip=1,df_basis_exch=jk,df_basis=df,ri_basis=ri
shift,.5,.5 ; maxit,50 ; core,16 }
dkroll=1
basis={ co=aug-cc-pwcvtz-dk ; c=cc-pvdz-dk ; o=cc-pvdz-dk ; h=cc-pvdz-dk }
{ hf }
{ccsd(t) ; core,16 ; maxit,50 ; shift,.5,.5 }
```

A.2 Detailed mechanism of propene hydroformylation.

The catalytic cycle shown in the main article is simplified and only the steps and transition states that are important for kinetic modelling are depicted and on top of that the full pathway is shown only for iso-cycle. Here the full mechanism containing reactants, intermediates and products is presented in Scheme A.1. All the DFT and CCSD(T) energies of stationary points are juxtaposed in Table A.1 in which the values for complementary structures omitted in the main paper are presented as well.

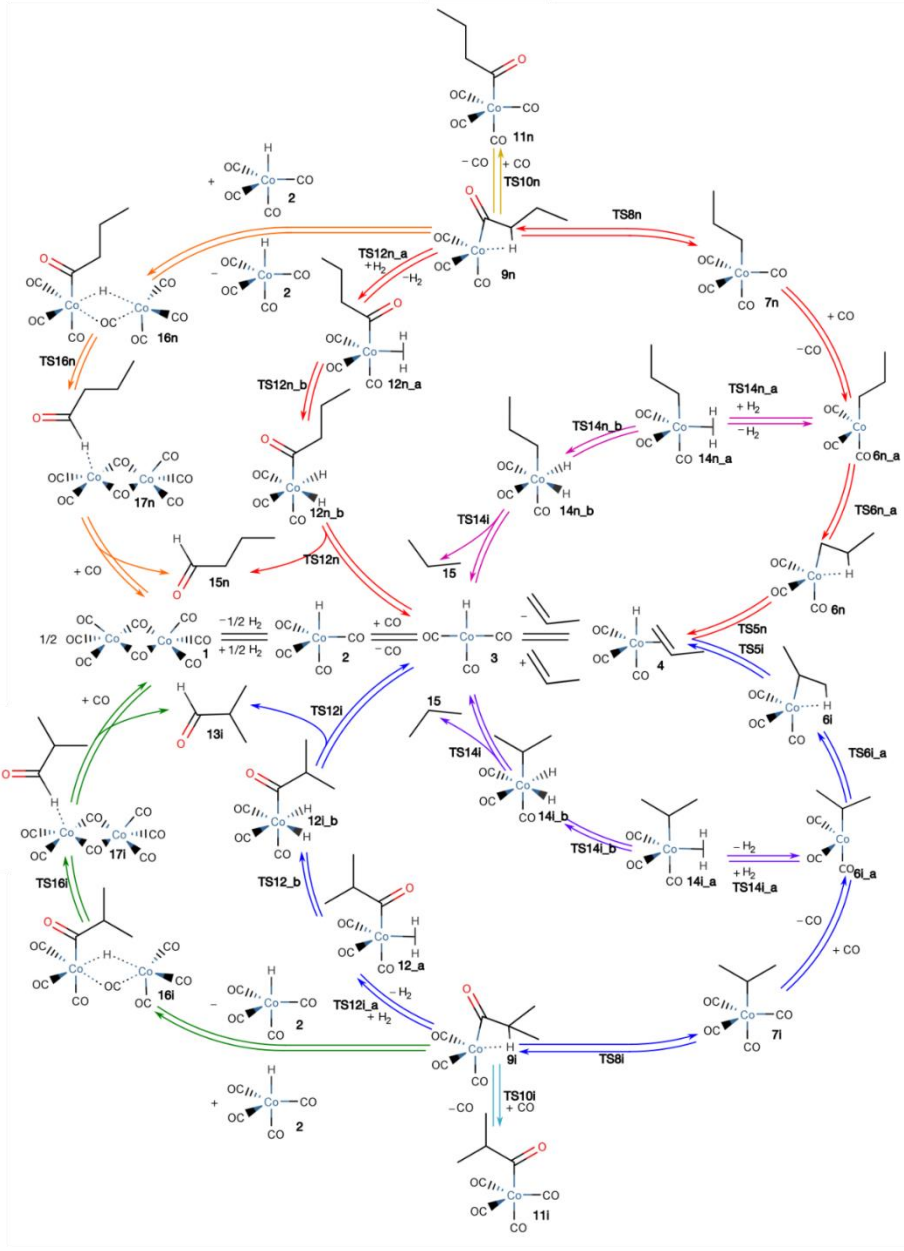

Scheme A.1 Catalytic cycle of propene hydroformylation indicating pathways leading to production of butyraldehyde isomers: n-butyraldehyde and iso-butyraldehyde by H_2 cleavage (red cycle and blue cycle respectively) and by catalyst cleavage (orange and green pathway) as well an unwanted hydrogenation to propane (pink and purple arrows).

Table A.1 Relative energies of the species in propene hydroformylation process, units: [kJ mol^{-1}].

Species	ΔE DFT		ΔE CCSD(T)		ΔG CCSD(T) 383 K		ΔG CCSD(T) 403 K		ΔG CCSD(T) 423 K	
	n	iso	n	iso	n	iso	n	iso	n	iso
1[a] -**2**+C_3H_6 +2H_2 +CO	-33.2		-33.2		-27.5		-27.2		-27.0	
2 +C_3H_6 +H_2 +CO	0.0		0.0		0.0		0.0		0.0	
3 +C_3H_6 +H_2 +2CO	137.1		152.8		84.9		81.8		78.6	
4 +H_2 +2 CO	28.3		33.7		34.1		33.8		33.5	
TS5 +H_2 +2CO	69.0	69.3	65.1	66.0	61.0	62.2	60.7	61.9	60.4	61.7
6 +H_2 +2CO	25.4	26.3	28.3	26.8	33.1	31.3	32.8	30.9	32.4	30.5
TS6_a +H_2 +2 CO	36.2	37.2	58.5	66.2	64.2	72.8	64.0	72.6	63.8	72.5
6a +H_2 +2CO	33.2	37.2	65.0	68.0	65.2	69.6	64.6	69.0	63.9	68.4
7 + H_2 + CO	-81.8	-80.5	-66.7	-65.7	1.6	4.9	4.0	7.5	6.4	10.1
TS8 +H_2 +CO	-26.8	-30.6	-7.4	-8.7	59.8	59.8	62.4	62.5	65.0	65.2
9 +H_2 +CO	-47.2	-57.4	-25.9	-33.9	43.4	36.0	45.9	38.6	48.4	41.2
TS10 + H_2	-70.2	-76.7	-24.2	-28.4	94.7	93.8	99.7	99.0	104.6	104.1
11 +H_2	-150.0	-155.2	-118.6	-124.7	14.5	10.7	19.9	16.3	25.3	21.8
TS12_a +CO	-47.3	-51.8	-9.0	-15.3	97.3	96.9	101.6	101.6	105.9	106.2
12_a +CO	-61.6	-66.3	-45.5	-51.4	81.4	78.5	86.3	83.6	91.2	88.6
TS12_b +CO	-32.2	-35.5	-22.0	-25.4	99.6	98.0	104.7	103.1	109.7	108.2
12_b +CO	-48.4	-51.8	-24.3	-28.6	103.3	101.0	108.3	106.2	113.4	111.3
TS12 +CO	-31.3	-36.2	-9.4	-15.5	116.5	111.8	121.7	117.0	126.8	122.3
13 + **3** +CO	-32.1	-35.4	5.3	0.8	76.9	72.7	79.3	75.1	81.7	77.5
13 +**2**	-169.2	-172.5	-147.5	-152.0	-7.9	-12.2	-2.4	-6.6	3.1	-1.1
TS14_a +2CO	32.5	34.9	58.8	58.9	95.7	102.8	96.8	104.3	97.9	105.8
14_a +2CO	15.4	15.83	12.9	12.8	76.8	80.1	78.8	82.3	80.8	84.4
TS14_b +2CO	41.8	43.1	38.1	39.09	95.5	98.6	97.6	100.9	99.7	103.1
14_b +2CO	33.0	35.3	39.4	40.1	100.7	104.4	102.7	106.6	104.7	108.8
TS14 +2CO	60.8	62.1	62.4	65.3	119.6	125.1	121.6	127.3	123.6	129.5
15 +**3** +2CO	-21.9		-0.5		9.4		8.9		8.4	
15 +**2** +CO	-159.0		-153.3		-75.5		-72.8		-70.2	
16[b] -**2** +H_2 +CO	-114.2	-110.9	-93.0	-87.4	51.8	57.6	57.4	63.2	62.9	68.6
TS16[b] -**2** +H_2 +CO	-63.1	-67.8	-41.8	-44.3	88.3	91.2	93.7	96.7	99.1	102.2
17[b] -**2** +H_2 +CO	-122.1	-127.2	-100.8	-103.8	37.8	29.1	43.1	34.1	48.3	39.2

[a] All value for Co_2CO_8 from DFT calculations [b] Values for CCSD(T) energies of bimetallic species obtained from equation $\Delta E = \Delta E_{DFT} + (\Delta E9_{CCSDT} - \Delta E9_{DFT})$

A.3 Calculations of Rate Constants

For kinetic modelling one needs to calculate the rate constants for relevant steps in the catalytic cycle. The reduced mechanism on which the modelling in this paper is based is presented in Scheme A.2. The labels of the rate constants on the Scheme A.2 are different compared to those in the schematic catalytic cycle presented in the main paper. This is done in order to be consistent with the notation used in the kinetic modelling programs and below. Rate constants are derived employing the equations of Transition State Theory. Below the equations used for calculating rate constants k and equilibrium constants K are listed:

$$k = \frac{k_B T}{h} e^{-\frac{\Delta G^{\ddagger}}{RT}} \quad \text{(A. 1)}$$

$$K = e^{-\frac{\Delta G^{\theta}}{RT}} \quad \text{(A. 2)}$$

$$K = \frac{k_+}{k_-} \quad \text{(A. 3)}$$

$$k_{diff} = \frac{8 k_B T}{3\eta} \quad \text{(A. 4)}$$

Each step is described in details in the following paragraphs. The derivation of rate and equilibrium constants is presented for the reaction at 423 K, however the values for two other modelled temperatures are shown as well. Starting from the bifurcation step, the explanation is provided only for the n-cycle but values are provided for the i-cycle as well). The equations describing the equilibria and rates for each step considered are given in the following paragraphs, the values in square brackets used in these equations are concentrations in M for solutes (e.g. [**1**] – concentration of dicobalt octacarbonyl) and atm for gases: [H_2] – pressure of hydrogen; [CO] – pressure of carbon monoxide] At the end of this section an input for Tenua program is presented. The presented values of Gibbs free energies are for a mixed standard

state of 1 M (solutes) and 1 atm (gases). One should remember that standard free energies do not immediately provide information on relative rates since these changes when considering non-standard concentrations and pressures.

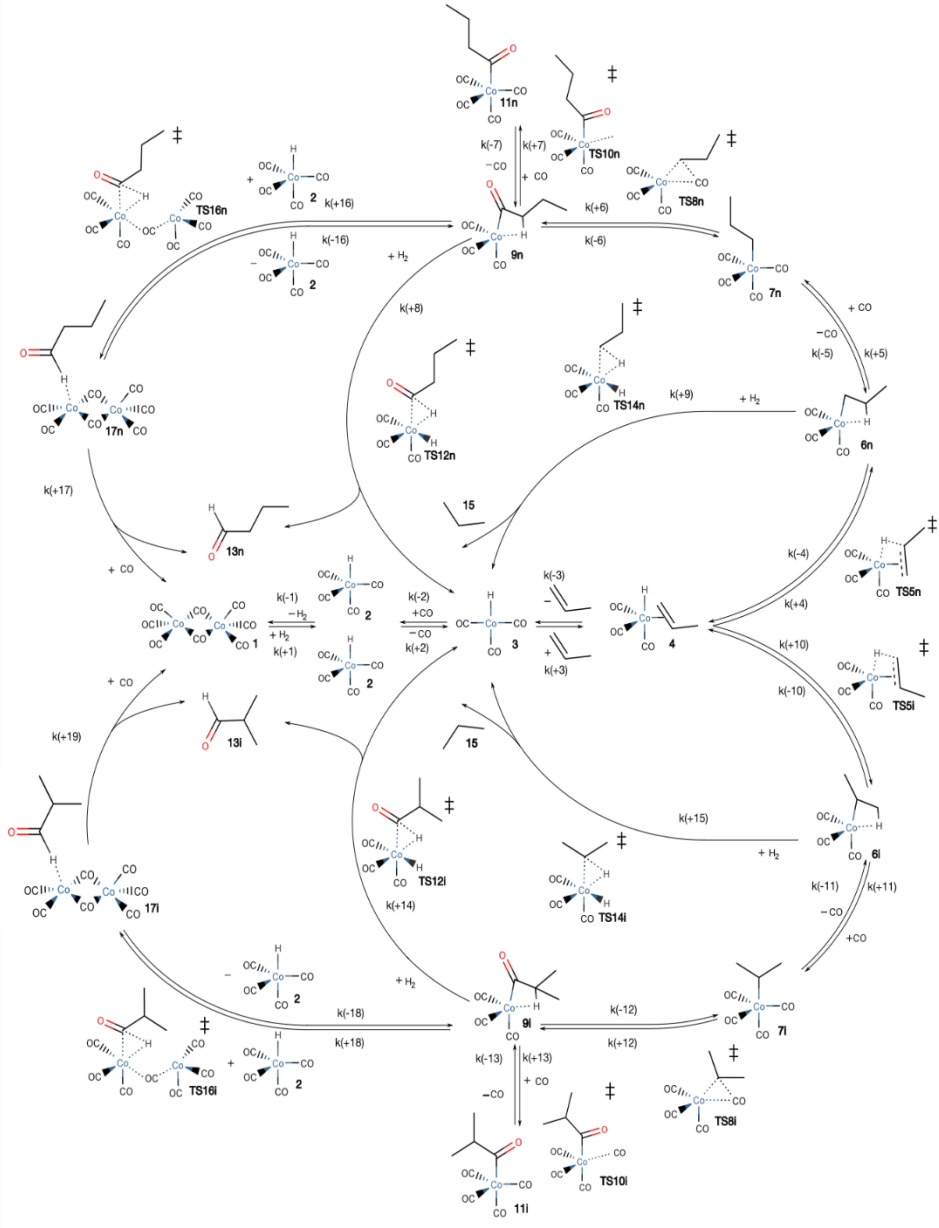

Scheme A.2 Simplified hydroformylation mechanism used in kinetic modelling.

Step 1: $Co_2(CO)_8 + H_2 <-> 2HCo(CO)_4$

1 + H_2 <-> 2 **2**
K(1) = [**2**]^2 / [**1**] [H_2] – equilibrium constant of step 1
R(1) = k(+1) [**1**] [H_2] - k(-1) [**2**]^2 – rate of step 1

For the transformation of dicobalt octacarbonyl into two molecules of cobalt tetracarbonyl hydride upon addition of hydrogen molecule no detailed exploration of the PES was performed. It was assumed that the species **1** and **2** are in equilibrium . The measured ΔH and ΔS for the reaction are 4.3 kcal mol^{-1} and -2.6 cal mol^{-1} respectively [9]. The calculated value of $\Delta G(1)$ is based on DFT energies as the $Co_2(CO)_8$ species is too computationally demanding for CCSD(T) calculations, this standard free energy change is equal to 27 kJ mol^{-1}. This value is close to the experimentally measured [9] value in n-heptane of 22.6 kJ mol^{-1} ($\Delta G = \Delta H - T\Delta S$). We have decided to use the latter value in the kinetic modelling, which corresponds to an equilibrium constant $K(1)$ equal to 1.62 10^{-3} atm^{-1} M. As the used protocol is based on rate constants not equilibrium constants, we used arbitrary (and quite large) values of $k(+1)$ and $k(-1)$ maintaining their ratio to be equal to $K(1)$. In this way we ensure the rapid equilibrium between catalyst species that is believed to be occurring under reaction conditions.

T [K]	423	403	383
K(1) [atm^{-1} M]	1.62E-03	1.26E-03	9.51E-04
k(+1) [atm^{-1} s^{-1}]	1.00E+04	1.00E+04	1.00E+04
k(-1) [M^{-1} s^{-1}]	6.16E+06	7.95E+06	1.05E+07
ΔG^{θ}(1) [kJ mol^{-1}]	22.6	22.4	22.2
$\Delta G^{\ddagger}$(1) [kJ mol^{-1}]	72.4	68.9	65.3

Step 2: $HCoCO_4 <-> HCoCO_3 + CO$

2 <-> **3** + **CO**
K(2) = [3] [CO] / [2]
R(2) = k(+3) [2] – k(-3) [3] [CO]

For the reaction of the loss of one carbonyl ligand from cobalt tetracarbonyl hydride leading to the formation of active catalyst $HCo(CO)_3$ we did not locate a saddle point on the potential energy surface. Hence the reverse reaction is assumed to be diffusion limited. Based on the experimental measurements of viscosity η [10] one can calculate the diffusion-limited rate constant from Equation A.4, which gives a value of 4.53×10^{10} M^{-1} s^{-1}. However because in this reaction a CO molecule is diffusing and the standard state used in this paper for CO is 1 atm the molar rate constant has to be divided by the volume occupied by 1 mol of gas under the pressure of 1 atm (value for ideal gas which is 34.7 dm^3 mol^{-1} for the temperature of 423 K is used). So $k(-2)$ equals to 1.31×10^{-9} atm^{-1} s^{-1}. $K(2)$ can be calculated from the $\Delta G^{\theta}(2)$ = 78.6 kJ mol^{-1} between species **3** and **2**. The forward rate constant k(+2) is derived from Equation A.3, yielding a value of 2.55×10^{-1} s^{-1}. The apparent barrier $\Delta G^{\ddagger}(2)$ calculated from Equation A.1 is 109.6 kJ mol^{-1}.

T [K]	423	403	383
K(2) [atm]	1.95E-10	2.54E-11	2.66E-12
k(+2) [s^{-1}]	2.55E-01	2.89E-02	2.63E-03
k(-2) [atm^{-1} s^{-1}]	1.31E+09	1.14E+09	9.90E+08
η [kg m^{-1} s^{-1}]	2.07E-04	2.37E-04	2.73E-04
ΔG^{θ}(2) [kJ mol^{-1}]	78.6	81.8	84.9
$\Delta G^{\ddagger}$(2) [kJ mol^{-1}]	109.6	111.6	113.6

Step 3: $HCoCO_3$ + C_3H_6 <-> $HCoCO_3$pr

3 + **C3H6** <-> **4**
K(3) = [4] / [3] [C3H6]
R(3) = k(+3) [3] [CH6] – k(-3) [4]

The alkene addition step is assumed to be diffusion-limited also, that is why $k(+3) = 4.53 \times 10^{10}$ M^{-1} s^{-1} as explained in the previous paragraph. $K(3) = 3.72 \times 10^5$ M is calculated using $\Delta G(3)$ = -45.11 kJ mol^{-1} between species **4** and **3**. $k(-3)$ = 1.22 10^5 M^{-2} s^{-1} as

calculated from Equation A.3. The relative value of activation barrier of this step is located at 97.17 kJ mol^{-1}.

T [K]	423	403	383
K(3) [M^{-1}]	3.72E+05	1.63E+06	8.43E+06
k(+3) [M^{-1} s^{-1}]	4.53E+10	3.77E+10	3.11E+10
k(-3) [s^{-1}]	1.22E+05	2.31E+04	3.69E+03
η [kg m^{-1} s^{-1}]	2.07E-04	2.37E-04	2.73E-04
ΔG^{0}(3) [kJ mol^{-1}]	-45.11	-47.94	-50.78
$\Delta G^{\ddagger}$(3) [kJ mol^{-1}]	18.54	18.11	17.67

Step 4 :
$HCo(CO)_3$pr <-> ag$Co(CO)_3$npr

4 <-> **6n**
K(4) = [6n] / [4]
R(4) = k(+4) [4] – k(-4) [6n]

Step 10:
$HCo(CO)_3$pr <-> ag$Co(CO)_3$ipr

4 <-> **6i**
K(10) = [6i] / [4]
R(10) = k(+10) [4] – k(-10) [6i]

The alkene insertion step is the bifurcation point of the reaction. Here the catalytic cycle splits and can lead to production of linear (n-cycle) and branched (i-cycle) butyraldehyde. The pathways for both cycles are parallel so they can be explained together. The description of the first step is rather straightforward as it is an elementary reaction. The forward kinetic constant is calculated from Equation A.1 as the **TS5** placed at relative value of 60.42 kJ mol^{-1} leading from **4** to **6** was localized. $k(+4)$ is equal to 4.20×10^{10} s^{-1}, while $k(+11)$ equals 2.96×10^{9} s^{-1}. Even though this reaction is very fast it cannot be merged with other steps, because it is a bifurcation step. The equilibrium constants and backward rate constant are calculated from Equation A.2 and A.3 respectively.

T [K]	423	403	383
K(4)	1.38E+00	1.37E+00	1.35E+00
k(+4) [s^{-1}]	4.20E+09	2.73E+09	1.70E+09
k(-4) [s^{-1}]	3.04E+09	1.99E+09	1.26E+09
ΔG^0(4) [kJ mol^{-1}]	-1.14	-1.06	-0.96
$\Delta G^{\ddagger}$(4) [kJ mol^{-1}]	26.90	26.91	26.92
K(10)	2.33E+00	2.38E+00	2.43E+00
k(+10) [s^{-1}]	2.96E+09	1.90E+09	1.16E+09
k(-10) [s^{-1}]	1.27E+09	7.98E+08	4.80E+08
ΔG^0(10) [kJ mol^{-1}]	-2.98	-2.90	-2.83
$\Delta G^{\ddagger}$(10) [kJ mol^{-1}]	28.13	28.13	28.13

Step 5:
agCo(CO)$_3$npr + CO <-> Co(CO)$_4$npr

6n + CO <-> **7n**
K(5) = [7n] / [6n] [CO]
R(5) = k(+5) [6n] [CO] – k(-5) [7n]

Step 11:
agCo(CO)$_3$ipr + CO <-> Co(CO)$_4$ipr

6i + CO <-> **7i**
K(11) = [7i] / [6i] [CO]
R(11) = k(+11) [6i] [CO] – k(-11) [7i]

For the reaction of CO addition into **6** two mechanisms were located on PES. The first one is the simple associative one in which an incoming CO is added to the metal centre while the agostic Co-H interaction is broken. The second one is the dissociative route in which firstly the Co-H agostic interaction of species **6** is broken through **TS6_a** yielding an unsaturated species and then CO is added to the metal centre. For this second step, no barrier was located, so it was assumed to be diffusion limited. The latter mechanism was found to be lower in terms of Gibbs free energy. The diffusion to unsaturated **6n_a** yielded a relative barrier of 94.9 kJ mol^{-1} (addition of $\Delta G^{\ddagger}_{diff}$ calculated using k_{diff} to value of ΔG for **6_a**), as the value of **TS6n_a** is lower (63.8 kJ mol^{-1}), the two elementary steps could be merged and values for overall reaction calculated using the relative Gibbs Free Energies for **6** and **7** and apparent value for the diffusion TS calculated with Equation A.4.

T [K]	423	403	383
K(5) [atm^{-1}]	1.59E+03	5.33E+03	2.03E+04
k(+5) [atm^{-1} s^{-1}]	1.69E+05	8.61E+04	4.13E+04
k(-5) [s^{-1}]	1.06E+02	1.62E+01	2.04E+00
ΔG^0(5) [kJ mol^{-1}]	-25.93	-28.75	-31.58
$\Delta G^{\ddagger}$(5) [kJ mol^{-1}]	62.50	61.64	60.76
K(11) [atm^{-1}]	3.30E+02	1.07E+03	3.92E+03
k(+11) [atm^{-1} s^{-1}]	2.73E+04	1.31E+04	5.88E+03
k(-11) [s^{-1}]	8.26E+01	1.23E+01	1.50E+00
ΔG^0(11) [kJ mol^{-1}]	-20.40	-23.37	-26.35
$\Delta G^{\ddagger}$(11) [kJ mol^{-1}]	68.91	67.95	66.97

Step 6:
$Co(CO)_4$npr <-> $Co(CO)_3$nbut

7n <-> **9n**
K(6) = [9n] / [7n]
R(6) = k(+6) [7n] – k(-6) [9n]

Step 12:
$Co(CO)_4$ipr <-> $Co(CO)_3$ibut

7i <-> **9i**
K(12) = [9i] / [7i]
R(12) = k(+12) [7i] – k(-12) [9i]

The step of insertion of CO ligand from **7** through **TS8** yielding unsaturated species **9** stabilized by an agostic H-Co interaction is an elementary reaction. So for calculations of kinetic and equilibrium constants one only needs to know the relative Gibbs free energy values for all species and employ Equations A.1, A.2 and A.3.

T [K]	423	403	383
K(6)	6.55E-06	3.67E-06	1.94E-06
k(+6) [s^{-1}]	5.25E+05	2.29E+05	9.19E+04
k(-6) [s^{-1}]	8.01E+10	6.24E+10	4.74E+10
ΔG^0(6) [kJ mol^{-1}]	41.98	41.93	41.89
$\Delta G^{\ddagger}$(6) [kJ mol^{-1}]	58.51	58.36	58.21
K(12)	1.48E-04	9.41E-05	5.69E-05
k(+12) [s^{-1}]	1.41E+06	6.37E+05	2.64E+05
k(-12) [s^{-1}]	9.52E+09	6.76E+09	4.65E+09
ΔG^0(12) [kJ mol^{-1}]	31.01	31.06	31.13
$\Delta G^{\ddagger}$(12) [kJ mol^{-1}]	55.03	54.93	54.85

Step 7:	**Step 13:**
$Co(CO)_3$nbut + CO <-> $Co(CO)_4$nbut	**$Co(CO)_3$ibut + CO <-> $Co(CO)_4$ibut**
9n + CO <-> **11n**	**9i + CO** <-> **11i**
K(7) = [11n] / [9n] [CO]	K(13) = [11i] / [9i] [CO]
R(7) = k(+7) [9n] [CO] – k(-7) [11n]	R(13) = k(+13)[9i] [CO] – k(-13) [11i]

Species **9n** can coordinate one CO molecule and transform into the quite stable cobalt tetracarbonyl acyl **11n**. The lowest lying **TS10n** for this reaction was located on the PES lying at 104.64 kJ mol^{-1}. As values of ΔG for all involved species are known one can simply calculate all constants as explained in a previous example.

T [K]	423	403	383
K(7) [atm^{-1}]	7.17E+02	2.37E+03	8.89E+03
k(+7) [atm^{-1} s^{-1}]	1.01E+06	9.03E+05	8.02E+05
k(-7) [s^{-1}]	1.41E+03	3.81E+02	9.03E+01
ΔG^0(7) [kJ mol^{-1}]	-23.13	-26.04	-28.95
$\Delta G^{\ddagger}$(7) [kJ mol^{-1}]	56.21	53.76	51.31
K(13) [atm^{-1}]	2.46E+02	7.88E+02	2.85E+03
k(+13) [atm^{-1} s^{-1}]	1.49E+05	1.26E+05	1.06E+05
k(-13) [s^{-1}]	6.04E+02	1.60E+02	3.71E+01
ΔG^0(13) [kJ mol^{-1}]	-19.37	-22.35	-25.34
$\Delta G^{\ddagger}$(13) [kJ mol^{-1}]	62.94	60.35	57.76

Step 8: $Co(CO)_3$nbut + H_2 <-> <-> $HCo(CO)_3$ + nbut	**Step 14: $Co(CO)_3$ibut + H_2 <-> <-> $HCo(CO)_3$ + ibut**
9n + H2 -> **13n** + **3**	**9i + H2** -> **13i** + **3**
K(8) = [13n] [3] / [9n] [H2]	K(14) = [13i] [3] / [9i] [H2]
R(8) = k(+8) [9n] [H2]	R(14) = k(+14) [9i] [H2]

The production of the final product of hydroformylation – butyraldehyde involves several elementary steps. Firstly H_2 molecule is added into the cobalt centre to species **9** through **TS12_a** yielding species **12_a**. Then oxidative addition of H_2 takes place and the involved TS and minimum are respectively **TS12_b** and **12_b**. From **12_b** reductive elimination through **TS12** follows and the **13** is finally produced together with catalyst species **3**. In all these reactions the highest lying TS is the last one - **TS12** and it

is assumed to be the rate limiting TS. For the n-cycle its ΔG = 126.84 kJ mol^{-1} value is used to calculate the forward rate constant together with ΔG = 48.43 kJ mol^{-1} of species **9n**, yielding k(+8) = 1.83 10^{3} atm^{-1} s^{-1}. The equilibrium constant and backward rate constant can be calculated as well, however in the model presented it is assumed that k(-8) = 0 and the reaction is irreversible.

T [K]	423	403	383
K(8) [M atm^{-1}]	-	-	-
k(+8) [atm^{-1} s^{-1}]	1.83E+03	1.28E+03	8.61E+02
k(-8) [M^{-1} s^{-1}]	0	0	0
ΔG^{0}(8) [kJ mol^{-1}]	33.29	33.38	33.51
$\Delta G^{\ddagger}$(8) [kJ mol^{-1}]	78.41	75.74	73.08
K(14) [M atm^{-1}]	-	-	-
k(+14) [atm^{-1} s^{-1}]	8.47E+02	5.78E+02	3.78E+02
k(-14) [M^{-1} s^{-1}]	0	0	0
ΔG^{0}(14) [kJ mol^{-1}]	36.37	36.50	36.65
$\Delta G^{\ddagger}$(14) [kJ mol^{-1}]	81.12	78.41	75.71

Step 9: agCo(CO)$_3$npr + H$_2$ <-> <-> prop + HCo(CO)$_3$

6n + **H2** -> **15** + **3**
K(9) = [15] [3] / [6n] [H2]
R(9) = k(+9) [6n] [H2]

Step 15: agCo(CO)$_3$ipr + H$_2$ <-> <-> prop + HCo(CO)$_3$

6i + **H2** -> **15** + **3**
K(15) = [15] [3] / [6i] [H2]
R(15) = k(+15) [6i] [H2]

The undesirable hydrogenation step producing alkene **15** happens in a similar way to the aldehyde 13 production however not from species **9** but from species **6**. Firstly the agostic H-Co interaction is broken yielding 16-electron species **6_a** which can coordinate H_2 molecule through **TS14_a** producing **14_a**. Oxidative addition of H_2 takes place through **TS14_b** yielding species **14_b**. Finally propane **15** is produced through reductive elimination **TS14** (note that in our earlier study, in which B3LYP rather than dispersion-corrected B3LYP, the minimum 14_b vanished, yielding a concerted oxidative addition/reductive elimination step). Again the reductive elimination TS is the highest point on the PES for this transformation and for the n-cycle the difference between ΔG =

123.61 kJ mol^{-1} of **TS14n** and ΔG = 32.38 kJ mol^{-1} is employed for calculations of k(+9) equal to 5.30 10^{-2} atm^{-1} s^{-1}. This step is assumed to be irreversible as well.

T [K]	423	403	383
K(9) [M atm^{-1}]	-	-	-
k(+9) [atm^{-1} s^{-1}]	4.78E+01	2.57E+01	1.29E+01
k(-9) [M^{-1} s^{-1}]	0	0	0
ΔG^0(9) [kJ mol^{-1}]	-23.93	-23.85	-23.75
$\Delta G^{\ddagger}$(9) [kJ mol^{-1}]	91.23	88.84	86.46
K(15) [M atm^{-1}]	-	-	-
k(+15) [atm^{-1} s^{-1}]	5.28E+00	2.67E+00	1.26E+00
k(-15) [M^{-1} s^{-1}]	0	0	0
ΔG^0(15) [kJ mol^{-1}]	-22.10	-22.01	-21.89
$\Delta G^{\ddagger}$(15) [kJ mol^{-1}]	98.98	96.42	93.88

Step 16: Co(CO)$_3$nbut + HCo(CO)$_4$ <-> nald_hept

9n + **2** <-> **17n**

K(16) = [17n] / [9n] [2]

R(16) = k(+16) [9n] [2] - k(-16) [17n]

Step 18: Co(CO)$_3$ibut + HCo(CO)$_4$ <-> iald_hept

9i + **2** <-> **17i**

K(18) = [17i] / [9i] [2]

R(18) = k(+18) [9i] [2] - k(-18) [17i]

The second modelled process in propene hydroformylation enabling production of the different aldehyde isomers proceeds by transfer of an H atom from the catalyst species **2** instead of H_2 molecule. As for the 'normal' reductive elimination, this process involves multiple elementary steps, which are combined for the purpose of kinetic modelling. It is assumed that the catalyst is added to species **9**, followed by reductive elimination by catalyst through **TS16** yielding the weakly-bonded species **17** in which there is an interaction between aldehyde **15** and dicobalt heptacarbonyl. The values of rate constants k(+16) = 4.89 10^6 M^{-1} s^{-1} and k(-16) = 4.73 10^6 s^{-1} as well as equilibrium constant K(16) = 1.03 M^{-1} are obtained based on ΔG = 99.09 kJ mol^{-1} for **TS16n**, ΔG=48.43 kJ mol^{-1} for **9n** and ΔG = 48.31 for the weakly-bonded complex **17n**.

T [K]	423	403	383
K(16) [M^{-1}]	1.03E+00	2.35E+00	5.86E+00
k(+16) [M^{-1} s^{-1}]	4.89E+06	5.39E+06	6.04E+06
k(-16) [s^{-1}]	4.73E+06	2.29E+06	1.03E+06
ΔG^0(16) [kJ mol^{-1}]	-0.12	-2.86	-5.63
$\Delta G^{\ddagger}$(16) [kJ mol^{-1}]	50.66	47.78	44.88
K(18) [M^{-1}]	1.76E+00	3.78E+00	8.85E+00
k(+18) [M^{-1} s^{-1}]	2.59E+05	2.50E+05	2.43E+05
k(-18) [s^{-1}]	1.47E+05	6.61E+04	2.74E+04
ΔG^0(18) [kJ mol^{-1}]	-2.00	-4.46	-6.94
$\Delta G^{\ddagger}$(18) [kJ mol^{-1}]	61.00	58.07	55.12

Step 17: nald_hept + CO <-> $Co_2(CO)_8$ + nbut

17n + CO -> 1 + 15n
K(17) = [15n] [1] / [17n] [CO]
R(17) = k(+17) [17n] [CO]

Step 19: iald_hept + CO <-> $Co_2(CO)_8$ + ibut

17i + CO -> 1 + 15i
K(19) = [15i] [1] / [17i] [CO]
R(19) = k(+19) [17i] [CO]

The last step closing the catalytic cycle is the release of butyraldehyde and the incorporation of CO ligand into dicobalt heptacarbonyl reviving the substrate **1**. As the interaction between aldehyde and metallic centre is thought to be weak it is assumed to be very fast, as well as the incorporation of CO. It is modelled here that this step is diffusion-limited and irreversible, yielding the value of $k(+17) = 1.31\ 10^9$ from Equation A.4.

T [K]	423	403	383
K(17) [M atm^{-1}]	-	-	-
k(+17) [atm^{-1} s^{-1}]	1.31E+09	1.14E+09	9.90E+08
k(-17) [M^{-1} s^{-1}]	0	0	0
ΔG^0(17) [kJ mol^{-1}]	-70.90	-65.45	-59.96
$\Delta G^{\ddagger}$(17) [kJ mol^{-1}]	31.01	29.84	28.64
K(19) [M atm^{-1}]	-	-	-
k(+19) [atm^{-1} s^{-1}]	1.31E+09	1.14E+09	9.90E+08
k(-19) [M^{-1} s^{-1}]	0	0	0
ΔG^0(19) [kJ mol^{-1}]	-61.75	-56.52	-51.26
$\Delta G^{\ddagger}$(19) [kJ mol^{-1}]	31.01	29.84	28.64

A.4 Symmetry numbers

As it is explained in the main paper the so called "raw model" presented here is fitted with the permutational symmetry numbers that seem to be essential for the proper ratio of n-butyraldehyde to i-butyraldehyde. This is why in the final simulations the backward rate constant *k*(-4) for propene insertion into the H-Co bond for the n-cycle is multiplied by *2* and *k*(-10) for the respective step in i-cycle is multiplied by *6*.

A.5 Tenua Modelling

Below is an example of Tenua [11] input for one of the simulated reaction conditions ([CO] = 50 bar, [H2] = 50 bar, [**1**] = 0.0073 M, [C3H6] = 1.19 M). It is assumed the pressures and propene concentration are constant, which is an acceptable description for the initial rates of hydroformylation measured experimentally[12].

```
Co2CO8 + H2 <-> 2HCoCO4 ;
k(+1) : 10000 ;
k(-1) : 6166000 ;
H2 : 50 ;
rate(H2) = 0 ;
Co2CO8 : 0.0073 ;
HCoCO4 <-> HCoCO3 + CO ;
k(+2) : 2.55E-01 ;
k(-2) : 1.31E+09 ;
CO : 50 ;
rate(CO) = 0 ;
HCoCO3 + C3H6 <-> HCoCO3pr ;
k(+3) : 4.53E+10 ;
k(-3) : 1.22E+05 ;
C3H6 : 1.19 ;
rate(C3H6) = 0 ;
HCoCO3pr <-> agCoCO3npr ;
k(+4) : 4.20E+09 ;
k(-4) : 2*3.04E+09 ;
agCoCO3npr + CO <-> CoCO4npr ;
```

k(+5) : 1.69E+05 ;
k(-5) : 1.06E+02 ;
CoCO4npr <-> CoCO3nbut ;
k(+6) : 5.25E+05 ;
k(-6) : 8.01E+10 ;
CoCO3nbut + CO <-> CoCO4nbut ;
k(+7) : 1.01E+06 ;
k(-7) : 1.41E+03 ;
CoCO3nbut + H2 <-> nbut_red + HCoCO3 ;
k(+8) : 1.83E+03 ;
k(-8) : 0 ;
agCoCO3npr + H2 <-> prop + HCoCO3 ;
k(+9) : 4.78E+01 ;
k(-9) : 0 ;
HCoCO3pr <-> agCoCO3ipr ;
k(+10) : 2.96E+09 ;
k(-10) : 6*1.27E+09 ;
agCoCO3ipr + CO <-> CoCO4ipr ;
k(+11) : 2.73E+04 ;
k(-11) : 8.26E+01 ;
CoCO4ipr <-> CoCO3ibut ;
k(+12) : 1.41E+06 ;
k(-12) : 9.52E+09 ;
CoCO3ibut + CO <-> CoCO4ibut ;
k(+13) = 1.49E+05 ;
k(-13) = 6.04E+02 ;
CoCO3ibut + H2 <-> HCoCO3 + ibut_red ;
k(+14) = 8.47E+02 ;
k(-14) = 0 ;
agCoCO3ipr + H2 <-> HCoCO3 + prop ;
k(+15) = 5.28E+00 ;
k(-15) = 0 ;
CoCO3nbut + HCoCO4 <-> nald_hept ;
k(+16) = 4.89E+06 ;
k(-16) = 4.73E+06 ;
nald_hept + CO <-> Co2CO8 + nbut_clev ;

```
k(+17) = 1.31E+09 ;
k(-17) = 0 ;
CoCO3ibut + HCoCO4 <-> iald_hept ;
k(+18) = 2.59E+05 ;
k(-18) = 1.47E+05 ;
iald_hept + CO <-> Co2CO8 + ibut_clev ;
k(+19) = 1.31E+09 ;
k(-19) = 0 ;
nbut = nbut_red + nbut_clev ;
ibut = ibut_red + ibut_clev ;
ratio = nbut / ibut ;
*output
nbut ; ibut ; prop ;
*script
mechanism.solver = "stiff" ;
go
```

A.6 Kinetic Modelling and Fitting

The kinetic modelling was done for the 34 different reaction conditions (Table A.2) for which experimental results were available. In the experimental paper pressures were reported in bar, and here we employ atm units. Because the error introduced by the simplification that 1 bar = 1 atm is negligible compared to other errors in our model the pressure units have not been converted and bar units are used for experimental description throughout.

Table A.2 Detailed conditions for each experiment

Exp. Nr	Temperature K	$Co_2(CO)_8$ conc. mol m^{-3}	C_3H_6 conc. mol dm^{-3}	CO pressure bar	H_2 pressure bar
1	423	7.30	1.19	50	50
2	423	2.92	1.19	50	50
3	423	1.46	1.19	50	50
4	403	14.6	1.19	50	50
5	403	7.30	1.19	50	50
6	403	2.92	1.19	50	50
7	383	14.6	1.19	50	50
8	383	7.30	1.19	50	50
9	383	2.92	1.19	50	50
10	423	2.92	2.20	50	50
11	423	2.92	0.595	50	50
12	403	2.92	2.20	50	50
13	403	2.92	1.79	50	50
14	403	2.92	0.595	50	50
15	383	2.92	3.57	50	50
16	383	2.92	2.20	50	50
17	383	2.92	1.79	50	50
18	383	2.92	0.595	50	50
19	423	7.30	1.19	50	25
20	423	7.30	1.19	25	25
21	423	7.30	1.19	10	25
22	403	7.30	1.19	50	25
23	403	7.30	1.19	25	25
24	403	7.30	1.19	10	25
25	383	7.30	1.19	75	25
26	383	7.30	1.19	50	25
27	383	7.30	1.19	25	25
28	383	7.30	1.19	10	25
29	423	7.30	1.19	25	75
30	423	7.30	1.19	25	50
31	403	7.30	1.19	25	75
32	403	7.30	1.19	25	50
33	383	7.30	1.19	25	75
34	383	7.30	1.19	25	50

As discussed in the paper the model presented in the previous chapter of Appendix A gave good agreement for the experiments conducted at the temperature of 423 K. The agreement is less good for the lower temperature of 403 K and even less good for the

lowest temperature of 383 K. As even small errors in calculated Gibbs free energies may lead to large errors in calculated rate constants *k*, because of the exponential dependence on Δ*G* values, we proposed a fitting scheme in order to check if small variations of 2-3 kcal mol^{-1} of key values used for *k* calculations could improve the agreement between experimental and theoretical values of rates. In the program written by us we allowed the values of Δ*H* and Δ*S* of chosen minima and barriers to vary incrementally up to a maximum value of 4 kJ mol^{-1} and 0.035 kJ mol^{-1} respectively. Altogether *H* and *S* were varied for eight species, for which most probably the theoretical values are the least accurate. The fitted energies are for:

I ΔG_1 - bimetallic precatalyst **1**

II $\Delta G^{\ddagger}_1$ – the apparent TS from **1** to **2** based only on experimental equilibrium constant

III $\Delta G^{\ddagger}_2$ – diffusion limited barrier of CO loss from **2** to **3**

IV $\Delta G^{\ddagger}_3$ – diffusion limited barrier in propene addition from **3** to **4**

V $\Delta G^{\ddagger}_5$ – diffusion limited barrier for CO diffusion to **6n** forming **7n**

VI $\Delta G^{\ddagger}_{11}$ – diffusion limited barrier for CO diffusion to **6i** forming **7i**

VII $\Delta G^{\ddagger}_{16}$ – bimetallic reductive elimination **TS16n**

VIII $\Delta G^{\ddagger}_{16}$ – bimetallic reductive elimination **TS16i**

Our best fit gave a final merit function of 22 % (root-mean square error of the calculated vs. experimental rate, as defined by Equation 5 in the main text) compared to 69 % for the "raw model". The raw and fitted values of Δ*H* and Δ*S* for concerned species are juxtaposed in Table A.3.

Table A.3 The raw and fitted values of relative enthalpies and entropies for fitted species in kJ mol^{-1} (H) or kJ mol^{-1} K^{-1} (S)

Nr	ΔH(raw)	ΔS(raw)	ΔH(fitted)	ΔS(fitted)
I	-17.991	0.010878	-16.080	0.027209
II	-21.336	-0.168283	-22.561	-0.191429
III	150.632	0.096896	149.467	0.131405
IV	153.977	0.134296	155.070	0.167019
V	84.362	-0.024861	83.626	-0.051714
VI	86.497	-0.030637	84.233	-0.052769
VII	-14.803	-0.269245	-14.107	-0.254968
VIII	-14.040	-0.274693	-12.350	-0.258970

To conclude the values of the rates of butyraldehyde production are summarized in Table A.4, in which the experimentally measured rates ($R_{exp,\,\mathbf{n}}$ and $R_{exp,\,\mathbf{i}}$) are compared to rates calculated with the "raw" model ($R_{calc\text{-}raw,\,\mathbf{n}}$ and $R_{calc\text{-}raw,\,\mathbf{i}}$) and the "fitted" model ($R_{calc\text{-}fitted,\,\mathbf{n}}$ and $R_{calc\text{-}fitted,\,\mathbf{i}}$) for n-butyraldehyde and iso-butyraldehyde respectively.

Table A.4 Comparison of experimental and calculated rates

Exp. Nr	Rates of n-butyraldehyde formation			Rates of iso-butyraldehyde formation		
	$R_{exp,\ n}$	$R_{calc\text{-}raw,\ n}$	$R_{calc\text{-}fitted,\ n}$	$R_{exp,\ i}$	$R_{calc\text{-}raw,\ i}$	$R_{calc\text{-}fitted,\ i}$
	mol m^{-3} s^{-1}					
1	0.777	0.5071	0.9255	0.2760	0.3891	0.3701
2	0.376	0.1992	0.3431	0.1420	0.1854	0.1776
3	0.227	0.0979	0.1588	0.0924	0.0997	0.0978
4	0.66	0.1823	0.8576	0.1800	0.0922	0.2378
5	0.349	0.1022	0.4689	0.1260	0.0653	0.1467
6	0.182	0.0441	0.1904	0.0560	0.0363	0.0731
7	0.206	0.0160	0.1970	0.0494	0.0050	0.0482
8	0.151	0.0087	0.1204	0.0368	0.0035	0.0306
9	0.063	0.0035	0.0563	0.0150	0.0019	0.0159
10	0.654	0.3379	0.5910	0.3050	0.3173	0.3111
11	0.22	0.1052	0.1791	0.0743	0.0974	0.0917
12	0.355	0.0722	0.3188	0.1350	0.0597	0.1250
13	0.302	0.0616	0.2699	0.1120	0.0509	0.1049
14	0.113	0.0238	0.1011	0.0303	0.0195	0.0384
15	0.167	0.0066	0.1327	0.0523	0.0034	0.0385
16	0.11	0.0052	0.0935	0.0324	0.0027	0.0267
17	0.0849	0.0046	0.0794	0.0230	0.0024	0.0225
18	0.0346	0.0021	0.0301	0.0063	0.0011	0.0084
19	0.478	0.3366	0.5585	0.2420	0.2203	0.1994
20	0.676	0.3920	0.5667	0.3540	0.2565	0.2019
21	0.791	0.4350	0.5718	0.6100	0.2846	0.2035
22	0.246	0.0796	0.3145	0.0919	0.0442	0.0930
23	0.311	0.1152	0.3323	0.1500	0.0641	0.0980
24	0.365	0.1565	0.3440	0.2190	0.0874	0.1013
25	0.0564	0.0040	0.0736	0.0134	0.0013	0.0151
26	0.0793	0.0060	0.0875	0.0217	0.0021	0.0201
27	0.105	0.0101	0.1058	0.0357	0.0039	0.0265
28	0.152	0.0157	0.1199	0.0601	0.0062	0.0306
29	1.41	0.8142	1.2435	0.5370	0.6653	0.5145
30	1.07	0.6285	0.9423	0.4710	0.4828	0.3761
31	0.642	0.1833	0.6178	0.2510	0.1221	0.1950
32	0.516	0.1559	0.4992	0.1950	0.0999	0.1558
33	0.21	0.0178	0.1712	0.0590	0.0073	0.0448
34	0.159	0.0146	0.1452	0.0490	0.0060	0.0378

A.5 References

[1] M. J. Frisch, G. W. Trucks, H. B. Schlegel, G. E. Scuseria, M. A. Robb, J. R. Cheeseman, G. Scalmani, V. Barone, B. Mennucci, G. A. Petersson, H. Nakatsuji, M. Caricato, X. Li, H. P. Hratchian, A. F. Izmaylov, J. Bloino, G. Zheng, J. L. Sonnenberg, M. Hada, M. Ehara, K. Toyota, R. Fukuda, J. Hasegawa, M. Ishida, T. Nakajima, Y. Honda, O. Kitao, H. Nakai, T. Vreven, J. A. Montgomery, Jr., J. E. Peralta, F. Ogliaro, M. Bearpark, J. J. Heyd, E. Brothers, K. N. Kudin, V. N. Staroverov, T. Keith, R. Kobayashi, J. Normand, K. Raghavachari, A. Rendell, J. C. Burant, S. S. Iyengar, J. Tomasi, M. Cossi, N. Rega, J. M. Millam, M. Klene, J. E. Knox, J. B. Cross, V. Bakken, C. Adamo, J. Jaramillo, R. Gomperts, R. E. Stratmann, O. Yazyev, A. J. Austin, R. Cammi, C. Pomelli, J. W. Ochterski, R. L. Martin, K. Morokuma, V. G. Zakrzewski, G. A. Voth, P. Salvador, J. J. Dannenberg, S. Dapprich, A. D. Daniels, O. Farkas, J. B. Foresman, J. V. Ortiz, J. Cioslowski, and D. J. Fox, *Gaussian 09, Revision E.01*, **2013**, Gaussian, Inc., Wallingford CT.

[2] A. D. Becke, *J. Chem. Phys.* **1993**, 98, 5648–5652.

[3] S. Grimme, S. Ehrlich, L. Goerigk, *J. Comp. Chem.* **2011**, 32, 1456-1465.

[4] a) K. Raghavachari, J. S. Binkley, R. Seeger, J. A. Pople, *J. Chem. Phys.* **1980**, 72, 650-654; b) K. Raghavachari, G. W. Trucks, *J. Chem. Phys.* **1989**, 91, 1062-65.

[5] a) R. F. Ribeiro, A. V. Marenich, C. J. Cramer, D. G. Truhlar, *J. Phys. Chem. B* **2011**, 115, 14556–14562; b) Y. Zhao, D. G. Truhlar, *Phys. Chem. Chem. Phys.* **2008**, 10, 2813–2818.

[6] a) H.-J. Werner, P. J. Knowles, G. Knizia, F. R. Manby, M. Schütz, *WIREs Comput. Mol. Sci.* **2012**, 2, 242-253; b) H.-J. Werner, P. J. Knowles, G. Knizia, F. R. Manby, M. Schütz, P. Celani, T. Korona, R. Lindh, A. Mitrushenkov, G. Rauhut, K. R. Shamasundar, T. B. Adler, R. D. Amos, A. Bernhardsson, A. Berning, D. L. Cooper, M. J. O. Deegan, A. J. Dobbyn, F. Eckert, E. Goll, C. Hampel, A. Hesselmann, G. Hetzer, T. Hrenar, G. Jansen, C. Köppl, Y. Liu, A. W. Lloyd, R. A. Mata, A. J. May, S. J. McNicholas, W. Meyer, M. E. Mura, A. Nicklass,

D. P. O'Neill, P. Palmieri, D. Peng, K. Pflüger, R. Pitzer, M. Reiher, T. Shiozaki, H. Stoll, A. J. Stone, R. Tarroni, T. Thorsteinsson, and M. Wang, *MOLPRO, version 2012.1*, a package of ab initio programs, http://www.molpro.net.
[7] a) T. B. Adler, G. Knizia, H.-J. Werner, *J. Chem. Phys.* **2007**, 127, 221106; b) H.-J. Werner, G. Knizia, F. R. Manby, *Mol. Phys*. **2011**, 109, 407-417.
[8] a) M. Reiher, A. Wolf*, J. Chem. Phys.* **2004**, 121, 2037-2047; b) M. Reiher, A. Wolf, *J. Chem. Phys.* **2004**, 121, 10945-10956; c) A. Wolf, M. Reiher, B. A. Hess, *J. Chem. Phys.* **2002**, 117, 9215-9226.
[9] a) F. Ungváry, *J. Organomet. Chem* **1972**, 36, 363-370; b) J. W. Rathke, R. J. Klingler, T. R. Krause, *Organometallics* **1992**, 11, 585-588.
[10] A. H. Krall, J. V. Sengers, J. Kestin, *J. Chem. Eng. Data* **1992**, 37, 349 – 355.
[11] D. Wachsstock*, Tenua 2.1—the kinetics simulator for Java, by Daniel Wachsstock, MD*., http://bililite.com/tenua/.
[12] R. V. Gholap, O. M. Kut, J. R. Bourne, *Ind. Eng. Chem. Res.* **1992**, 31, 2446-2450.

Appendix B

This appendix is the supplementary information part of Chapter 3

B.1 Additional computational results

The PES of methane activation by alternant pnictogen chalcogen ring cations was explored at the DFT level of theory with the B2-PLYP functional [1] with D3BJ empirical dispersion [2] and standard 6-311g(d) [3] basis set on all atoms using Gaussian 16 revision A.03 program [4]. The geometries of all of the located stationary points on PES were optimized and their single point energies calculated. Frequency analysis was conducted as well. On the optimized structures of $N_2O_2^{\bullet+}$ and $N_2S_2^{\bullet+}$ reaction with CH_4 the CCSD(T) single-point energy calculations employing aug-cc-pvtz [5] basis set were performed.

B.2 $N_2S_2^{\bullet+}$

In order to confirm the qualitative validity of the obtained values of the energies we have repeated some of the DFT geometry optimization calculations employing two different functionals, namely ωB97X-D [6] and M06-2X [7] with D3 dispersion correction [8], and 6-311+g(d) basis set on all atoms. Moreover we have calculated the single-point energy at the CCSD(T) level of theory for geometries of stationary points optimized with ωB97X-D functional. The calculated DFT and CCSD(T) relative energies reported in kJ mol^{-1} for the reaction of CH_4 with $N_2S_2^{\bullet+}$ (Figure 3.3 in the Chapter 3) explained in the article are compared in Table B.1.

Table B.1 Relative energies for the CH_4 + $N_2S_2^{\bullet+}$ reaction. [a] TS was not localized with M06-2X functional

Species	$\Delta E_{B2\text{-}PLYP}$	$\Delta E_{B2\text{-}PLYP\_CCSDT}$	$\Delta E_{\omega B97X\text{-}D}$	$\Delta E_{\omega B97X\text{-}D\_CCSDT}$	$\Delta E_{M06\text{-}2X}$
$N_2S_2^{\bullet+}$ + CH_4	0.0	0.0	0.0	0.0	0.0
EC_{NS}	-17.9	-23.3	-17.5	-23.3	-21.9
TS_{NS}	-14.6	-15.3	-16.7	-21.0	— [a]
I_{NS}	-81.8	-82.8	-77.2	-82.6	-86.4
$HN_2S_2^{+}$ + $CH_3^{\bullet}$	-43.6	-40.0	-38.3	-39.7	-48.6

As mentioned in the paper some of the pathways leading to low-energy minima on PES of CH_4 activation were localized. They are presented below. The relative energy values ΔE are calculated at CCSD(T) level of theory employing aug-cc-pvtz basis set for the structures which geometries were optimized at DFT level of theory with the B2-PLYP functional with D3BJ empirical dispersion and standard 6-311g(d) basis set on all atoms. All energies presented are relative to $N_2S_2^{\bullet+}$ + CH_4 energy of separated reactants which is set to zero. The concerted reaction pathway leading to $Min5_{NS}$ was not localized.

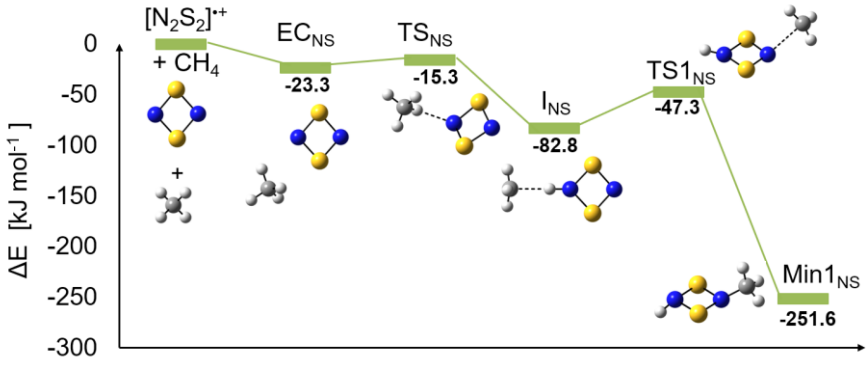

Figure B.1 PES for the reaction $N_2S_2^{\bullet+}$ + CH_4 ↔ I_{NS} ↔$Min1_{NS}$.

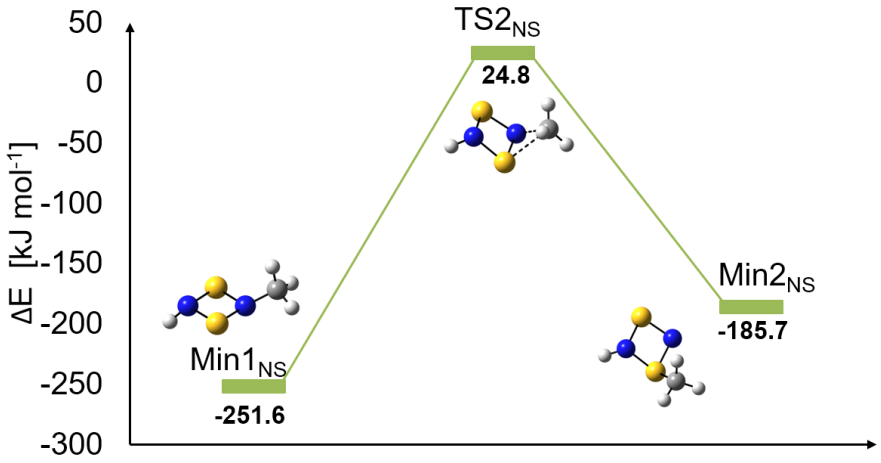

Figure B.2 PES of the reaction $Min1_{NS}$ ↔ $Min2_{NS}$.

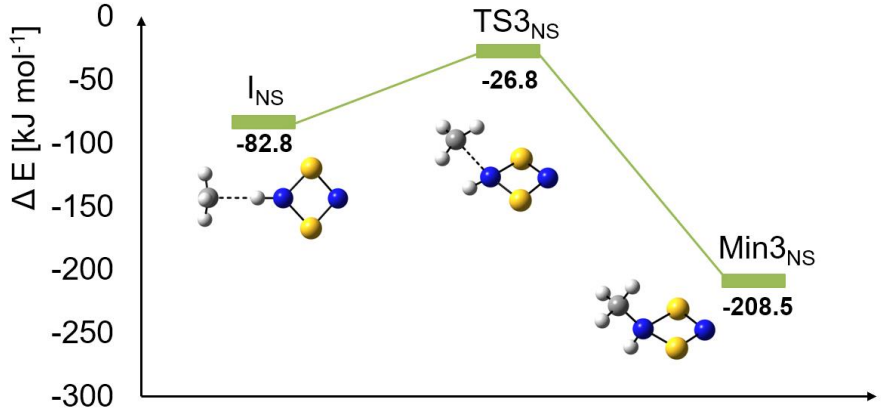

Figure B.3 PES of the reaction I_{NS} ↔ $Min3_{NS}$.

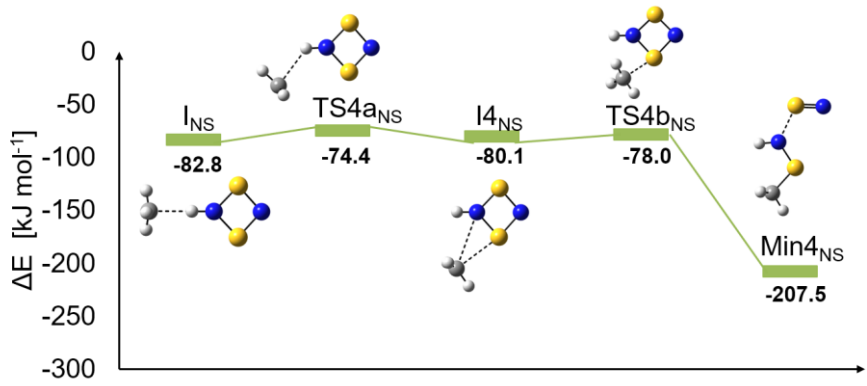

Figure B.4 PES of the reaction I_{NS} ↔ $Min4_{NS}$.

The calculated vibrational spectra of low- energy minima localized on PES of CH_4 activation by alternant $N_2S_2^{\bullet+}$ radical cation ring are given in Table B.2. They were calculated employing B2-PLYP functional with D3BJ empirical dispersion and standard 6-311g(d) basis set on all atoms.

Table B.2 Peak information of IR spectra of five low- energy minima localized on PES of CH_4 activation by $N_2S_2^{\bullet+}$

	$Min1_{NS}$		$Min2_{NS}$		$Min3_{NS}$		$Min4_{NS}$		$Min5_{NS}$	
	Freq	**D** 10^{-40} esu^2 cm^2	**Freq**	**D** 10^{-40} esu^2 cm^2	**Freq**	**D** 10^{-40} esu^2 cm^2	**Freq**	**D** 10^{-40} esu^2 cm^2	**Freq**	**D** 10^{-40} esu^2 cm^2
Nr	cm^{-1}		cm^{-1}		cm^{-1}		cm^{-1}		cm^{-1}	
1	161	417	146	88	83	222	41	198	62	17
2	191	10	169	39	230	7	88	6	104	18
3	273	13	247	108	270	2	120	207	161	153
4	285	268	350	123	322	18	172	0	273	95
5	531	15	502	37	505	13	190	576	273	551
6	574	308	595	369	514	44	324	1061	499	72
7	680	636	679	62	597	82	412	1317	672	190
8	733	6	690	208	721	3	435	859	711	43
9	835	0	713	55	767	5	690	10	713	497
10	865	273	828	63	979	62	931	244	895	186
11	1123	74	922	231	1127	59	979	27	968	16
12	1164	17	982	19	1129	31	1009	45	976	221
13	1208	4	1021	38	1230	57	1216	32	1030	103
14	1303	100	1309	144	1397	17	1398	26	1094	245
15	1477	1	1385	20	1477	8	1404	86	1397	8
16	1503	70	1450	62	1506	44	1482	61	1470	63
17	1510	31	1461	73	1511	70	1482	34	1471	43
18	3080	1	3071	19	3094	1	3078	5	3084	13
19	3177	2	3172	13	3188	2	3185	3	3194	5
20	3186	1	3212	11	3219	2	3186	1	3194	5
21	3524	154	3495	102	3452	112	3507	64	3481	206

B.3 $N_2O_2^{\bullet+}$

The localized pathways leading to the formation of the low-energy species for the reaction of CH_4 with $N_2O_2^{\bullet+}$ are presented below. The energies shown are relative to $N_2O_2^{\bullet+}$ + CH_4 energy of separated reactants which is set to zero. Their values were calculated employing the same protocol as for $N_2S_2^{\bullet+}$, single-point energies are calculated at CCSD(T) level of theory employing aug-cc-pvtz basis set on each atom for the structures which geometries

were optimized at DFT level of theory with the B2-PLYP functional with D3BJ empirical dispersion and standard 6-311g(d) basis set on all atoms. We did not localize a concerted pathway leading to $Min4_{NO}$ and $Min5_{NO}$

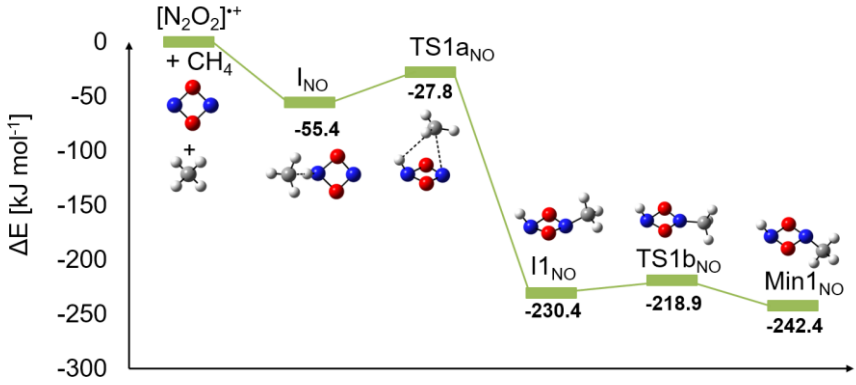

Figure B.5 PES of the reaction $N_2O_2^{\bullet+}$ + CH_4 ↔ I_{NO} ↔ $Min1_{NO}$.

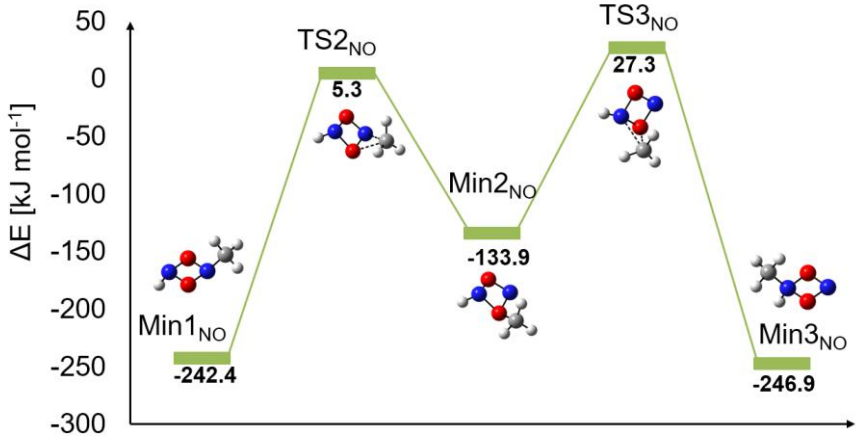

Figure B.6 PES of the reaction $Min1_{NO}$ ↔ $Min2_{NO}$ ↔ $Min3_{NO}$.

The calculated vibrational spectra of low- energy minima localized on PES of CH_4 activation by alternant $N_2O_2^{\bullet+}$ radical cation ring are juxtaposed in Table B.3. They were calculated employing B2-PLYP functional with D3BJ empirical dispersion and standard 6-311g(d) basis set on all atoms.

Table B.3 Peak information of IR spectra of five low- energy minima localized on PES of CH_4 activation by $N_2O_2^{\bullet+}$.

	$Min1_{NO}$		$Min2_{NO}$		$Min3_{NO}$		$Min4_{NO}$		$Min5_{NO}$	
	Freq	D 10^{-40} esu^2	Freq	D 10^{-40} esu^2	Freq	D 10^{-40} esu^2	Freq	D 10^{-40} esu^2	Freq	D 10^{-40} esu^2
Nr	cm^{-1}	cm^2	cm^{-1}	cm^2	cm^{-1}	cm^2	cm^{-1}	cm^2	cm^{-1}	cm^2
1	219	23	177	7	182	4	143	35	111	21
2	220	825	189	65	242	0	481	142	173	5
3	357	93	304	25	354	4	548	686	260	147
4	457	95	374	328	494	223	967	108	286	1051
5	659	195	592	159	781	100	1150	107	428	177
6	846	118	719	403	841	163	1192	6	552	481
7	928	128	789	260	925	269	1240	130	642	164
8	1008	58	902	13	972	163	1491	3	754	93
9	1087	13	940	67	990	44	1513	23	982	182
10	1152	12	1113	74	1058	4	1523	110	1080	126
11	1180	39	1187	12	1174	23	1546	18	1172	1
12	1186	561	1205	37	1206	23	2352	31	1194	274
13	1202	40	1304	249	1359	25	3075	44	1353	508
14	1357	101	1392	113	1449	10	3157	41	1479	53
15	1448	20	1465	11	1463	23	3191	24	1490	1
16	1484	50	1480	69	1495	85	3417	12	1500	122
17	1489	89	1491	57	1509	64			1520	314
18	3082	14	3115	4	3090	19			3119	4
19	3193	15	3245	13	3191	17			3252	6
20	3197	6	3260	9	3232	12			3259	9
21	3373	154	3382	81	3391	120			3420	86

B.4 $P_2O_2^{\bullet+}$

The energies for the reaction of CH_4 or SiH_4 with $P_2O_2^{\bullet+}$ were calculated only at the DFT level of theory using the B2-PLYP functional with D3BJ empirical dispersion and standard 6-311g(d) basis set on all atoms. As mentioned in the paper the hydrogen atom transfer from methane appeared not to take place for the phosphorous cluster. However the transition state corresponding to proton coupled electron transfer mechanism for CH_4 cleavage

TS_{PO_pcet} was localized although its relative energy is lying very high compared to separated reactants. The corresponding PES is depicted in Figure B.7. The energy of $P_2O_2^{\bullet+}$ + CH_4 separated reactants is set to zero and the shown energies of other species are relative to it.

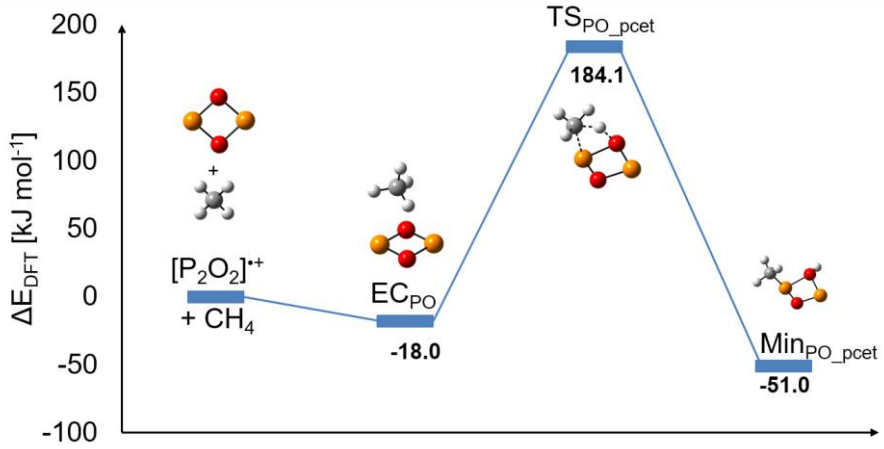

Figure B.7 PES of the reaction $P_2O_2^{\bullet+}$ + CH_4 ↔ Min_{PO_pcet}.

The HAT-type reaction was found for the reaction with silane. For the latter system no transition state was localized and the intermediate was more stable than separated reactants. The PES for the $P_2O_2^{\bullet+}$ + SiH_4 (the system energies are set to zero) reaction is presented in Figure B.8 with energies calculated as in the previous example.

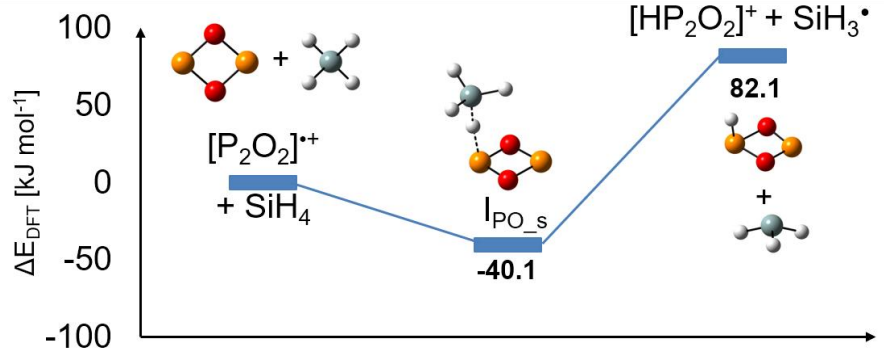

Figure B.8 PES of the reaction $P_2O_2^{\bullet+}$ with SiH_4.

B.5. References

[1] S. Grimme, *Chem. Phys.* **2006**, 124, 034108.
[2] (a) L. Goerigk, S. Grimme, *J. Chem. Theory Comput.* **2011**, 7, 291–309; (b) S. Grimme, S. Ehrlich, L. Goerigk*, J. Comput. Chem.* **2011**, 32, 7, 1456-1465.
[3] (a) K. Raghavachari, J. S. Binkley, R. Seeger, J. A. Pople, J. Chem. Phys. 1980, 72, 650-654; (b) K. Raghavachari, G. W. Trucks, J. Chem. Phys. 1989, 91, 1062-65.
[4] M. J. Frisch, G. W. Trucks, H. B. Schlegel, G. E. Scuseria, M. A. Robb, J. R. Cheeseman, G. Scalmani, V. Barone, G. A. Petersson, H. Nakatsuji, X. Li, M. Caricato, A. V. Marenich, J. Bloino, B. G. Janesko, R. Gomperts, B. Mennucci, H. P. Hratchian, J. V. Ortiz, A. F. Izmaylov, J. L. Sonnenberg, D. Williams-Young, F. Ding, F. Lipparini, F. Egidi, J. Goings, B. Peng, A. Petrone, T. Henderson, D. Ranasinghe, V. G. Zakrzewski, J. Gao, N. Rega, G. Zheng, W. Liang, M. Hada, M. Ehara, K. Toyota, R. Fukuda, J. Hasegawa, M. Ishida, T. Nakajima, Y. Honda, O. Kitao, H. Nakai, T. Vreven, K. Throssell, J. A. Montgomery, Jr., J. E. Peralta, F. Ogliaro, M. J. Bearpark, J. J. Heyd, E. N. Brothers, K. N. Kudin, V. N. Staroverov, T. A. Keith, R. Kobayashi, J. Normand, K. Raghavachari, A. P. Rendell, J. C. Burant, S. S. Iyengar, J. Tomasi, M. Cossi, J. M. Millam, M. Klene, C. Adamo, R. Cammi, J. W. Ochterski, R. L. Martin, K. Morokuma, O. Farkas, J. B. Foresman, D. J. Fox, *Gaussian 16, Revision A.03*, **2016**, Gaussian, Inc., Wallingford CT.
[5] R. A. Kendall, T. H. Dunning Jr., R. J. Harrison, *J. Chem. Phys.* **1992**, 96, 6796-6806.
[6] J. D. Chai, M. Head-Gordon, *Phys. Chem. Chem. Phys.* **2008**, 10, 6615-6620.
[7] Y. Zhao, D. G. Truhlar, *Theor. Chem. Acc.* **2008**, 120, 215-41.
[8] S. Grimme, J. Antony, S. Ehrlich, H. Krieg, *J. Chem. Phys.* **2010**, 132, 154104.